University of Nottingham

School of Mathematical Science

Quantum-enhanced strategies for surface and phase discrimination

Carmine Napoli

A thesis submitted to the University of Nottingham

for the degree of

Doctor of Philosophy

December 24, 2020

alla mia famiglia

Abstract

The ability to perform high precision measurements underpins a plethora of applications. Several techniques for force sensing, phase estimation and discrimination, as well as surface reconstruction for complex features of three-dimensional samples, have been developed in recent years. The main aim of this thesis is to investigate metrology enhancements due to quantum resources (probes and measurements), by using quantum parameter estimation and channel discrimination techniques.

The thesis focuses on two main scenarios.

In the first one, we deal with three-dimensional superlocalisation. By using tools from multiparameter quantum metrology, we show that a simultaneous estimation of all three components of the separation between two incoherent point sources in the paraxial approximation is achievable by a single quantum measurement, with a precision saturating the ultimate limit stemming from the quantum Cramér-Rao bound. Such a precision is not degraded in the sub-wavelength regime, thus overcoming the traditional limitations of classical direct imaging derived from Rayleigh's criterion. Our results are qualitatively independent of the point spread function of the imaging system, and quantitatively illustrated in detail for Gaussian beams. In this case, we show that a method of measuring the position of each photon at the imaging plane based on discrimination in terms of Hermite-Gaussian spatial modes reaches the quantum precision bound in the limit of infinitesimal separation.

In the second part of the thesis, we investigate the role of quantum coherence as a resource for channel discrimination tasks. We consider a probe state of arbitrary dimension entering a black box, in which a phase shift is implemented, with the unknown phase randomly sampled from a finite set of predetermined possibilities. At the output, an optimal measurement is performed in order to guess which specific phase was applied in the process. We show that the presence of quantum coherence (superposition with respect to the eigenbasis of the generator of the phase shift) in the input probe directly determines an enhancement in the probability of success for this task, compared to the use of incoherent probes. We prove that such a quantum advantage is exactly quantified by the robustness of coherence, a full monotone with respect to the recently formulated resource theories of quantum coherence, whose properties and applications are developed and explored in detail.

Acknowledgements

First, I would like to express my sincere gratitude to my PhD supervisors Gerardo Adesso, Samanta Piano and Tommaso Tufarelli for their precious help and constant encouragement throughout these years. They have generously shared with me their knowledge, experience and time, and I will always be grateful to them for this. Not a single sentence of this thesis would have been written without his careful support.

A huge thank is for the all members of the two groups that adopted me during this journey: the Manufacturing and Metrology Group leaded by the Prof. Richard Leach and the Quantum Correlation Group leaded by the Prof. Gerardo Adesso.

A special person that I would thank is Luisa, for her sweetness and her love. We supported each other trough this long writing period (for me), and ”lab things” (for her) done during the lockdown, and when things where going bad we have always find a way to tackle the meeting day: friends and milkshake. She teach me what means walk togheter.

Then, I would like to thank all the amazing people I have met in Nottingham and that have made my experience here unforgettable. First of all to the infinite amount of people that have lived with me: to Giorgio, Eliana, Mariele, Antoine, thanks with them it was possible to build something that I could call ”home”. Moreover, I have to say thank you to all the people that I have met here in Nottingham: Fabio, Davide, Nicola, Elisabetta, Pete, Gordon, Mauro, Marco Perin, Pietro, Marco Baffetti, Marco Cianciaruso, Luis, Patri, Lemmon,Eugenia, Giulia, Anna, Anahita

and Eugenio and to all the people with whom I shared the love for theatre: all the members that have been in Post Graduate New Theatre Group.
I would also like to thank all friends back in Mercato San Severino that have supported me for many years. To Angelantonio, Diana, Emanuele, Filomena, Mario Ferrentino, Mario Loffredo, Mario Venezia and Rosa. They were able to make me feel with them where ever I was and I was able to do same with them.
Above all, I would like to thank my family that has always been by my side in every step I have taken: my mother and father, Luisa and Vincenzo, for being the solid pillars of my life and for their unconditional love, my sisters and brother-in-law Gilda, Maria and Leonardo, with whom the bond of affection becomes stronger and stronger each year, and I am sure it will always be like this, with my nephews Raffaele, Vincenzo and Gian Domenico for their infinite sweetness, and moreover I would thank my grandmother Gilda which supported me over and over and whole my family.

Contents

Introduction

The ability to perform high precision measurements, sensing, and imaging at micro- and nano-scale underpins a plethora of applications in manufacturing industry, biomedical sciences, fundamental physics and information technology [1]. Several techniques to scan and reconstruct complex features of three-dimensional inert or living samples have been developed in recent years [2], and the quest to enhance the signal-to-noise ratio and the acquisition rate in these setups is still very much open. The majority of optical imaging techniques (e.g. fringe projection, or focus variation) utilise light sources which are essentially modelled as classical, which means that the precision achievable in such setups is a priori limited by the so-called shot noise limit. On the other hand, it is well known that quantum features such as superposition and entanglement can give rise to an enhanced precision in metrology and imaging, allowing one to beat those limitations [3, 4]. The applications of quantum metrology to a wide range of technologies (e.g. communication, navigation, clocks) are currently being pursued as a national priority in the UK, and the detection of elusive signals like gravitational waves will only be possible by exploiting quantum-enhanced techniques.

The thesis is organized as follows.

This thesis is focused mainly on three-dimensional superlocalization and on the role of quantum coherence as a resource for channel discrimination tasks.

The dissertation starts with a brief introduction over the elements of quantum mechanics, where are showed the basics axioms of quantum mechanics that describe

the states, observables and the dynamical evolution of a quantum system.
Then, in the first part, we investigate the imaging theory starting from the classical scheme. Here we look from the diffraction theory [5, 6] to led through the classical resolution limit: Rayleigh's criterion [7, 8]. Then we look at some scenarios that beat this limit as the Abbe theory of formation that lead to the Abbe's [9, 10, 11] limit and the a priori information from the Fourier analysis [6, 12, 13]. From here we move to a quantum setting, where with use of quantum metrology analysis [14, 15, 16, 17] we show how the Rayleigh's curse is beaten [18, 19, 20]. In particular we focus on the estimation of relative distances in a scheme of two light point sources (initially focusing on angular and axial distances between them, then we specialize in a 3-D setting). In both cases we find that Rayleigh's curse does not occur, indeed this measurement is distance-independent [21]. Then we specialize to Gaussian beams deriving formulas and showing that in the limit of small distances all the parameters become statistically independent. In the end we propose an experimental implementation that use the method of spatial mode demultiplexing [18]. We show, that using this method is possible to estimate the 3-D separation between the two sources with quantum optimal Fisher information.
In the second part we start to analyze the quantum coherence as resource theory [22, 23], showing the general structure of a quantum resource theory [24]: free states, resource states and free operation where they are respectively the states that can be implemented for free, the states which are not free and the operation that cannot convert a free state into a resources state. From here we we approach quantum coherence as a resource theory, defining the resource states and free states for it, and proposing a class of free operation suitable for quantum coherence. In the last part we define robustness of coherence as a measure for quantum coherence [23], giving an operational interpretation of it that quantifies the advantage enabled by a quantum state in a phase discrimination task.

1 — Elements of quantum mechanics

1.1 The postulates of quantum mechanics

We set the stage of this thesis by briefly reviewing the basic axioms [25] of quantum mechanics, describing the states, observables and dynamical evolution of a quantum system. These postulates provide a connection between the physical world and the mathematical formalism of quantum mechanics.

1.1.1 Pure state space

The first postulate of quantum mechanics establishes what the pure states of a quantum system are, i.e. the states of a quantum system whose knowledge is in principle the best possible one.

Postulate 1.1.1. Any quantum system is associated with a complex Hilbert space $\mathcal{H}$, also known as the carrier Hilbert space. The set of pure states of a quantum system is characterised by the projective Hilbert space $\mathbb{P}(\mathcal{H})$ of the carrier Hilbert space $\mathcal{H}$, i.e. the set of equivalence classes of vectors of $\mathcal{H}$ differing by

multiplication through a non-zero complex number. Specifically,

$$\begin{aligned}\mathbb{P}(\mathcal{H}) = \{\,[|\psi\rangle] : |\psi\rangle, |\psi'\rangle \in [|\psi\rangle] \Leftrightarrow |\psi\rangle = \lambda\,|\psi'\rangle\,,\\ |\psi\rangle\,,\ |\psi'\rangle \in \mathcal{H}\backslash\{\mathbf{0}\}\,,\ \lambda \in \mathbb{C}\backslash\{\mathbf{0}\}\,\}.\end{aligned} \tag{1.1}$$

For the sake of simplicity, according to common practice, in the following we will denote an arbitrary pure state simply by a so-called state vector $|\psi\rangle$, i.e. a vector of $\mathcal{H}$ satisfying the condition $\langle\psi|\psi\rangle = 1$, also known as normalisation condition. However, it is worthwhile to note that the state vectors are not in one-to-one correspondence with the pure states, as it can be easily seen by considering the two state vectors $|\psi\rangle$ and $|\psi\rangle' = e^{i\phi}\,|\psi\rangle$ which are both normalised but are equivalent up to an unobservable phase factor, thus corresponding to the same pure state.

The simplest quantum system is the so-called quantum bit, also known as *qubit*. A qubit is associated with a two-dimensional complex Hilbert space, i.e. $\mathcal{H} \simeq \mathbb{C}^2$. Therefore, if $|0\rangle$ and $|1\rangle$ form an orthonormal basis of such space, then an arbitrary pure state of a qubit can be written as follows:

$$|\psi\rangle = a\,|0\rangle + b\,|1\rangle\,, \tag{1.2}$$

where a and b are complex numbers such that $|a|^2 + |b|^2 = 1$. The most general pure state of a qubit, Eq. (1.2), can be thus written in the following form:

$$|\psi\rangle = \cos\theta\,|0\rangle + e^{i\phi}\sin\theta\,|1\rangle\,, \tag{1.3}$$

where $\theta \in [0, \pi/2]$ and $\phi \in [0, 2\pi[$. Consequently, the set of pure states of a qubit enjoys a nice geometrical representation, that is the two-dimensional unit sphere.

1.1.2 Closed dynamics

How does an initial pure state $|\psi\rangle$ of a closed quantum system vary with time? The following postulate gives a prescription for such dynamical evolution.

Postulate 1.1.2. The evolution of a closed quantum system is described by a *unitary transformation*. More precisely, the pure state $|\psi(t)\rangle$ of the system at a subsequent time $t > t_0$ is obtained by applying to the state $|\psi(t_0)\rangle$ of the system at the initial time t_0 a unitary operator $U(t, t_0)$ which depends only on the times t and t_0, i.e.

$$|\psi(t)\rangle = U(t, t_0)\,|\psi(t_0)\rangle\,, \tag{1.4}$$

where $U(t, t_0)^\dagger\, U(t, t_0) = U(t, t_0)\, U^\dagger(t, t_0) = \mathbb{1}$, with $\mathbb{1}$ being the identity over $\mathcal{H}$.

The evolution of a closed quantum system is thus deterministic, in the sense that the state of the system at a subsequent time t is entirely determined by the state of the system at the initial time t_0.

1.1.3 Quantum measurements

However, when a measurement is performed on a quantum system, the latter is in general disturbed and such determinism is lost. The next postulate describes the intrinsically indeterministic effect of a measurement performed on a quantum system.

Postulate 1.1.3. Quantum measurements are described by a collection $\{M_m\}$ of semi-positive definite operators $M_m \geq 0$ over the carrier Hilbert space satisfying the *completeness relation*,

$$\sum_m M_m^\dagger M_m = \mathbb{1}. \tag{1.5}$$

The index m refers to the corresponding measurement outcome that may occur in the experiment. If, immediately before the measurement, the state of the quantum

system is $|\psi\rangle$, then the probability that the result m occurs is given by

$$p(m) = \langle\psi \left| M_m^\dagger M_m \right| \psi\rangle, \tag{1.6}$$

and the state of the system after the measurement is

$$\frac{M_m |\psi\rangle}{\sqrt{\langle\psi \left| M_m^\dagger M_m \right| \psi\rangle}}. \tag{1.7}$$

The completeness relation thus ensures that the probabilities $p(m)$ of obtaining all the possible outcomes sum up to one, i.e.:

$$\sum_m p(m) = \sum_m \langle\psi \left| M_m^\dagger M_m \right| \psi\rangle = \langle\psi|\psi\rangle = 1. \tag{1.8}$$

1.1.4 Composite systems

Suppose we are interested in a quantum system composed of two (or more) distinguishable particles. How should we describe it in terms of its subsystems? The following postulate provides us with the answer.

Postulate 1.1.4. The carrier Hilbert space of a composite quantum system is given by the tensor product of the carrier Hilbert spaces associated with the subsystems.

For example, if we have a quantum system composed of two distinguishable particles A and B, whose carrier Hilbert spaces are given by $\mathcal{H}_A$ and $\mathcal{H}_B$ with dimensions d_A and d_B, respectively, then we have that the Hilbert space associated with the composite system is given by $\mathcal{H}_{AB} = \mathcal{H}_A \otimes \mathcal{H}_B$. Specifically, if $\left\{|i^A\rangle\right\}_{i=0}^{d_A-1}$ and $\left\{|j^B\rangle\right\}_{j=0}^{d_B-1}$ are orthonormal bases of $\mathcal{H}_A$ and $\mathcal{H}_B$, respectively, then $\left\{|i^A\rangle \otimes |j^B\rangle\right\}$, also denoted by $\left\{|i^A\rangle\,|j^B\rangle\right\}$, is an orthonormal basis of $\mathcal{H}_{AB}$. In other words, a generic

pure quantum state of such composite system can be written as follows:

$$|\psi_{AB}\rangle = \sum_{i=0}^{d_A-1} \sum_{j=0}^{d_B-1} c_{ij} \, |i^A\rangle \, |j^B\rangle \,, \tag{1.9}$$

where $\sum_{i=0}^{d_A-1} \sum_{j=0}^{d_B-1} \left|c_{ij}\right|^2 = 1$.

1.1.5 Mixed states

Density operators over the carrier Hilbert space, which are defined as trace-one semi-positive definite operators over $\mathcal{H}$, provide a convenient way to describe the states of quantum systems whose knowledge is not the best possible one, also known as mixed states. More precisely, suppose we only know that a quantum system is in one of a number of pure states $|\psi_i\rangle$, with corresponding probabilities p_i. We shall call $\{p_i, |\psi_i\rangle\}$ an *ensemble of pure states*. The mixed state of the system corresponding to such ensemble of pure states is characterised by the following density operator:

$$\rho \equiv \sum_i p_i \, |\psi_i\rangle \, \langle\psi_i| \,. \tag{1.10}$$

The density operator is also known as *density matrix* when represented in a particular basis of the carrier Hilbert space. We immediately recover the set of pure states within the density operator formalism by restricting to the rank-one density operators, i.e. the normalised projectors over the carrier Hilbert space, which are in one-to-one correspondence with the elements of the projective Hilbert space of the carrier Hilbert space.

It turns out that all the postulates of quantum mechanics can be readily extended from pure states to mixed states as follows.

Since the evolution of a closed quantum system in a pure state is described by a unitary operator U, if the system was initially in the state $|\psi_i\rangle$ with probability p_i, then after the evolution has occurred the system will be in the state $U \, |\psi_i\rangle$ with

probability p_i. Consequently, the evolution of the mixed state corresponding to the ensemble $\{p_i, |\psi_i\rangle\}$ is described by the following equation:

$$\rho = \sum_i p_i |\psi_i\rangle \langle\psi_i| \xrightarrow{U} \sum_i p_i U |\psi_i\rangle \langle\psi_i| U^\dagger = U\rho U^\dagger. \tag{1.11}$$

Measurements are also easily extendible to mixed states through the density operator formalism. Suppose we perform a measurement described by the collection of semi-positive definite operators $\{M_m\}$. Given that the initial state is $|\psi_i\rangle$, the probability of getting the m-th result is:

$$p(m|i) = \langle\psi_i | M_m^\dagger M_m | \psi_i\rangle = \mathrm{Tr}\left[M_m^\dagger M_m |\psi_i\rangle \langle\psi_i|\right], \tag{1.12}$$

while the state of the system after obtaining the result m is:

$$|\psi_i^m\rangle = \frac{M_m}{\sqrt{\langle\psi_i|M_m^\dagger M_m|\psi_i\rangle}} |\psi_i\rangle. \tag{1.13}$$

Consequently, the mixed state corresponding to the ensemble $\{p_i, |\psi_i\rangle\}$ after obtaining the result m is given by:

$$\rho_m = \sum_i p(i|m) |\psi_i^m\rangle \langle\psi_i^m| = \sum_i p(i|m) \frac{M_m |\psi_i\rangle \langle\psi_i| M_m^\dagger}{\langle\psi_i|M_m^\dagger M_m|\psi_i\rangle}, \tag{1.14}$$

where $p(i|m)$ is the probability that the state prior to the measurement was $|\psi_i\rangle$ given that the measurement outcome is the m-th one. By using Bayes' rule, $p(i|m) = p_i \frac{p(m|i)}{p(m)}$, and the fact that $p(m) = \sum_i p_i p(m|i)$, we obtain:

$$\rho_m = \sum_i p_i \frac{M_m |\psi_i\rangle \langle\psi_i| M_m^\dagger}{\mathrm{Tr}\left[M_m^\dagger M_m \rho\right]} = \frac{M_m \rho M_m^\dagger}{\mathrm{Tr}\left[M_m^\dagger M_m \rho\right]} \tag{1.15}$$

We can now reformulate the postulates of quantum mechanics within the *density operator formalism*.

Postulate 1.1.5. The set of states of a quantum system is characterised by the set of density operators over the carrier Hilbert space.

Again, if we restrict ourselves to the case of a qubit, we get that the set of all states, as given by all the possible convex mixtures of two-qubit pure states, i.e. all the possible convex combinations of points lying on the two-dimensional unit-sphere, is the unit ball, also known as Bloch sphere.

Postulate 1.1.6. The evolution of a closed quantum system is described by a *unitary transformation*. More precisely, the state $\rho(t)$ of the system at a subsequent time $t > t_0$ is obtained by applying to the state $\rho(t_0)$ of the system at the initial time t_0 a unitary operator $U(t, t_0)$ which depends only on the times t and t_0, i.e.

$$\rho(t) = U(t, t_0)\,\rho(t_0)\,U^{\dagger}(t, t_0)\,. \tag{1.16}$$

However, as soon as an open quantum system is considered, its evolution is in general no longer unitary. The most general dynamical evolution that a quantum system can undergo is described by a so-called completely positive trace preserving (CPTP) map, i.e. any channel Λ

$$\rho \to \Lambda(\rho)\,, \tag{1.17}$$

such that $\mathrm{Tr}\left[\Lambda(\rho)\right] = 1$ and $\Lambda(\rho) \otimes \mathbb{1}_n$ is a density operator for any ρ and any dimension n of the $n \times n$ identity $\mathbb{1}_n$. CPTP maps enjoy a nice characterisation in terms of the so-called Kraus operators $\{V_i\}$ [26]:

$$\Lambda(\rho) = \sum_i V_i \rho V_i^{\dagger}, \tag{1.18}$$

where $\sum_i V_i^{\dagger} V_i = \mathbb{1}$. Eq. (1.18) can be easily written as a classical mixture $\Lambda(\rho) = \sum_i p_i \rho_i$, with probabilities given by $p_i = Tr\left(V_i \rho V_i^{\dagger}\right)$ and states $\rho_i = V_i \rho V_i^{\dagger}/p_i$. Consequently, the general evolved state of an open quantum system is a mixed

state, thus justifying why we are facing the extension of the rules of quantum mechanics from the set of pure states to the set of mixed ones.

Postulate 1.1.7. Quantum measurements are described by a collection $\{M_m\}$ of semi-positive definite operators $M_m \geq 0$ over the carrier Hilbert space satisfying the *completeness relation*,

$$\sum_m M_m^\dagger M_m = \mathbb{1}. \tag{1.19}$$

The index m refers to the corresponding measurement outcome that may occur in the experiment. If, immediately before the measurement, the state of the quantum system is ρ, then the probability that the result m occurs is given by

$$p(m) = \mathrm{Tr}\left[M_m^\dagger M_m \rho\right], \tag{1.20}$$

and the state of the system after the measurement is

$$\frac{M_m \rho M_m^\dagger}{\mathrm{Tr}\left[M_m^\dagger M_m \rho\right]}. \tag{1.21}$$

In this postulate is given a description of the statistics of measurements, indeed is given the probabilities of all possible measurement outcomes. Moreover, the postulate gives a description of the state of the system after the measurement. In some applications, instead of the post-measurement description of the state of the system, is taken, as main item of interest, the probabilities of the respective measurement outcomes. An example is for an experiment where the system is measured only once. In this case there a mathematical tool known as POVM (Positive Operator-Valued Measure) formalism. This formalism is a consequence of the general description of the measurements introduced in the previous postulate.

Postulate 1.1.8. The state space of a quantum system composed of distinguishable particles is given by the set of density operators over the tensor product of the carrier Hilbert spaces corresponding to each subsystem.

Let us consider again a quantum system composed of two distinguishable particles in the overall state ρ_{AB}. A natural question arises: what are the corresponding states of the two subsystems? The latter are described by the so-called reduced density operators, obtained by marginalising each of the two subsystems as follows:

$$\begin{aligned} \rho_A &= \mathrm{Tr}_{\mathcal{H}_B}\left[\rho_{AB}\right] = \sum_{j=0}^{d_B-1} \langle j^B \left|\rho_{AB}\right| j^B \rangle \,, \\ \rho_B &= \mathrm{Tr}_{\mathcal{H}_A}\left[\rho_{AB}\right] = \sum_{i=0}^{d_A-1} \langle i^A \left|\rho_{AB}\right| i^A \rangle \,. \end{aligned} \tag{1.22}$$

Part I

2 — Classical imaging theory

In this chapter we are going to show a brief introduction on the area of image formation, studying several cases based on the diffraction theory. From this we analyze the several criterion which regulate when a direct measurement of the optical intensity provides resolution limited. This help us to build up the starting point to study the optical resolution and to find the tools to beat this limited resolution.

2.1 Diffraction theory

The optical resolution sets the ability of an imaging system to distinguish spatial dimension of an object. The classical resolving power of an optical instrument is well-known from the works by Abbe [10, 11, 9] and Rayleigh [7], indeed, according to these works, the sources can be resolved by direct imaging only if they are separated, at least, by the diffraction-limited size of their point-spread function (PSF).

The PSF can be imaged as the transfer function of the imaging system, hence from [27] the imaging process is naturally described by: $g(\mathbf{r}) = \int S(\mathbf{r}, \mathbf{r}') f(\mathbf{r}')\, d\mathbf{r}'$, where $f(\mathbf{r}')$ and $g(\mathbf{r})$ are respectively the complex amplitude of the input object and the image, while $S(\mathbf{r}, \mathbf{r}')$ is the PSF of the system. Physically, the PSF represents the image at point $\mathbf{r}$ of a source situated at the point $\mathbf{r}'$. In case of space-invariant systems, the PSF depends only on the difference of the variables

$\mathbf{r} - \mathbf{r}'$, in which case the imaging process is given by the convolution integral

$$g(\mathbf{r}) = \int S(\mathbf{r} - \mathbf{r}') f(\mathbf{r}') \, d\mathbf{r}'. \tag{2.1}$$

To understand the mechanism that regulates the image formation and physical resolution limits, it is helpful to start with the easy monochromatic light beam case [28].

When a light beam is partly blocked by an obstacle, some of the light is scattered around the object. At the edge of the shadow of the object on the screen, is imprinted a pattern of light and dark bands. This effect is called diffraction [29]. This phenomenon is the starting point of many effects, for example the recorded tracks of a CD or DVD act as a diffraction grating, generating the rainbow effect pattern on the surface [30].

Consider the general form of the wave equation propagation [5] $\nabla^2 u - \frac{1}{c^2}\frac{\partial^2 u}{\partial t^2} = 0$, where c is the light speed, $u(\mathbf{r}, t)$ is the generic wave amplitude function of a time variable t and spatial variables $\mathbf{r} = (x, y, z)$, with a monochromatic point source C, propagated through an opening in a plane opaque screen, and let P be the point at which the light disturbance is determined. The disturbance at the point P is given taking the Kirchhoff's integral [31] over the surface S formed by the opening and the opaque portion of the screen (see Figure 2.1), joined and closed by the spherical surface centred in P [30]. The Kirchhoff formulation of diffraction for strictly monochromatic scalar wave ($u(\mathbf{r}, t) = \psi(\mathbf{r}) \exp[-ikct]$) with wavenumber k gives

$$\psi(P) = \psi(\mathbf{r}) = -\frac{1}{4\pi} \int_S \left\{ \left(\frac{\partial \psi(\mathbf{r})}{\partial n} \right) \frac{\exp[ik\xi]}{\xi} - \psi(\mathbf{r}) \frac{\partial}{\partial n} \left(\frac{\exp[ik\xi]}{\xi} \right) \right\} dS, \tag{2.2}$$

where ξ is the distance of the element dS from P and $\frac{\partial}{\partial n}$ denotes differentiation along the inward normal to the surface of integration [5].

Supposing that the wave propagates along the z-axis, and the object and image

plane are fixed at $z = 0$ and $z = d$ respectively, the input and output complex amplitude are defined as [30]

$$\begin{aligned} f(\mathbf{r}') &= f(x', y') = \psi(x', y', z')\big|_{z=0} \\ g(\mathbf{r}) &= g(x, y) = \psi(x, y, z)\big|_{z=d}. \end{aligned} \tag{2.3}$$

In literature [32] is well known the solution of Eq. (2.2) in near field and far field regime, respectively the Fresnel diffraction and the Fraunhofer diffraction, which occurs when the amplitude of the slit and the wavenumber varies linearly with the distance from the aperture. For example [6], when a 2 mm size hole is illuminated by light of wavelength $5x10^{-4}$ mm, the Fresnel diffraction is observed for distance less than 2 m, then the Fraunhofer diffraction occurs at greater distances.

For a monochromatic light source with a wavenumber k, the total amplitude at the point $P \equiv (u, v)$ of Fraunhofer diffraction [6] in the image plane, as shown in

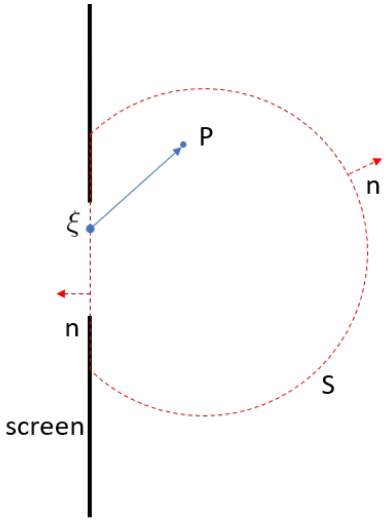

Figure 2.1: Description of the contour of integration and the quantities used to deduce Fresnel-Kirchhoff's diffraction formula. Here ξ is shown as a point on the aperture, which is a subset of the aperture plane.

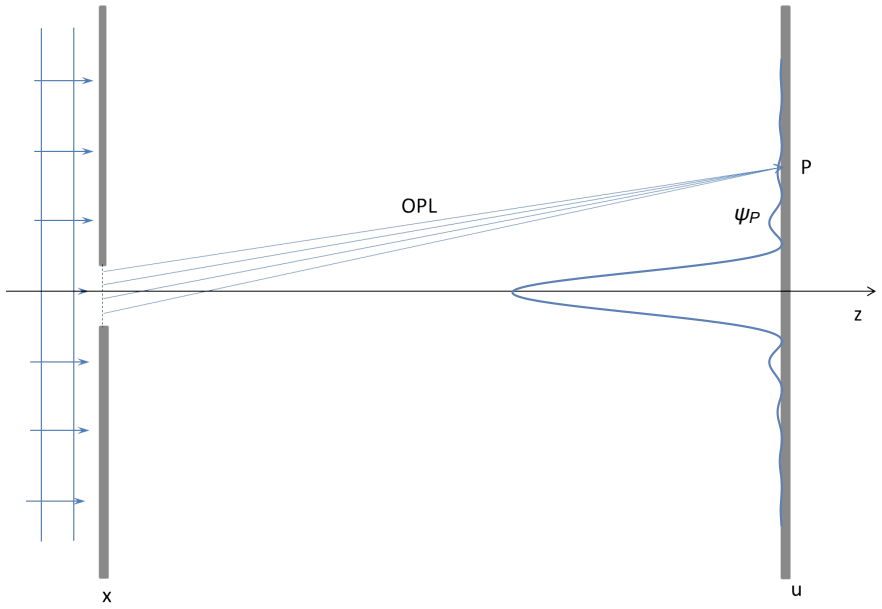

Figure 2.2: Illustration of the Fraunhoffer diffraction given by a single slit, here we can see that the intensity at each point P on the screen is given by the superposition of all point sources into the object plane.

Figure 2.2, is obtained by

$$\psi(u,v) = \exp\left[ik\overline{OPL}\right] \int_S f(x,y) \exp\left[-ik(ux+vy)\right] dx\, dy, \tag{2.4}$$

where $f(x,y)$ is the transmission function of the object, and OPL is the Optical Path Length of the light beam from the source to the screen. However, when we measure the diffraction pattern, we estimate the intensity of total amplitude: $I(u,v) = |\psi(u,v)|^2$, for this reason OPL is irrelevant.

This approach can be generalized if the light beam illuminating the mask does not travel along the z-axis. However, this is not a huge problem, indeed, from the knowledge of the direction cosines of the incident wave-vector (l_0, m_0, n_0) it is

possible to redefine the coordinates on the image plane by [5, 32, 6, 33]

$$u = k_0 (l - l_0), \qquad v = k_0 (m - m_0). \tag{2.5}$$

It is not difficult to see that even if we consider the most general case, the result strongly depends on the geometrical shape of the slit, then we propose some crucial cases.

2.1.1 Single-slit case

Let's assume that the transmission function is defined for the slit of width a along x-direction

$$f(x, y) = \text{rect}(x/a) = \begin{cases} 1 \text{ if } & |x| \leq a/2 \\ 0 \text{ if } & |x| > a/2. \end{cases} \tag{2.6}$$

Furthermore, on the y-axis the slit is infinity.
Then, the amplitude function, using the transmission function Eq. (2.6), separates the double integral Eq. (2.4) in a product of two integral of x and y, then from Eq. (2.4)

$$\begin{aligned} \psi(u, v) &= \int_{-a/2}^{a/2} \exp(-iux)\, dx \int_{-\infty}^{\infty} \exp(-ivy)\, dy \\ &= a\, \text{sinc}\left(\frac{au}{2}\right) \delta(v). \end{aligned} \tag{2.7}$$

After this, it is trivial to show the intensity of the pattern impressed on the screen [33, 6, 5] for $v = 0$

$$I(u, 0) = a^2\, \text{sinc}^2\left(\frac{au}{2}\right). \tag{2.8}$$

As we can see in Figure 2.3, the function Eq. (2.8) has a maximum a for $u = 0$, and is zero for a regular period given by $au/2 = m\pi$, where $m \in \mathbb{Z} \setminus \{0\}$. The other maximum values are given by this proportional law: $(2m + 1)^{-2}$, as given from

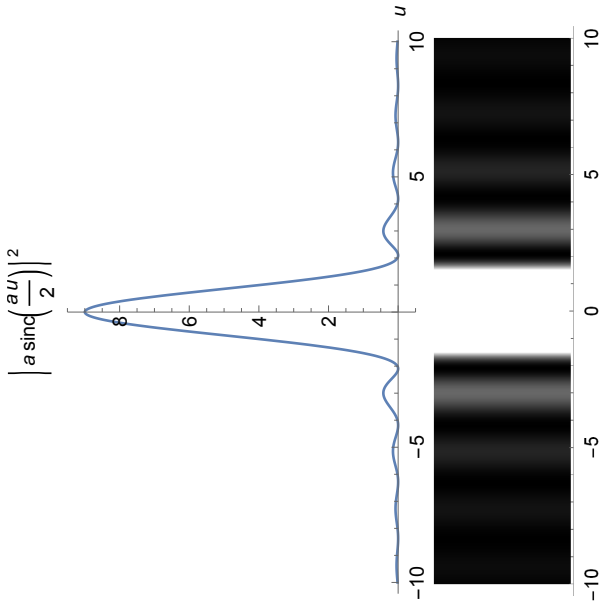

Figure 2.3: Analytic form and pattern given by a single slit.

[6]. Moreover, the intensity is zero for the angles given by $\frac{1}{2}k_0 a \sin(\theta) = m\pi$, where k_0 is the wave number.

The pattern impressed on the screen is characterized by the function Eq. (2.8), and consists of a succession of bright and dark fringes parallel to the line source and the slit.

2.1.2 Double-slit case

An interesting example is given by the double-slit experiment. In this case we consider an optical system composed of two slits with the same aperture a and spacing d, as shown in the Figure 2.4.

Following the same idea used in the single-slit, we define the transmission func-

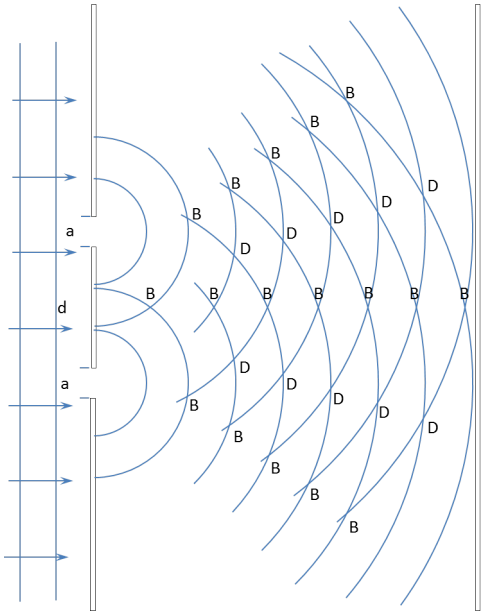

Figure 2.4: Double slits experiment scheme.

tion as

$$f(x,y) = \begin{cases} 1 & \text{if } -\left(\frac{d}{2}+a\right) \leq x \leq \left(\frac{d}{2}-a\right) \\ 1 & \text{if } \left(a-\frac{d}{2}\right) \leq x \leq \left(\frac{d}{2}+a\right) \\ 0 & \text{otherwise.} \end{cases} \tag{2.9}$$

Using the similarity between Eq. (2.9) and Eq. (2.6), even in this case the transmission function separates the integral Eq. (2.4) into a product of functions of x and y, and so

$$\psi(u,v) = 2d\ \mathrm{sinc}\left(\frac{du}{2}\right)\cos(au)\,\delta(v)\,, \tag{2.10}$$

with intensity

$$I(u,0) = 4d^2\ \mathrm{sinc}^2\left(\frac{du}{2}\right)\cos^2(au)\,. \tag{2.11}$$

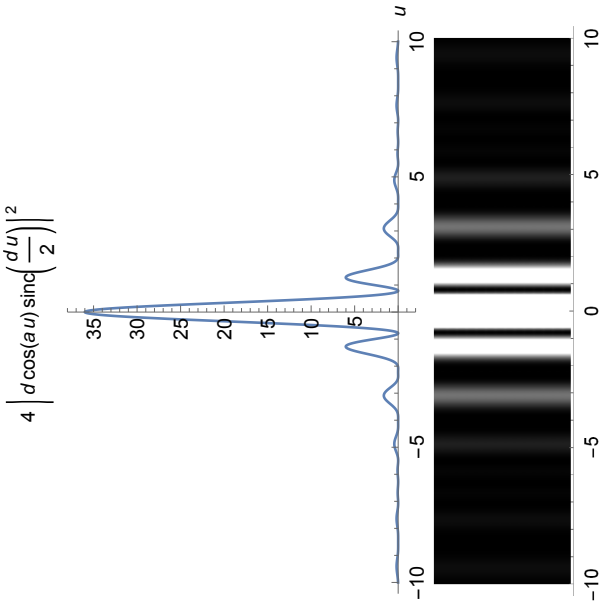

Figure 2.5: Analytic form and pattern given by a double-slits.

The angular spacing of the fringes, θ_f, is given

$$\theta_f \approx \frac{\lambda_0}{d}, \tag{2.12}$$

where λ_0 is the light wavelength , and d is the distance between the two slits.

2.1.3 Rectangular hole

From the analysis of the examples we are able to study the diffraction pattern from a hole. In the case of a rectangular hole we can represent it as two different single slits: two of them on x-axis and the other two on y-axis [5, 32, 6, 33]. Supposing that the origin is at the center of the aperture, the double integral can be factorized and written as

$$\psi(u,v) = \int_{-a/2}^{a/2} \exp(-iux)\ da \int_{-b/2}^{b/2} \exp(-ivy)\ db. \tag{2.13}$$

Thus, the amplitude becomes

$$\psi(u,v) = ab\ \mathrm{sinc}\left(\frac{ua}{2}\right)\ \mathrm{sinc}\left(\frac{vb}{2}\right), \tag{2.14}$$

and then

$$I(u,v) = a^2b^2\ \mathrm{sinc}^2\left(\frac{ua}{2}\right)\ \mathrm{sinc}^2\left(\frac{vb}{2}\right) \tag{2.15}$$

The diffraction pattern is zero at values of ua and vb equal to non-zero multiples of 2π, as we have seen in the single-slit case. Furthermore, the zeros lie on lines parallel to the edge of slit, and are given by

$$ua = m_1 2\pi, \quad \text{and} \quad vb = m_2 2\pi. \tag{2.16}$$

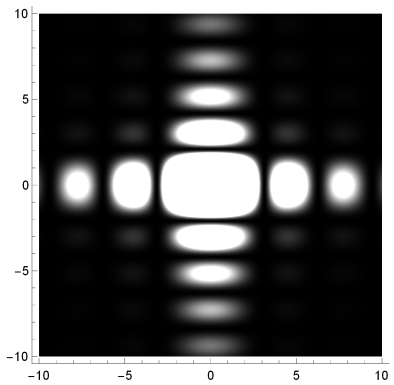

Figure 2.6: The observed diffraction pattern from a rectangular hole.

2.1.4 Circular hole

The last example is given by the circular hole. Furthermore, for this case, unlike previous cases, the limits are not independent. If we consider a hole of radius R it is a good idea to use polar coordinates for points in the aperture plane (ρ, θ) and

in the diffraction plane (ξ, ϕ)

$$\begin{cases} x = \rho \cos\theta \\ y = \rho \sin\theta \end{cases} \qquad \begin{cases} u = \xi \cos\phi \\ v = \xi \sin\phi, \end{cases} \tag{2.17}$$

then Eq. (2.4) becomes

$$\begin{aligned} \psi(u, v) =& \psi(\xi, \theta) = \\ &= \int_0^r \int_0^{2\pi} \exp\left[-i\rho\xi \cos(\theta - \phi)\right] \, d\rho \, d\phi. \end{aligned} \tag{2.18}$$

A simple way to solve this integral is using the Bessel functions [6, 34]

$$\psi(\xi, \theta) = \frac{2\pi R J_1(\xi R)}{\xi} = \pi R^2 \left[\frac{2J_1(\xi R)}{\xi R}\right], \tag{2.19}$$

hence the intensity, as we said before, is

$$I(\xi, \theta) = \pi^2 R^2 \left[\frac{2J_1(\xi R)}{\xi R}\right]^2. \tag{2.20}$$

As it could be expected, the results show that the pattern consists of a bright disc, centred on the geometrical image of the source, surrounded by concentric bright and dark rings Figure 2.7 . The intensity of the bright rings decreases rapidly with the rings radius and usually only the first one or two rings can be seen by eyes. Even in this case, as in the single-slit aperture, the amplitude profile has a maximum for $u = 0$, moreover, the first zero from the maximum defines a circle known as *Airy disk* [35, 36]. The first zero is given at the angle $\xi/k_0 = 0.61\lambda/R$, which corresponds to $x = \xi R = 3.83$.

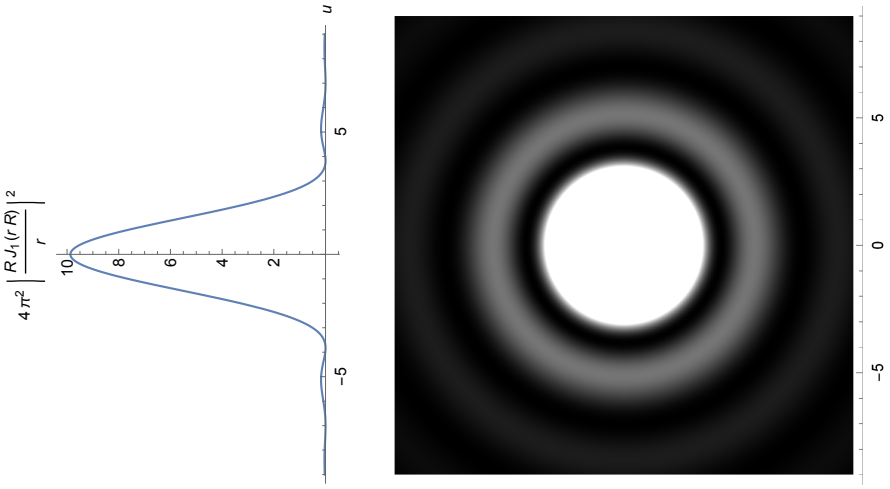

(a) (b)

Figure 2.7: (a) Form of the circular hole intensity function; (b) Form of the circular hole intensity function.

2.1.5 Diffraction grating

The first diffraction grating experiment was proposed by David Rittenhouse in 1785 [37]. It is a useful tool for modeling phenomena, indeed is an optical structure with a periodic structure that splits and diffracts light into several beams travelling in different directions. Then, the characterization of any particular grating is made by its transmission function.

The diffraction grating can be described as a one-dimensional periodic array of similar apertures. By following the approach in Ref. [37, 6, 5, 32], each hole is described by a profile $b(x)$ and they are spaced by d, then the transmission function is

$$f(x) = b(x) \otimes \sum_{n=N/2}^{N/2} \delta(x - nd), \tag{2.21}$$

where N is the total number of the slits, and n is the order of diffraction. In the approximation when $N \to \infty$ (fundamental point for Abbe's theory of imaging

formation [10, 9]) the complex amplitude, given by[5, 32, 6, 33], is

$$\psi(u) = B(u) \sum_{m=-\infty}^{\infty} \delta\left(u - \frac{2\pi m}{d}\right), \tag{2.22}$$

where $B(u)$ is the amplitude of the various orders of diffraction.
In this case, to find each zero points we have to consider the approach when the light beam is not along the z-axis. Indeed, supposing that the incident beam is at the angle θ_0 and the diffracted light at θ to the z-axis, from Eq. (2.5), the coordinate on the diffraction screen is

$$\begin{aligned} u = k_0 (l - l_0) =& k_0 (\sin\theta - \sin\theta_0) = \\ =& \frac{2\pi}{\lambda} (\sin\theta - \sin\theta_0) . \end{aligned} \tag{2.23}$$

Since $\sin\theta$ and $\sin\theta_0$ are between -1 and 1, we have that $\frac{4\pi}{\lambda}$ is the maximum value of u observable. Then, even if Eq. (2.22) is defined for all m, the general diffraction condition will be

$$m\lambda = d (\sin\theta - \sin\theta_0) , \tag{2.24}$$

where, fixed θ

$$(-1 - \sin\theta_0) \frac{d}{\lambda} \leq m \leq (1 - \sin\theta_0) \frac{d}{\lambda}. \tag{2.25}$$

2.2 Classical resolution limit

An optical system is said to be able to resolve two point sources if the corresponding diffraction patterns are sufficiently small or sufficiently separated to be distinguished.

2.2.1 Rayleigh's and Sparrow's criterion

In the previous section we have seen how the diffraction pattern given from a circular hole defines the Airy disk, the best-known resolution criterion formulated by Rayleigh [7, 38, 32, 6, 5, 39] is applied to a case of an incoherent illuminated object based on the definition of the Airy disk.

Initially, we suppose the light from the two object points is assumed to be incoherent. This assumption is warranted when we are working with self-luminous objects, e.g. with stars viewed by a telescope. Then the intensity observed at any point in the image plane is equal to the sum of the intensities due to each point source.

Let us consider an aperture with diameter D, the intensity of this diffraction pattern, expressed as a function of the incident angle θ, is given from [7, 6] by Eq. (2.19)

$$I(\theta) = \left[\frac{2J_1(x)}{x}\right]^2, \qquad x = \frac{k_0 D \sin\theta}{2}, \tag{2.26}$$

where $J_1(x)$ is the Bessel function of the first order. From the Bessel function analysis [34], the first minimum occurs at $x = 3.83$, then the minimum angular separation is

$$\theta_{min}^{Ray.} = 1.22\frac{\lambda}{D}. \tag{2.27}$$

On this result enter only the angular separation of the sources and on the other side we have got only the diameter of the aperture D and the incident wavelength λ.

An alternative is given by the angular resolution criterion given by Sparrow. In this case the minimum distance resolved into an optical system is given by the maximum distance between two point sources where the images no longer have a dip in brightness between the central peaks, but have a constant brightness in the region between the peaks [6, 5, 38, 40, 39]. This limit corresponds to the human eyes resolution limit. Mathematically, it means that the two point sources

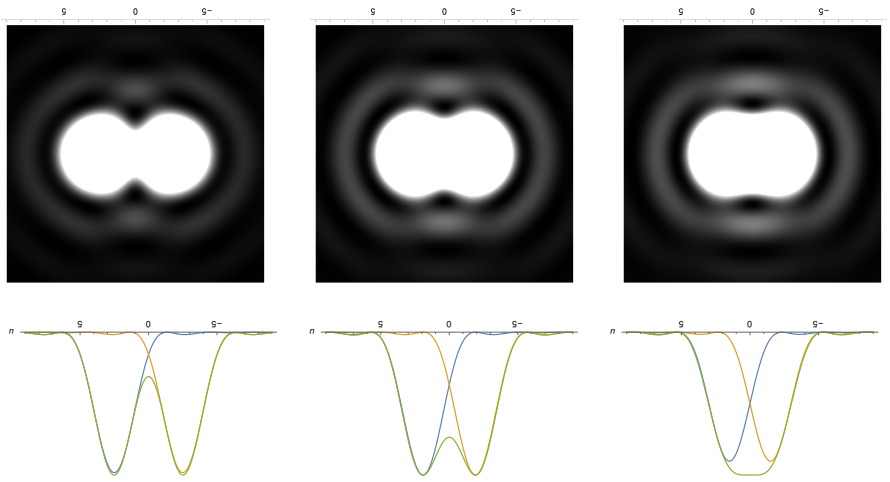

(a) (b) (c)

Figure 2.8: Airy diffraction patterns, and their analytic profiles, generated by from two incoherent light sources (orange and blue lines) and their sum (green line) passing through a circular shape. (a) The two points sources are well separated. (b) The distance between the two points sources correspond to the minimum distance resolvable by the Rayleigh's criterion. (c) The distance between the two points sources correspond to the minimum distance resolvable by the Sparrow's criterion.

intensity function has a minimum on the line joining their centers

$$\left(\frac{\mathrm{d}^2 I}{\mathrm{d}\theta^2}\right)_{\theta=\frac{\theta}{2}} = 0 \tag{2.28}$$

Then, without entering into details about Bessel function [34] this gives

$$\theta_{min}^{Sp.} = 0.95\frac{\lambda}{D}. \tag{2.29}$$

Even in this case, it is interesting to study what happens when are taking in account two coherent light beams. Following the same idea used in Rayleigh's criterion [6, 5, 38, 41, 42, 43, 44], we have to add the phase information to the complex

amplitude functions. Nevertheless, the different definition, between the two cases, gives even a difference in the approach when we consider coherent light. Indeed, we have to add amplitudes before squaring to find the intensity for the two criteria, but in this case the Sparrow criterion gives

$$\theta_{min}^{Sp.\,coh.} = 1.46\frac{\lambda}{D}. \tag{2.30}$$

2.2.2 Abbe's theory of image formation

A satisfactory theory about the formation, and then the resolution limit of an object uniformly and coherently illuminated was formulated by Abbe [10, 11, 9]. The first step to approach Abbe's theory of image formation to consider the assumptions of a periodic object, indeed the Figure 2.10 shows that in this case the object is composed by a diffraction grating in the object plane. A useful setting is considering a light beam which makes a small angle θ to the optical axis see Figure 2.9. This allows the approximation

$$\sin\theta \approx \theta, \quad \tan\theta \approx \theta, \quad \cos\theta \approx 1. \tag{2.31}$$

In the *paraxial approximation* we can consider each order as a plane-wave, and its set can be refracted by a lens converging individually to a set of points S in the focal plane of the lens. The last step is given by the overlapping of each plane-wave of the set in the screen, composing the complicated diffraction pattern called image. This set up is useful even to describe and to improve the optical performance of microscopes [10, 11, 8, 9].

The diffraction grating helps us because, according to Abbe [10], not only every element of the aperture of the object, but even the other elements of the object have to be taken into account, so as to determine the complex perturbation at any points in the image screen. Mathematically, this means that the transmission

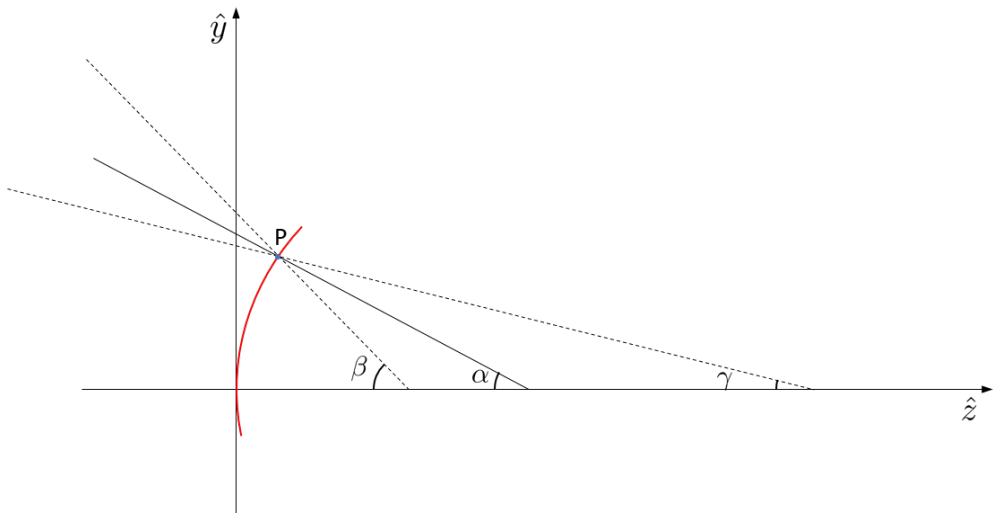

Figure 2.9: Schematisation of the paraxial approximation where θ may be any of α, β or γ.

function involves two integrations that describe two distinct stages. In Abbe's theory of formation, in the first step one considers the diffraction given by the object and after that the effect of the aperture.

Following [6, 5], we consider a light beam directly orthogonal to the grating. The plane-waves are diffracted by the object giving the grating Fraunhofer diffraction pattern Eq. (2.22) in the focal plane of the lens. The orders become like a set of equally spaced sources, such that the image impressed on the screen detector is given by their diffraction.

Supposing to be in the vacuum and the periodic spacing of each grating order is d, the order S_j appears at angle θ_j given, in the small angles approximation, by

$$\theta_j \approx \sin\theta_j = \frac{j\lambda}{U}. \tag{2.32}$$

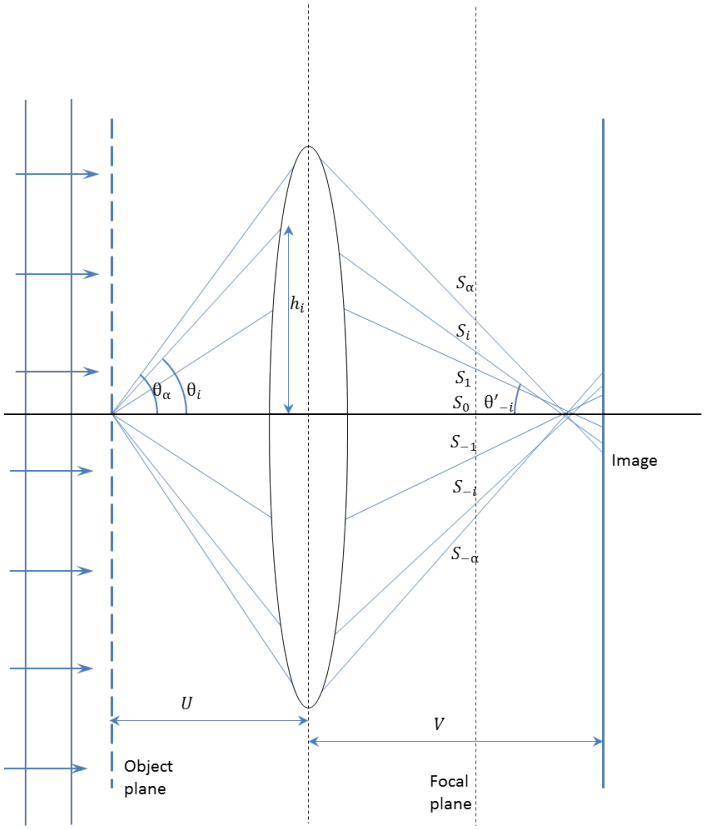

Figure 2.10: Formation of the image of the diffraction grating. We show five orders of diffraction that produce five focal points S in the focal plane.

Using simple geometry, from Figure 2.10, we can see that

$$\begin{aligned} \theta_j \approx \tan\theta_j &= \frac{h}{U}, \\ \theta'_j \approx \tan\theta'_j &= \frac{h}{V}, \end{aligned} \tag{2.33}$$

which is equivalent to

$$\theta'_j \approx \frac{U\theta_j}{V}. \tag{2.34}$$

Taking in account the first orders: S_1 and S_{-1}, the waves converge on the image

at angles of angle of $\pm\theta_1$. Then, using Eq. (2.32), Eq. (2.34) becomes

$$d' \approx d\frac{V}{U}. \tag{2.35}$$

The high order fringes generate harmonics with periodic pattern $m = V/U$ (called magnification), and spacing by d'/j. This means [6], that the finest detail observable in the image is given by the highest order of the diffraction which is transmitted by the lens. From this, the zero order contribution plays a crucial role, because without it the interference pattern of the first orders appear to have the half of the period of the image, because, as we said before, we observe (and measure) the intensity and not the amplitude.

Abbe's limit

Now, the natural question is which resolution is achievable for this imaging system Figure 2.10 [5, 10, 11]. As said before, the resolution that can be obtained with a given imaging system is limited by the highest order of diffraction admitted by the finite aperture of the lens. Supposing that the angular semi-aperture of the lens is given by θ_α, the smallest period attainable is given by

$$d_{min} = \frac{\lambda}{\sin\theta_\alpha}, \tag{2.36}$$

as a direct consequence of the Abbe's theory of imaging formation. It is possible to improve this limit [6, 8, 9] supposing a medium with refractive index μ, such as the wavelength becomes λ/μ. A further improvement is given if we consider the incident light traveling at angle θ_α to the axis, so that the zero order passes through, then using Eq. (2.5) we obtain

$$d_{min} = \frac{\lambda}{2\mu\sin\theta_\alpha} = \frac{\lambda}{2\mathrm{NA}}, \tag{2.37}$$

where NA represents the numerical aperture, that is a dimensionless number that characterizes the range of the angle over which the system can accept or emit light. This limit represent the best resolution achievable with a given lens.

2.2.3 A priori information

The imaging detection can be estimated even with the help of Fourier analysis. Indeed, from the beginning until nowadays it is implemented several systems in order to study and improve the resolution limit achievable. One of the most important system is undoubtedly the *4-f imaging system* [6, 12, 13] Figure 2.11. This system, as it is shown in the scheme Figure 2.11, is realized with two lenses

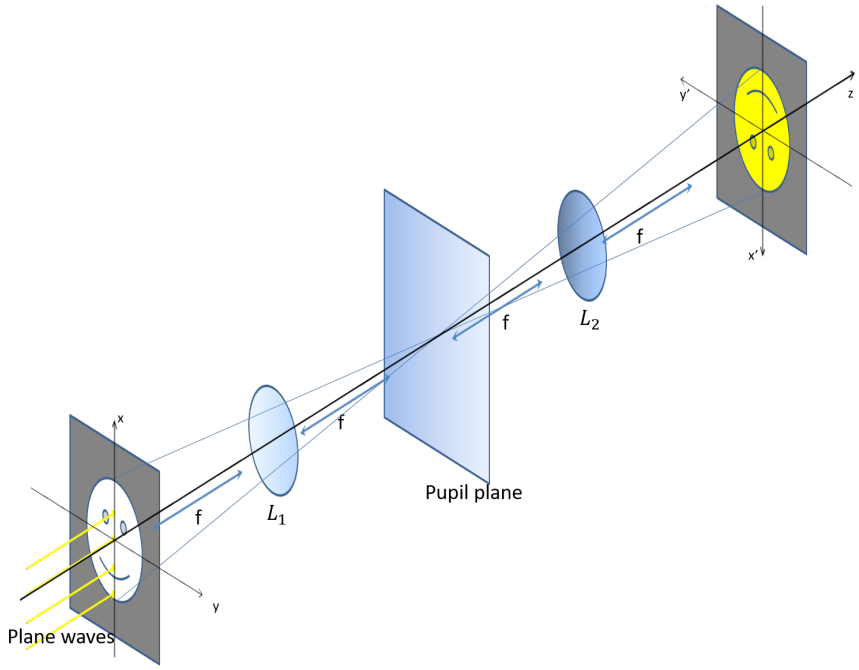

Figure 2.11: The 4-f system executes a Fourier image with the lens L_1 on the pupil plane and the anti-Fourier transform performed by the L_2 lens on the screen.

which perform respectively a Fourier transform (L_1) and anti-Fourier transform (L_2). The hallmark of this system, which determines the name Figure 2.11, is

that all parts of it are placed in the focal plane of the corresponding lens. Thanks to this schematization, the analysis of the propagation through this system becomes simple. Indeed, the Fourier and anti-Fourier transform performed by the two lenses, can be described easily [45, 46, 47] taking into account the impulse-response function of the system $h(r, r')$, which describe the response of the system to a point sources between the input plane and the output plane respectively with coordinates $r' = (x', y')$ $r = (x, y)$, and this function is also called as *point-spread function*. When $h(r, r')$ is a function only of $r - r'$ then we are working with an isoplanatic system or invariant under translation [47]. Then all imaging process can be described by this function and the complex amplitude of the light beam in input $a(r')$ and in output $e(r)$, linked by [47]

$$e(r) = \int_{-\infty}^{\infty} h(r, r')\, a(r')\, dr'. \tag{2.38}$$

In this case the impulse-response function is given by [45]

$$h(s - s')' = \frac{\sin[c(s - s')]}{\pi(s - s')}, \tag{2.39}$$

where s and s' are the dimensionless coordinates, according to [45] and c is the space-bandwidth product, which contains all the information about the system and the input light beam. Translating in 1-dimension words, these quantities become: $c = \frac{\pi dX}{x\lambda f}$, $s = \frac{2x}{X}$ and $s' = \frac{2x'}{X}$.

Following studies of Kobolov [45, 46], we can write the input and output complex amplitude functions as a superposition of prolate spheroidal wave functions [48]

$$\varphi_k(s) = \begin{cases} \frac{1}{\sqrt{\lambda_k}}\psi_k(s) & |s| \leq 1 \\ 0 & |s| > 1 \end{cases} \tag{2.40}$$

where $\varphi_k(s)$ is the orthonormal basis of the eigenfunction of operator corresponding to the product of $h(r, r')$ and is adjoint, λ_k are the corresponding eigenvalues

and $\psi_k(s)$ are the prolate spheroidal wave function. Then the corresponding input and output light beams become

$$\begin{aligned} a(s) &= \sum_{k=0}^{\infty} a_k \varphi_k(s) \quad |s| \leq 1, \\ e(s) &= \sum_{k=0}^{\infty} a_k \psi_k(s) \quad -\infty < s < -\infty, \end{aligned} \tag{2.41}$$

where the coefficients are $a_k = \int_{-\infty}^{\infty} a(s)\varphi_k(s)\, ds$ and $e_k = \int_{-\infty}^{\infty} a(s)\psi_k(s)\, ds$. Then when we study the relation between the input and output signal, we are studying their coefficients related by Eq. (2.38), using Eq. (2.40) and Eq. (2.41)

$$e_k = \sqrt{\lambda_k} a_k. \tag{2.42}$$

In this system, achieve a good resolution means how better is possible to reconstruct the input coefficients a_k from the coefficients detected e_k. In this point of view, the reconstructed coefficient given from this analysis is

$$a_k^r = \frac{1}{\sqrt{\lambda_k}} e_k = a_k. \tag{2.43}$$

This relation means that in an ideal case, where we can detect an image without any kind of fluctuation, we are able to reconstruct perfectly the input signal. In other words we can achieve a super-resolution detection of an image.

Achieve the super-resolution means beat the phenomenon known as Rayleigh's curse. When the sources are incoherent, then direct measurement of the optical intensity provides resolution limited by Rayleigh's curse, i.e., the precision diminishes to zero as the separation is reduced to zero, which occurs when an optical system is regulated by a minimum distance resolvable as in Eq. 2.27.

3 — Quantum imaging theory

In this chapter we are going to show some results presented in [21]. High-resolution imaging is a cornerstone of modern science and engineering, which has enabled revolutionary advances in astronomy, manufacturing, biochemistry, and medical diagnostics. In traditional direct imaging based on classical wave optics, two incoherent point sources with angular separation smaller than the wavelength of the emitted light cannot be resolved due to fundamental diffraction effects [7], a phenomenon recently dubbed "Rayleigh's curse" see Eqs. (2.27) and (2.29) in the section 2.2.1 [18]. Several techniques, including most prominently fluorescence microscopy [49], have been introduced in recent years to overcome this limitation and achieve sub-wavelength imaging [50, 51]. Nevertheless, to determine the ultimate limits of optical resolution one needs to resort to a full quantum mechanical description of the imaging process [52]. These results, which stem from the fundamental quantum Cramér-Rao bound [14, 15] and *de facto* banish Rayleigh's curse [18], have been corroborated by proof-of-principle experiments [53, 54, 55, 56].

The most relevant toolbox to tackle the light sources localization problem is a branch of quantum mechanics: multiparameter quantum metrology. In this area, a starting point has been reported in a series of works [18, 57, 19, 20, 58, 59, 60, 61, 62, 63, 64, 65, 66] initiated by Tsang and his collaborators [18], who shown that the achievable error in angular distance estimation, of two incoherent point light sources in paraxial approximation, does not depend of that separation, by using

of quantum metrology [14, 15, 16, 3], and providing an optimal detection scheme supporting it [53, 20]. In this chapter, we address the problem of estimating both axial and angular separation of two point sources by following a similar approach to [18], which is in turn inspired by Rayleigh's work. We find that Rayleigh's curse does not occur even when the sources have a nonzero axial separation, indeed this measurement is distance-independent. Moreover, both axial and angular distances can be estimated simultaneously meeting the compatibility requirements for saturation of the multiparameter quantum Cramér-Rao bound [67, 68]. These results are obtained analytically and are valid for any point spread function of the imaging system obeying the paraxial wave equation. Then, we specialize to a point-spread function with a Gaussian shape, and derive formulas for the achievable estimation error and its scaling with the parameters of interest as determined by the quantum Fisher information matrix, showing that in the limit of small angular and axial distances all the parameters, including the centroid coordinates, become statistically independent.

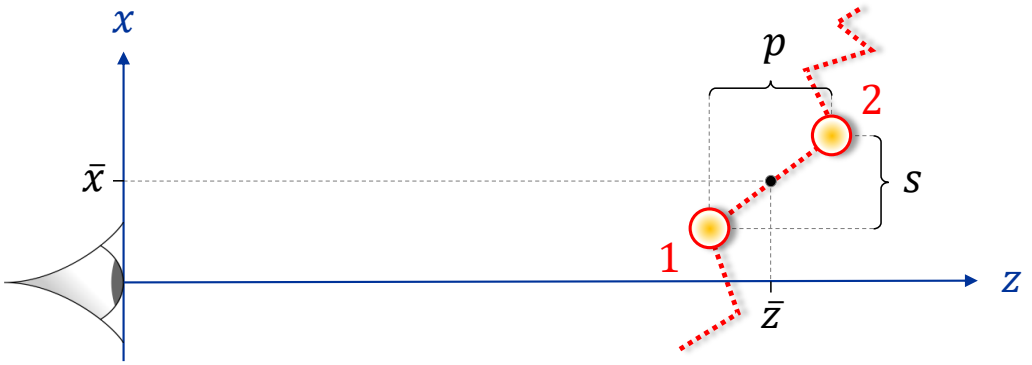

Figure 3.1: Schematic of the two sources. The four parameters to be estimated are: the angular separation s, the axial separation p, the angular centroid coordinate $\bar{x}$, and the axial centroid coordinate $\bar{z}$.

3.1 Sources and imaging model

In the present model we assume that the detectable light on the image plane can be described as an incoherent mixture of two quasimonochromatic scalar paraxial waves, one coming from each source. Considering thermal sources at optical frequencies, we divide the total emission time into short coherence time intervals τ_c, so that within each interval the sources can be assumed weak, i.e., effectively emitting at most one photon. This is a standard approach for modeling incoherent thermal sources [69, 70, 71, 72, 73, 74, 75], and it allows us to describe the quantum state ρ of the optical field on the image plane as a mixture of a zero-photon state ρ_0 and a one-photon state ρ_1 in each time interval (neglecting contributions from higher photon numbers) [19, 20]

$$\rho = (1 - \varepsilon)\rho_0 + \varepsilon\rho_1 + o\left(\varepsilon^2\right), \tag{3.1}$$

where $\varepsilon \ll 1$ is the average number of photons arriving on the image plane. This mean that a detectable signal is obtained by measuring the optical field for a time $t \gg \tau_c$, so that many coherence time intervals are included, resulting in a non-negligible mean photon number. In general that the image-plane field amplitude generated by each source takes the form

$$\Psi_j(x, y) \equiv \psi\left(x - x_j, y, z_j\right) \tag{3.2}$$

where (x, y) are the image-plane coordinates $\left(x_j, z_j\right)$ are the unknown coordinates of the sources $j = 1, 2$, x_j being the coordinate perpendicular to the optical axis, and z_j the axial distance to the image-plane. Assuming that the coordinate $y_j = 0$ is known. The amplitude function $\psi(x, y, z)$ obeys a paraxial wave equation, which in free space it would have the form

$$i\partial_z\psi = G\psi, \tag{3.3}$$

where G is a self-adjoint differential operator featuring only x and y derivatives-for example, in free space one would have $G = \frac{1}{2k}\left(\partial_x{}^2 + \partial_y{}^2\right) + k$, where k is the wave number. Since $[G, \partial_x] = 0$, it follows

$$\Psi_j(x,y) = \exp\left[-iGz_j - x_j\partial_x\right]\psi(x,y,0). \tag{3.4}$$

Indicating with $a(x,y)$ the field annihilation operator at position (x,y) on the image plane, satisfying the bosonic commutation rule $\left[a(x,y), a^\dagger(x',y')\right] = \delta(x - x')\delta(y - y')$. Then the one-photon state ρ_1 for two incoherent point sources as the incoherent mixture become

$$\rho_1 = \frac{1}{2}\left(|\Psi_1\rangle\langle\Psi_1| + |\Psi_2\rangle\langle\Psi_2|\right), \tag{3.5}$$

where the quantum state of the optical field on the image plane corresponding to the emission of one photon by the source j may be expressed as

$$|\Psi_j\rangle = \exp\left[-iGz_j - x_j\partial_x\right]|\psi\rangle, \tag{3.6}$$

$$|\psi\rangle \equiv \int_{\mathbb{R}^2} \psi(x,y,0)\, a^\dagger(x,y)\,|0\rangle\, dxdy, \tag{3.7}$$

where $|0\rangle$ is the vacuum state and we take $\psi(x,y,0)$ real, which results in some simplifications later on. This can be assumed without loss of generality, as the complex phase of $\psi(x,y,0)$ may be compensated by redefinition of $a^\dagger(x,y)$ that is independent of the source parameters [76, 77]. However, $\psi(x,y,z)$ will keep a general phase profile.

3.2 Multiparameter estimation and quantum Cramér-Rao lower bound

Working under the assumption that the photon statistics of our sources is Poissonian, following a similar approach as in [18], we can assume that in a single run of the experiment, which lasts for M coherence time intervals, M copies of the state ρ in Eq. (3.1) are prepared and measured (equivalently, one may consider the input state $\rho^{\otimes M}$). On average, this yields $M\varepsilon$ photons per run. In order to apply the standard tools of estimation theory, we further suppose that $\nu \gg 1$ runs are performed, after which the measurement data are processed to build estimators for the unknown parameters.

In our case, the parameters of interest are the angular and axial relative coordinates and the centroid coordinates of the sources, indicated as s, $\bar{x}$, p, $\bar{z}$ as in Figure 3.1. Thus it is possible to write the state ρ as a function of four parameters $\left\{\lambda_\mu\right\}_{\mu=1,\dots,4}$, where

$$\begin{aligned} \lambda_1 \equiv s = x_2 - x_1, \qquad & \lambda_2 \equiv \bar{x} = \frac{x_1 + x_2}{2}, \\ \lambda_3 \equiv p = z_2 - z_1, \qquad & \lambda_4 \equiv \bar{z} = \frac{z_1 + z_2}{2}. \end{aligned} \tag{3.8}$$

The statistical error (variance) $\Delta\lambda_\mu^2$ of any *unbiased* estimator of the unknown parameter λ_μ is lower bounded via the quantum Cramér-Rao bound (qCRb) [14, 15]

$$\sum_{\mu=1}^{4} \Delta\lambda_\mu^2 \geq \frac{1}{\nu M \varepsilon} \mathrm{Tr}\left[H^{-1}\right], \tag{3.9}$$

where H is the quantum Fisher information matrix (qFim) of the single-photon state ρ_1 (equivalently, this can be seen as the qFim per coherence time interval per photon). The prefactors on the right-hand side of Eq. (3.9) is obtained by exploiting the additivity property $qFim\left(\rho^{\otimes M}\right) = M \times qFim\left(\rho\right)$, and by approximating

that $qFim(\rho) \approx \varepsilon \times qFim(\rho_1)$ at leading order in ε (since the field vacuum state ρ_0 is independent of all source parameters and is always orthogonal to ρ_1). The resulting linear dependence on the total photon number $\nu M\varepsilon$ is characteristic of classical light sources [3, 78].

The qCRb suggests that, the higher the qFim element $H_{\mu\mu}$, the more precisely (i.e., with lower statistical error) one may be able to estimate the parameter λ_μ, by performing a suitable measurement. While for a single parameter the qCRb can always be saturated asymptotically by means of an adaptive procedure [16], this in no longer the case for multiparameter estimation, as the parameters may not always be compatible [68].

The qFim elements are given by

$$H_{\mu\nu} = \mathrm{Re}\left[\mathrm{Tr}\left[\rho_1 L_\mu L_\nu\right]\right], \tag{3.10}$$

where L_μ is the symmetric logarithmic derivative (SLD) for the parameter λ_μ defined implicitly by the equation

$$2\frac{\partial \rho_1}{\partial \lambda_\mu} = L_\mu \rho_1 + \rho_1 L_\mu. \tag{3.11}$$

The following matrix (proportional to the averaged SLD commutators) will also be interest for our discussion

$$\Omega_{\mu\nu} \equiv \mathrm{Im}\left[\mathrm{Tr}\left[\rho_1 L_\mu L_\nu\right]\right]. \tag{3.12}$$

For the problem under investigation, we have derived the general analytical expressions for both matrices H and Ω, and it came from the expansion of ρ_1 in the generally nonorthogonal basis

$$\left\{|\Psi_1\rangle, |\Psi_2\rangle, \partial_{x_1}|\Psi_1\rangle, \partial_{x_2}|\Psi_2\rangle, \partial_{z_1}|\Psi_1\rangle, \partial_{z_2}|\Psi_2\rangle\right\}, \tag{3.13}$$

followed by standard linear algebraic manipulation to find out the elements of the SLDs matrices by using the equivalence in Eq. (3.11) for each μ.

3.2.1 Derivation in a non-orthogonal basis from the expansion of ρ_1

Observing that ρ_1 and all its derivatives are supported in the subspace spanned by the vectors $|\Psi_1\rangle$, $|\Psi_2\rangle$ and their derivatives

$$\begin{aligned} |\Psi_3\rangle &\equiv \partial_{x_1} |\Psi_1\rangle \\ |\Psi_4\rangle &\equiv \partial_{x_2} |\Psi_2\rangle \\ |\Psi_5\rangle &\equiv \partial_{z_1} |\Psi_1\rangle \\ |\Psi_6\rangle &\equiv \partial_{z_2} |\Psi_2\rangle . \end{aligned} \tag{3.14}$$

The set $\left\{|\Psi_j\rangle\right\}_j$ is linearly independent provided that $x_1 \neq x_2$ and $z_1 \neq z_2$, but it is not othonormal in general. Yet, we will use such basis to linearly expand any state or operator and in particular it will be used to expand the SLDs operators in such basis. The method, proposed by [79], depends on the matrix S of scalar products between the basis elements

$$S_{ij} \equiv \langle \Psi_i | \Psi_j \rangle . \tag{3.15}$$

Using the representation Eq. (3.4), the overlap matrix S depends only on the separations $s = x_2 - x_1$, $p = z_2 - z_1$, and not on the centroid coordinates, like

$$\begin{aligned} \delta \equiv \langle \Psi_1 | \Psi_2 \rangle &= \langle \psi | e^{iGz_1 + x_1 \partial_x} e^{-iGz_2 - x_2 \partial_x} | \psi \rangle \\ &= \langle \psi | e^{-iGp - s\partial_x} | \psi \rangle , \end{aligned} \tag{3.16}$$

where it has been considered that ∂_x is anti-Hermitian. Similar simplifications, together with the paraxial wave equation $\partial_{z_1} |\Psi_j\rangle = -iG |\Psi_j\rangle$, allow to write all the

matrix elements of S as

$$S = \begin{pmatrix} 1 & \delta & 0 & -i\langle G\rangle & \partial_{x_2}\delta & \partial_{z2}\delta \\ \delta^* & 1 & \partial_{x_1}\delta^* & \partial_{z_1}\delta^* & 0 & -i\langle G\rangle \\ 0 & \partial_{x_1}\delta & \langle\partial_x\psi|\partial_x\psi\rangle & 0 & \partial_{x_1}\partial_{x_2}\delta & \partial_{x_1}\partial_{z_2}\delta \\ i\langle G\rangle & \partial_{z_1}\delta & 0 & \langle G^2\rangle & \partial_{z_1}\partial_{x_2}\delta & \partial_{z_1}\partial_{z_2}\delta \\ \partial_{x_2}\delta^* & 0 & \partial_{x_1}\partial_{x_2}\delta^* & \partial_{z_1}\partial_{x_2}\delta^* & \langle\partial_x\psi|\partial_x\psi\rangle & 0 \\ \partial_{z_2}\delta^* & i\langle G\rangle & \partial_{x_1}\partial_{z_2}\delta^* & \partial_{z_1}\partial_{z_2}\delta^* & 0 & \langle G^2\rangle \end{pmatrix}, \tag{3.17}$$

where it worth noting that only $\delta = \delta(s, p)$ depends on the source separations, while $\langle\partial_x\psi|\partial_x\psi\rangle$, $\langle G\rangle$ and $\langle G^2\rangle$ are independent of all source parameters. In the Eq. (3.17) we made use of the further simplification $\langle\psi|\partial_x\psi\rangle = 0$, which follows from the assumptions that $\psi(x, y, 0) \in \mathbb{R}$. In the non-orthogonal basis $\left\{|\Psi_j\rangle\right\}_j$, the operator ρ_1 is represented by the matrix

$$R = \begin{pmatrix} 1 & S_{12} & S_{13} & S_{14} & S_{15} & S_{16} \\ S_{21} & 1 & S_{23} & S_{24} & S_{25} & S_{26} \\ 0 & 0 & 0 & 0 & 0 & 0 \\ 0 & 0 & 0 & 0 & 0 & 0 \\ 0 & 0 & 0 & 0 & 0 & 0 \\ 0 & 0 & 0 & 0 & 0 & 0 \end{pmatrix}. \tag{3.18}$$

It is important to emphasize that $\rho_1 = \rho_1^\dagger$ does not imply $R_{ij} = R_{ij}^*$, due to the use of a non-orthogonal basis. We note that the $j - th$ column of R features the coefficients of the expansion of $\rho_1|\Psi_j\rangle$ in the basis $\left\{\Psi_j\right\}$, that is, the first three columns are equivalent to the relations

$$\rho_1|\Psi_1\rangle = \frac{1}{2}\left(|\Psi_1\rangle + S_{21}|\Psi_2\rangle\right), \tag{3.19a}$$

$$\rho_1|\Psi_2\rangle = \frac{1}{2}\left(S_{12}|\Psi_1\rangle + |\Psi_2\rangle\right), \tag{3.19b}$$

$$\rho_1 |\Psi_3\rangle = \frac{1}{2} \left(S_{13} |\Psi_1\rangle + S_{23} |\Psi_2\rangle \right), \tag{3.19c}$$

and similarly for the remaining columns

$$\rho_1 |\Psi_4\rangle = \frac{1}{2} \left(S_{14} |\Psi_1\rangle + S_{24} |\Psi_2\rangle \right), \tag{3.20a}$$

$$\rho_1 |\Psi_5\rangle = \frac{1}{2} \left(S_{15} |\Psi_1\rangle + S_{25} |\Psi_2\rangle \right), \tag{3.20b}$$

$$\rho_1 |\Psi_6\rangle = \frac{1}{2} \left(S_{16} |\Psi_1\rangle + S_{26} |\Psi_2\rangle \right). \tag{3.20c}$$

Let us now find a matrix representation for the derivatives of ρ_1. To do so, we first express the derivatives of our state in terms of the chosen basis

$$2\partial_{x_1}\rho_1 = |\Psi_1\rangle \langle\Psi_3| + |\Psi_3\rangle \langle\Psi_1|, \tag{3.21a}$$

$$2\partial_{z_1}\rho_1 = |\Psi_1\rangle \langle\Psi_4| + |\Psi_4\rangle \langle\Psi_1|, \tag{3.21b}$$

$$2\partial_{x_2}\rho_1 = |\Psi_2\rangle \langle\Psi_3| + |\Psi_3\rangle \langle\Psi_2|, \tag{3.21c}$$

$$2\partial_{z_2}\rho_1 = |\Psi_2\rangle \langle\Psi_4| + |\Psi_4\rangle \langle\Psi_2|. \tag{3.21d}$$

From the above equation it is possible to find the explicit form of each matrix D_μ, the matrix representation of $\partial_\mu \rho_1$

$$2D_{x_1} = \begin{pmatrix} S_{31} & S_{32} & S_{33} & S_{34} & S_{35} & S_{36} \\ 0 & 0 & 0 & 0 & 0 & 0 \\ 1 & S_{12} & S_{13} & S_{14} & S_{15} & S_{16} \\ 0 & 0 & 0 & 0 & 0 & 0 \\ 0 & 0 & 0 & 0 & 0 & 0 \\ 0 & 0 & 0 & 0 & 0 & 0 \end{pmatrix}, \tag{3.22a}$$

$$2D_{z_1} = \begin{pmatrix} S_{41} & S_{42} & S_{43} & S_{44} & S_{45} & S_{46} \\ 0 & 0 & 0 & 0 & 0 & 0 \\ 0 & 0 & 0 & 0 & 0 & 0 \\ 1 & S_{12} & S_{13} & S_{14} & S_{15} & S_{16} \\ 0 & 0 & 0 & 0 & 0 & 0 \\ 0 & 0 & 0 & 0 & 0 & 0 \end{pmatrix}, \tag{3.22b}$$

$$2D_{x_2} = \begin{pmatrix} 0 & 0 & 0 & 0 & 0 & 0 \\ S_{51} & S_{52} & S_{53} & S_{54} & S_{55} & S_{56} \\ 0 & 0 & 0 & 0 & 0 & 0 \\ 0 & 0 & 0 & 0 & 0 & 0 \\ S_{21} & 1 & S_{23} & S_{24} & S_{25} & S_{26} \\ 0 & 0 & 0 & 0 & 0 & 0 \end{pmatrix}, \tag{3.22c}$$

$$2D_{z_2} = \begin{pmatrix} 0 & 0 & 0 & 0 & 0 & 0 \\ S_{61} & S_{62} & S_{63} & S_{64} & S_{65} & S_{66} \\ 0 & 0 & 0 & 0 & 0 & 0 \\ 0 & 0 & 0 & 0 & 0 & 0 \\ 0 & 0 & 0 & 0 & 0 & 0 \\ S_{21} & 1 & S_{23} & S_{24} & S_{25} & S_{26} \end{pmatrix}. \tag{3.22d}$$

3.3 Quantum estimation of angular and axial estimation

3.3.1 Analytical results

The SLD equations Eq. (3.11) are equivalent to the analogous set of matrix equations

$$L_\mu R + R L_\mu = 2 D_\mu, \tag{3.23}$$

and then interpreting the above equations as a linear system for the unknown matrix elements of L_μ. Then the qFim is composed on the diagonal elements

$$H_{ss} = \langle \partial_x \psi | \partial_x \psi \rangle , \tag{3.24a}$$

$$H_{pp} = \langle G^2 \rangle - \langle G \rangle^2 , \tag{3.24b}$$

$$H_{\bar{x}\bar{x}} = 4 \langle \partial_x \psi | \partial_x \psi \rangle + \frac{\left(\partial_s |\delta|^2 \right)^2 - 4 \partial_s \delta \partial_s \delta^*}{1 - |\delta|^2}, \tag{3.24c}$$

$$\begin{aligned} H_{\bar{z}\bar{z}} = \langle G^2 \rangle - \frac{4}{1 - |\delta|^2} \left\{ \langle G \rangle^2 - i \langle G \rangle \left(\delta \partial_p \delta^* - \partial_p \delta \delta^* \right) + \partial_p \delta \partial_p \delta^* \right\} + \\ + \frac{\left(\partial_p |\delta|^2 \right)^2}{1 - |\delta|^2}, \end{aligned} \tag{3.24d}$$

while the off-diagonal elements are all zeros except

$$H_{\bar{x}\bar{z}} = \frac{\left(\partial_s |\delta|^2\right)\left(\partial_p |\delta|^2\right) - 2\left(\partial_p \delta \partial_s \delta^* + \partial_s \delta \partial_p \delta^*\right)}{1 - |\delta|^2} + \\ - \frac{2i \langle G \rangle \left(\delta^* \partial_s \delta - \delta \partial_s \delta^*\right)}{1 - |\delta|^2}, \tag{3.25}$$

At the same time the only nonzero matrix elements of Ω are

$$\Omega_{s\bar{x}} = \frac{\delta^2 \partial_s \delta^{*2} - \delta^{*2} \partial_s \delta^2}{2\left(1 - |\delta|^2\right)}, \tag{3.26a}$$

$$\Omega_{p\bar{z}} = \frac{\partial_p |\delta|^2 \left[\left(\delta \partial_p \delta^* - \delta^* \partial_p \delta\right) + 2i \langle G \rangle |\delta|^2\right]}{2\left(1 - |\delta|^2\right)}, \tag{3.26b}$$

$$\Omega_{s\bar{z}} = \frac{\left(\delta \partial_s \delta^* - \delta^* \partial_s \delta\right) \partial_p |\delta|^2 - 2\left(\partial_p \delta \partial_s \delta^* - \partial_s \delta \partial_p \delta^*\right)}{2\left(1 - |\delta|^2\right)} + \\ + \frac{2i \langle G \rangle \partial_s |\delta|^2}{2\left(1 - |\delta|^2\right)}, \tag{3.26c}$$

$$\Omega_{\bar{x}p} = \frac{2i \langle G \rangle \left(1 - |\delta|^2\right) \partial_s |\delta|^2 - \partial_s |\delta|^2 \left(\delta \partial_p \delta^* - \delta^* \partial_p \delta\right)}{2\left(1 - |\delta|^2\right)} + \\ - \frac{2\left(\partial_p \delta \partial_s \delta^* - \partial_s \delta \partial_p \delta^*\right)}{2\left(1 - |\delta|^2\right)}, \tag{3.26d}$$

where the following notation has been used

$$\delta \equiv \langle \Psi_1 | \Psi_2 \rangle, \qquad \langle O \rangle \equiv \langle \psi | O | \psi \rangle,$$

and we emphasize that $\delta = \delta(s, p)$ is the only quantity depending on the source coordinates. A fundamental result came immediately from Eq. (3.24a) and Eq. (3.24b): for any point spread function that satisfies the paraxial wave equation, H_{ss} and H_{pp} are constant, because the only element that depends on the relative distance between the two sources is δ. This result is a further insight on the problem of subwavelenght imaging, while correctly reproducing what is known for $p = 0$. Moreover, the Rayleigh's curse does not affect the estimation of the angular separation s nor that of the axial separation p. Taking one step further, one can investigate how close it is possible to get to the limits imposed by the qCRb in practical experiments. In quantum estimation theory, multi-parameter problems embody a nontrivial generalization of the single-parameter case [67, 16, 80, 68]: if an estimation scheme is optimized for a particular parameter, it typically results into an increased error in estimating the others. However in the best case scenario, such a trade-off doses not apply, and one can identify an optimal protocol for the estimation of all the parameters simultaneously. This happens is and only if the parameters are *compatible*; i.e., they satisfy the following conditions [68]:

(i) There is a single probe state yielding the maximal qFim element for each of the parameters;

(ii) There is a single measurement which is jointly optimal for extracting information on all the parameters from the output state, ensuring the asymptotic saturability of the qCRb;

(iii) The parameters are statistically independent, meaning that the indeterminacy of one of them does not affect the error on estimating the others.

We recall also that (ii) holds if and only if $\Omega_{\mu\nu} = 0 \,\forall\, \mu \neq \nu$, while (iii) is equivalent to the condition $H_{\mu\nu} = 0 \,\forall\, \mu \neq \nu$. The first condition is not investigated, because this theory is built around a realistic imaging scenario in which the emission properties of the sources are fixed in advance. However, it is worth investigating the

other two conditions, indeed they have a crucial implications for the actual achievability of the statistical errors given by the qCRb. It is important to remark that the conditions (ii) and (iii) are always satisfied for the pair of parameters (s, p), independently of the specific point spread function. Then in the simplified scenario where $(\bar{x}, \bar{z})$ are estimated independently or given in advance, it is thus possible to construct a physical measurement and estimation strategy for s and p saturating Eq. (3.9) asymptotically [67, 68]. On the other hand, it is possible to see that conditions (ii) and (iii) do not hold in general for the full set of the parameters $(s, p, \bar{x}, \bar{z})$. Furthermore, it is possible to appreciate on the example below that there is at least one relevant type of point spread function for which conditions (ii) and (iii) are satisfied for all parameters in the limits $s \to 0$ and $p \to 0$.

3.3.2 Gaussian case

The following example takes in consideration what happens with a Gaussian beams in a free space under the paraxial approximation [81]

$$\psi(x, y, z) = \sqrt{\frac{kz_R}{\pi}} \frac{1}{z + iz_R} e^{-\frac{ik\left(x^2+y^2\right)}{2\left(z+iz_R\right)} - ikz}, \tag{3.27}$$

where z_R is a length parameter characterizing the beam which depend on the waist of the beam, the wave number and the index of refraction. Typically this parameter is assumed of the same order as the wavelength, i.e., $\approx \frac{1}{k}$. Eq. (3.27) can be obtained, e.g., is the fields generated by the two sources are well approximated by

Gaussian beam in the vicinity of the image plane [82]. Then it is obtained

$$\begin{aligned}
\delta &= \frac{2iz_R}{p+2iz_R} e^{-ik\left(p+\frac{s^2}{2p+4iz_R}\right)}, \\
\langle \partial_x\psi|\partial_x\psi\rangle &= \frac{k}{2z_R}, \\
\langle G\rangle &= k - \frac{1}{2z_R}, \\
\langle G^2\rangle &= k^2 - \frac{k}{z_R} + \frac{1}{2{z_R}^2}.
\end{aligned} \tag{3.28}$$

Substituting these values in the nonzero elements of the matrices $H_{\mu\nu}$ Eqs. (3.24) and (3.25) it is obtained for the diagonal elements

$$H_{ss} = \frac{k}{2z_R}, \tag{3.29a}$$

$$H_{\bar{x}\bar{x}} = \frac{2k}{z_R} - \frac{4\xi s^2\left(k^2 - 4{z_R}^2\xi^2 e^{-\xi s^2}\right)}{k\left(ke^{\xi s^2} - 2\xi z_R\right)}, \tag{3.29b}$$

$$H_{pp} = \frac{1}{4{z_R}^2}, \tag{3.29c}$$

$$\begin{aligned}
H_{\bar{z}\bar{z}} =& \frac{1}{{z_R}^2} + \frac{8p^2{z_R}^2\xi^4 e^{-\xi s^2}\left(s^2\xi - 1\right)}{2k^3{z_R}^2\left(ke^{\xi s^2} - 2\xi z_R\right)} + \\
&+ \frac{k^2\xi\left(2\xi\left(p^2s^2\xi + 4{z_R}^2\right) - kz_R\left(s^4\xi^2 + 4\right)\right)}{2k^3{z_R}^2\left(ke^{\xi s^2} - 2\xi z_R\right)},
\end{aligned} \tag{3.29d}$$

and the nonzero off-diagonal elements

$$H_{\bar{x}\bar{z}} = \frac{ps\xi^2 e^{-\xi s^2}\left(e^{\xi s^2}k^2\left(\xi s^2 - 2\right) - 8{z_R}^2\xi^2\left(\xi s^2 - 1\right)\right)}{k^2 z_R\left(ke^{\xi s^2} - 2\xi z_R\right)}. \tag{3.30}$$

While $\Omega_{\mu\nu}$ Eq. (3.26)

$$\Omega_{s\bar{x}} = \frac{4ie^{-\xi s^2} p s^2 z_R \xi^4}{k\left(e^{\xi s^2} - 2z_R\xi\right)}, \tag{3.31a}$$

$$\Omega_{p\bar{x}} = \frac{is\xi^3\left(k^2 s^2 + 2e^{-\xi s^2} z_R\left(k\left(\xi s^2 - 2\right) - 4z_R\xi\left(\xi s^2 - 1\right)\right)\right)}{k^2\left(e^{\xi s^2} - 2z_R\xi\right)}, \tag{3.31b}$$

$$\Omega_{s\bar{z}} = \frac{is\xi^3\left(k^2 s^2 - 4z_R e^{-\xi s^2}\left(\xi s^2 - 1\right)(k - 2z_R\xi)\right)}{k^2\left(e^{\xi s^2} - 2z_R\xi\right)}, \tag{3.31c}$$

$$\Omega_{p\bar{z}} = \frac{ie^{-\xi s^2} p\xi^3\left(\xi s^2 - 1\right)\left(k\left(\xi s^2 - 2\right) - 4z_R\xi\left(\xi s^2 - 1\right)\right)}{k^3\left(e^{\xi s^2} - 2z_R\xi\right)}, \tag{3.31d}$$

where $\xi \equiv \frac{2kz_R}{p^2+4{z_R}^2}$.

These results become particularly interesting in the regime $ks \ll 1$ and $kp \ll 1$, which is precisely the one of relevance to subwavelength imaging. In this limit we have

$$\lim_{(s,p)\to(0,0)} H = \mathrm{diag}\left\{\frac{k}{2z_R}, \frac{2k}{z_R}, \frac{1}{4{z_R}^2}, \frac{1}{{z_R}^2}\right\}, \tag{3.32}$$

$$\lim_{(s,p)\to(0,0)} \Omega = \mathrm{diag}\left\{0, 0, 0, 0\right\}, \tag{3.33}$$

meaning that the (optimal) estimators of the four parameters $s, \bar{x}, p, \bar{z}$ are approximately statistically independent; i.e., they have vanishingly small statistical correlations, when the two sources have infinitesimal angular and axial separations. The behavior of the four diagonal qFim elements $H_{\mu\mu}$ as a function of the separations s and p is illustrated in Figure 3.2; the top panel can be compared directly with Figure 3.2 of [18]. From the plots and from Eq. (3.32) the qFim diagonal elements tend to a nonzero value when $s, p \to 0$. Hence the fundamental lower bound on the total estimation error, $\propto \mathrm{Tr}\left[H^{-1}\right]$, stays finite even when the two sources are infinitesimally close, instead of diverging as in direct imaging as shown in Figure 3.2. Eq. (3.33) further suggests that it is be possible to construct

a single measurement that is approximately optimal for the estimation of all four parameters when $ks \ll 1$ and $kp \ll 1$. It is important to notice that this may require collective measurements over many copies of the state, i.e., many time intervals.

3.4 3-D super localization of 2 point light sources

In this section the work is extended further to calculate QFI and qCRb for the joint estimation of the position of the centroid and the separation of a pair of equally bright sources in the photon-counting (Poisson) limit in all three spatial dimensions. The approach to the 3-D case follows the approach shown in the previous section, considering the image-plane field amplitude generated by each sources

$$\Psi_j(x,y) \equiv \psi\left(x - x_j, y - y_j, z_j\right), \tag{3.34}$$

where (x,y) are the image-plane coordinates, while $\left(x_j, y_j, z_j\right)$ are the unknown coordinates of the sources $j = 1,2$. As shown, the amplitude function $\psi(x,y,z)$ obeys the paraxial wave equation Eq. (3.3). Since $[G, \partial_x] = 0$ and $\left[G, \partial_y\right] = 0$ it follows

$$\Psi_j(x,y) = \exp\left[-iGz_j - x_j\partial_x - y_j\partial_y\right]\psi(x,y,0). \tag{3.35}$$

Indicating with $a(x,y)$ the field annihilation operator at position (x,y) on the image plane, satisfying the bosonic commutation rule $\left[a(x,y), a^\dagger(x',y')\right] = \delta(x - x')\delta(y - y')$. Then the one-photon state ρ_1 for two incoherent point sources as the incoherent mixture becomes

$$\rho_1 = \frac{1}{2}\left(|\Psi_1\rangle\langle\Psi_1| + |\Psi_2\rangle\langle\Psi_2|\right), \tag{3.36}$$

where the quantum state of the optical field on the image plane corresponding to the emission of one photon by the source j may be expressed as

$$|\Psi_j\rangle = \exp\left[-iGz_j - x_j\partial_x - y_j\partial_y\right]|\psi\rangle\,, \tag{3.37}$$

$$|\psi\rangle \equiv \int_{\mathbb{R}^2} \psi\,(x,y,0)\,a^\dagger\,(x,y)\,|0\rangle\;dxdy, \tag{3.38}$$

where $|0\rangle$ is the vacuum state. The parameters of interest are the relative distances s_x, s_y, p and their centroid coordinates of the sources $(\bar{x},\bar{y},\bar{z})$. Thus is possible to rewrite the state ρ as a function of six parameters $\left\{\lambda_\mu\right\}_{\mu=1,\dots,6}$

$$\begin{aligned}
\lambda_1 \equiv s_x = x_2 - x_1, \qquad & \lambda_2 \equiv \bar{x} = \frac{x_1+x_2}{2},\\
\lambda_3 \equiv s_y = y_2 - y_1, \qquad & \lambda_4 \equiv \bar{y} = \frac{y_1+y_2}{2},\\
\lambda_5 \equiv p = z_2 - z_1, \qquad & \lambda_6 \equiv \bar{z} = \frac{z_1+z_2}{2}.
\end{aligned} \tag{3.39}$$

3.4.1 Analytical results

Following the same approach used in the previous section, we can build the scalar products matrix S for this case in the subspace spanned by the vectors $|\Psi_1\rangle$, $|\Psi_2\rangle$ and their derivatives

$$\begin{aligned}
|\Psi_3\rangle \equiv \partial_{x_1}|\Psi_1\rangle \qquad & |\Psi_4\rangle \equiv \partial_{x_2}|\Psi_2\rangle\\
|\Psi_5\rangle \equiv \partial_{y_1}|\Psi_1\rangle \qquad & |\Psi_6\rangle \equiv \partial_{y_2}|\Psi_2\rangle\\
|\Psi_7\rangle \equiv \partial_{z_1}|\Psi_1\rangle \qquad & |\Psi_8\rangle \equiv \partial_{z_2}|\Psi_2\rangle\,.
\end{aligned} \tag{3.40}$$

From Eq. (3.15), S becomes

$$S = \begin{pmatrix} 1 & \delta & 0 & 0 & -i\langle G\rangle & \partial_{x_2}\delta & \partial_{y_2}\delta & \partial_{z2}\delta \\ \delta^* & 1 & \partial_{x_1}\delta^* & \partial_{y_1}\delta^* & \partial_{z_1}\delta^* & 0 & 0 & -i\langle G\rangle \\ 0 & \partial_{x_1}\delta & \langle\partial_x\psi|\partial_x\psi\rangle & 0 & 0 & \partial_{x_1}\partial_{x_2}\delta & \partial_{x_1}\partial_{y_2}\delta & \partial_{x_1}\partial_{z_2}\delta \\ 0 & \partial_{y_1}\delta & 0 & \langle\partial_y\psi|\partial_y\psi\rangle & 0 & \partial_{y_1}\partial_{x_2}\delta & \partial_{y_1}\partial_{y_2}\delta & \partial_{y_1}\partial_{z_2}\delta \\ i\langle G\rangle & \partial_{z_1}\delta & 0 & 0 & \langle G^2\rangle & \partial_{z_1}\partial_{x_2}\delta & \partial_{z_1}\partial_{y_2}\delta & \partial_{z_1}\partial_{z_2}\delta \\ \partial_{x_2}\delta^* & 0 & \partial_{x_1}\partial_{x_2}\delta^* & \partial_{y_1}\partial_{x_2}\delta^* & \partial_{z_1}\partial_{x_2}\delta^* & \langle\partial_x\psi|\partial_x\psi\rangle & 0 & 0 \\ \partial_{y_2}\delta^* & 0 & \partial_{x_1}\partial_{y_2}\delta^* & \partial_{y_1}\partial_{y_2}\delta^* & \partial_{z_1}\partial_{y_2}\delta^* & 0 & \langle\partial_y\psi|\partial_y\psi\rangle & 0 \\ \partial_{z_2}\delta^* & i\langle G\rangle & \partial_{x_1}\partial_{z_2}\delta^* & \partial_{y_1}\partial_{z_2}\delta^* & \partial_{z_1}\partial_{z_2}\delta^* & 0 & 0 & \langle G^2\rangle \end{pmatrix}, \tag{3.41}$$

where $\delta \equiv \delta\left(s_x, s_y, p\right)$ depends on the source separations s_x, s_y, p, while $\langle\partial_x\psi|\partial_x\psi\rangle$, $\langle\partial_y\psi|\partial_y\psi\rangle$, $\langle G\rangle$ and $\langle G^2\rangle$ are independent of all sources parameters.
In the non-orthogonal basis $\left\{|\Psi_j\rangle\right\}_j$, the operator ρ_1 is represented by the matrix

$$R = \begin{pmatrix} 1 & S_{12} & S_{13} & S_{14} & S_{15} & S_{16} & S_{17} & S_{18} \\ S_{21} & 1 & S_{23} & S_{24} & S_{25} & S_{26} & S_{27} & S_{28} \\ 0 & 0 & 0 & 0 & 0 & 0 & 0 & 0 \\ 0 & 0 & 0 & 0 & 0 & 0 & 0 & 0 \\ 0 & 0 & 0 & 0 & 0 & 0 & 0 & 0 \\ 0 & 0 & 0 & 0 & 0 & 0 & 0 & 0 \\ 0 & 0 & 0 & 0 & 0 & 0 & 0 & 0 \\ 0 & 0 & 0 & 0 & 0 & 0 & 0 & 0 \end{pmatrix}. \tag{3.42}$$

From this it is possible to build the matrix representation for the derivatives of ρ_1. Then using Eq. (3.23), it follows that the qFim is composed on the diagonal elements

$$H_{s_x s_x} = \langle\partial_x\psi|\partial_x\psi\rangle\,, \tag{3.43a}$$

$$H_{s_y s_y} = \langle\partial_y\psi|\partial_y\psi\rangle\,, \tag{3.43b}$$

$$H_{pp} = \langle G^2\rangle - \langle G\rangle^2\,, \tag{3.43c}$$

$$H_{\bar{x}\bar{x}} = 4\langle \partial_x\psi|\partial_x\psi\rangle + \frac{\left(\partial_{s_x}|\delta|^2\right)^2 - 4\partial_{s_x}\delta\partial_{s_x}\delta^*}{1-|\delta|^2}, \tag{3.43d}$$

$$H_{\bar{y}\bar{y}} = 4\langle \partial_y\psi|\partial_y\psi\rangle + \frac{\left(\partial_{s_y}|\delta|^2\right)^2 - 4\partial_{s_y}\delta\partial_{s_y}\delta^*}{1-|\delta|^2}, \tag{3.43e}$$

$$\begin{aligned} H_{\bar{z}\bar{z}} = \langle G^2\rangle - \frac{4}{1-|\delta|^2}\left\{\langle G\rangle^2 - i\langle G\rangle\left(\delta\partial_p\delta^* - \partial_p\delta\delta^*\right) + \partial_p\delta\partial_p\delta^*\right\} + \\ + \frac{\left(\partial_p|\delta|^2\right)^2}{1-|\delta|^2}, \end{aligned} \tag{3.43f}$$

while the off-diagonal elements are all zeros except

$$H_{\bar{x}\bar{y}} = \frac{\left(\partial_{s_x}|\delta|^2\right)\left(\partial_{s_y}|\delta|^2\right) - 2\left(\partial_{s_y}\delta\partial_{s_x}\delta^* + \partial_{s_x}\delta\partial_{s_y}\delta^*\right)}{1-|\delta|^2}, \tag{3.44a}$$

$$\begin{aligned} H_{\bar{x}\bar{z}} = &\frac{\left(\partial_{s_x}|\delta|^2\right)\left(\partial_p|\delta|^2\right) - 2\left(\partial_p\delta\partial_{s_x}\delta^* + \partial_{s_x}\delta\partial_p\delta^*\right)}{1-|\delta|^2} + \\ &- \frac{2i\langle G\rangle\left(\delta^*\partial_{s_x}\delta - \delta\partial_{s_x}\delta^*\right)}{1-|\delta|^2}, \end{aligned} \tag{3.44b}$$

$$\begin{aligned} H_{\bar{y}\bar{z}} = &\frac{\left(\partial_{s_y}|\delta|^2\right)\left(\partial_p|\delta|^2\right) - 2\left(\partial_p\delta\partial_{s_y}\delta^* + \partial_{s_y}\delta\partial_p\delta^*\right)}{1-|\delta|^2} + \\ &- \frac{2i\langle G\rangle\left(\delta^*\partial_{s_y}\delta - \delta\partial_{s_y}\delta^*\right)}{1-|\delta|^2}. \end{aligned} \tag{3.44c}$$

At the same time the nonzero elements of Ω are

$$\Omega_{s_x\bar{x}} = \frac{\delta^2\partial_{s_x}\delta^{*2} - \delta^{*2}\partial_{s_x}\delta^2}{2\left(1-|\delta|^2\right)}, \tag{3.45a}$$

$$\Omega_{s_x\bar{y}} = \frac{\left(\delta\partial_{s_x}\delta^* - \delta^*\partial_{s_x}\delta\right)\partial_{s_y}|\delta|^2 - 2\left(\partial_{s_y}\delta\partial_{s_x}\delta^* - \partial_{s_x}\delta\partial_{s_y}\delta^*\right)}{2\left(1-|\delta|^2\right)}, \tag{3.45b}$$

$$\begin{aligned}\Omega_{s_x\bar{z}} =& \frac{\left(\delta\partial_{s_x}\delta^* - \delta^*\partial_{s_x}\delta\right)\partial_p|\delta|^2 - 2\left(\partial_p\delta\partial_{s_x}\delta^* - \partial_{s_x}\delta\partial_p\delta^*\right)}{2\left(1-|\delta|^2\right)} + \\ &+ \frac{2i\langle G\rangle\,\partial_{s_x}|\delta|^2}{2\left(1-|\delta|^2\right)},\end{aligned} \tag{3.45c}$$

$$\Omega_{\bar{x}s_y} = \frac{\partial_{s_x}|\delta|^2\left(\delta^*\partial_{s_y}\delta - \delta\partial_{s_y}\delta^*\right) - 2\left(\partial_{s_y}\delta\partial_{s_x}\delta^* - \partial_{s_x}\delta\partial_{s_y}\delta^*\right)}{2\left(1-|\delta|^2\right)}, \tag{3.45d}$$

$$\begin{aligned}\Omega_{\bar{x}p} =& \frac{2i\langle G\rangle\left(1-|\delta|^2\right)\partial_{s_x}|\delta|^2 - \partial_{s_x}|\delta|^2\left(\delta\partial_p\delta^* - \delta^*\partial_p\delta\right)}{2\left(1-|\delta|^2\right)} + \\ &- \frac{2\left(\partial_p\delta\partial_{s_x}\delta^* - \partial_{s_x}\delta\partial_p\delta^*\right)}{2\left(1-|\delta|^2\right)},\end{aligned} \tag{3.45e}$$

$$\Omega_{s_y\bar{y}} = \frac{\delta^2\partial_{s_y}\delta^{*2} - \delta^{*2}\partial_{s_y}\delta^2}{2\left(1-|\delta|^2\right)}, \tag{3.45f}$$

$$\Omega_{s_y\bar{z}} = \frac{\left(\delta\partial_{s_y}\delta^* - \delta^*\partial_{s_y}\delta\right)\partial_p|\delta|^2 - 2\left(\partial_p\delta\partial_{s_y}\delta^* - \partial_{s_y}\delta\partial_p\delta^*\right)}{2\left(1-|\delta|^2\right)} + \\ + \frac{2i\langle G\rangle\,\partial_{s_y}|\delta|^2}{2\left(1-|\delta|^2\right)}, \tag{3.45g}$$

$$\Omega_{\bar{y}p} = \frac{2i\langle G\rangle\left(1-|\delta|^2\right)\partial_{s_y}|\delta|^2 - \partial_{s_y}|\delta|^2\left(\delta\partial_p\delta^* - \delta^*\partial_p\delta\right)}{2\left(1-|\delta|^2\right)} + \\ - \frac{2\left(\partial_p\delta\partial_{s_y}\delta^* - \partial_{s_y}\delta\partial_p\delta^*\right)}{2\left(1-|\delta|^2\right)}, \tag{3.45h}$$

$$\Omega_{p\bar{z}} = \frac{\partial_p|\delta|^2\left[\left(\delta\partial_p\delta^* - \delta^*\partial_p\delta\right) + 2i\langle G\rangle|\delta|^2\right]}{2\left(1-|\delta|^2\right)}, \tag{3.45i}$$

where

$$\delta \equiv \langle\Psi_1|\Psi_2\rangle\,, \qquad \langle O\rangle \equiv \langle\psi|O|\psi\rangle\,.$$

As in the previous section, even in this case from Eqs. (3.43a), (3.43b) and (3.43c), for any light beam that satisfies the paraxial wave equation, the qFim elements corresponding to the relative distances between the two point light sources are constant, the Rayleigh's curse does not affect the estimation of any separations.

3.4.2 Gaussian case

Even in this case, it has been taken in consideration a Gaussian beam in a free space Eq. (3.27), then the elements of the matrix S Eq. (3.41) became

$$\begin{aligned}
&\delta = \frac{2iz_R}{p+2iz_R} e^{-\frac{ik\left(2p^2+{s_x}^2+{s_y}^2+4ipz_R\right)}{2(p+2iz_R)}}, \\
&\langle \partial_x\psi|\partial_x\psi\rangle = \frac{k}{2z_R}, \qquad \langle \partial_y\psi|\partial_y\psi\rangle = \frac{k}{2z_R}, \\
&\langle G\rangle = k - \frac{1}{2z_R}, \qquad \langle G^2\rangle = k^2 + \frac{1}{2{z_R}^2} - \frac{k}{z_R}.
\end{aligned} \tag{3.46}$$

Substituting these values in the nonzero elements of the matrices $H_{\mu\nu}$ Eqs. 3.43, 3.44 and $\Omega_{\mu\nu}$ Eq. 3.45, it is obtained

$$H_{s_x s_x} = \frac{k}{2z_R}, \tag{3.47a}$$

$$H_{\bar{x}\bar{x}} = \frac{2k}{z_R} - \frac{4\xi^2 {s_x}^2\left(k^2 - 4\xi^2 {z_R}^2 e^{-\xi\left({s_x}^2+{s_y}^2\right)}\right)}{k\left(ke^{\xi\left({s_x}^2+{s_y}^2\right)} - 2\xi z_R\right)}, \tag{3.47b}$$

$$H_{s_y s_y} = \frac{k}{2z_R}, \tag{3.47c}$$

$$H_{\bar{y}\bar{y}} = \frac{2k}{z_R} - \frac{4\xi^2 {s_y}^2\left(k^2 - 4\xi^2 {z_R}^2 e^{-\xi\left({s_x}^2+{s_y}^2\right)}\right)}{k\left(ke^{\xi\left({s_x}^2+{s_y}^2\right)} - 2\xi z_R\right)}, \tag{3.47d}$$

$$H_{pp} = \frac{1}{4{z_R}^2}, \tag{3.47e}$$

$$H_{\bar{z}\bar{z}} = \frac{1}{{z_R}^2} - \frac{4\xi^2 e^{-\xi\left({s_x}^2+{s_y}^2\right)}\left(\xi\left({s_x}^2+{s_y}^2\right)-1\right)^2(k-2z_R\xi)}{k^3} + \\ - \frac{\xi\left(k\left(\xi\left({s_x}^2+{s_y}^2\right)-2\right)-4z_R\xi\left(\xi\left({s_x}^2+{s_y}^2\right)-1\right)\right)^2}{2k^2 z_R\left(ke^{\xi\left({s_x}^2+{s_y}^2\right)}-2z_R\xi\right)}, \tag{3.47f}$$

while the off-diagonal elements are

$$H_{\bar{x}\bar{y}} = -\frac{4\xi^2 s_x s_y\left(k^2-4\xi^2{z_R}^2 e^{-\xi\left({s_x}^2+{s_y}^2\right)}\right)}{k\left(ke^{\xi\left({s_x}^2+{s_y}^2\right)}-2\xi z_R\right)} \tag{3.48a}$$

$$H_{\bar{x}\bar{z}} = \frac{\xi^2 s_x p e^{-\xi\left({s_x}^2+{s_y}^2\right)}}{k^2 z_R\left(ke^{\xi\left({s_x}^2+{s_y}^2\right)}-2\xi z_R\right)} \\ \left(k^2 e^{\xi\left({s_x}^2+{s_y}^2\right)}\left(\xi\left({s_x}^2+{s_y}^2\right)-2\right)-8{z_R}^2\xi^2\left(\xi\left({s_x}^2+{s_y}^2\right)-1\right)\right), \tag{3.48b}$$

$$H_{\bar{y}\bar{z}} = \frac{\xi^2 s_y p e^{-\xi\left({s_x}^2+{s_y}^2\right)}}{k^2 z_R\left(ke^{\xi\left({s_x}^2+{s_y}^2\right)}-2\xi z_R\right)} \\ \left(k^2 e^{\xi\left({s_x}^2+{s_y}^2\right)}\left(\xi\left({s_x}^2+{s_y}^2\right)-2\right)-8{z_R}^2\xi^2\left(\xi\left({s_x}^2+{s_y}^2\right)-1\right)\right). \tag{3.48c}$$

At the same time the nonzero elements of Ω from Eq. 3.45 are

$$\Omega_{s_x\bar{x}} = \frac{4ie^{-\xi\left({s_x}^2+{s_y}^2\right)}p z_R\xi^4{s_x}^2}{k\left(ke^{\xi\left({s_x}^2+{s_y}^2\right)}-2z_R\xi\right)} \tag{3.49a}$$

$$\Omega_{s_x\bar{y}} = \frac{4ie^{-\xi\left({s_x}^2+{s_y}^2\right)}p z_R\xi^4 s_x s_y}{k\left(ke^{\xi\left({s_x}^2+{s_y}^2\right)}-2z_R\xi\right)} \tag{3.49b}$$

$$\Omega_{s_x\bar{z}} = \frac{ie^{-\xi\left({s_x}^2+{s_y}^2\right)}ks_x\xi^3\left(2p^2\xi+\left({s_x}^2+{s_y}^2\right)\left(e^{\xi\left({s_x}^2+{s_y}^2\right)}k^2-2p^2\xi^2\right)\right)}{k^2\left(ke^{\xi\left({s_x}^2+{s_y}^2\right)}-2z_R\xi\right)} \tag{3.49c}$$

$$\Omega_{s_y\bar{x}} = \frac{4ie^{-\xi\left({s_x}^2+{s_y}^2\right)}pz_R\xi^4 s_x s_y}{k\left(ke^{\xi\left({s_x}^2+{s_y}^2\right)}-2z_R\xi\right)} \tag{3.49d}$$

$$\begin{aligned}\Omega_{p\bar{x}} =& \frac{ie^{-\xi\left({s_x}^2+{s_y}^2\right)}s_x\xi^3}{k^2\left(ke^{\xi\left({s_x}^2+{s_y}^2\right)}-2z_R\xi\right)} \\ & \left(4z_R\left(2z_R\xi-k\right)+\left({s_x}^2+{s_y}^2\right)\left(k^2e^{\xi\left({s_x}^2+{s_y}^2\right)}+2z_R\xi\left(k-4z_R\xi\right)\right)\right)\end{aligned} \tag{3.49e}$$

$$\Omega_{s_y\bar{y}} = \frac{4ie^{-\xi\left({s_y}^2+{s_y}^2\right)}pz_R\xi^4 {s_x}^2}{k\left(ke^{\xi\left({s_x}^2+{s_y}^2\right)}-2z_R\xi\right)} \tag{3.49f}$$

$$\Omega_{s_y\bar{z}} = \frac{ie^{-\xi\left({s_x}^2+{s_y}^2\right)}ks_y\xi^3\left(2p^2\xi+\left({s_x}^2+{s_y}^2\right)\left(e^{\xi\left({s_x}^2+{s_y}^2\right)}k^2-2p^2\xi^2\right)\right)}{k^2\left(ke^{\xi\left({s_x}^2+{s_y}^2\right)}-2z_R\xi\right)} \tag{3.49g}$$

$$\begin{aligned}\Omega_{p\bar{y}} =& \frac{ie^{-\xi\left({s_x}^2+{s_y}^2\right)}s_y\xi^3}{k^2\left(ke^{\xi\left({s_x}^2+{s_y}^2\right)}-2z_R\xi\right)} \\ & \left(4z_R\left(2z_R\xi-k\right)+\left({s_x}^2+{s_y}^2\right)\left(k^2e^{\xi\left({s_x}^2+{s_y}^2\right)}+2z_R\xi\left(k-4z_R\xi\right)\right)\right)\end{aligned} \tag{3.49h}$$

$$\begin{aligned}\Omega_{p\bar{z}} =& \frac{ie^{-\xi\left({s_x}^2+{s_y}^2\right)}p\xi^3\left(\xi\left({s_x}^2+{s_y}^2\right)-1\right)}{k^3\left(ke^{\xi\left({s_x}^2+{s_y}^2\right)}-2z_R\xi\right)} \\ & \left(k\left(\xi\left({s_x}^2+{s_y}^2\right)-2\right)-4z_R\xi\left(\xi\left({s_x}^2+{s_y}^2\right)-1\right)\right)\end{aligned} \tag{3.49i}$$

where $\xi = \frac{2kz_R}{p^2+4{z_R}^2}$. These results become particularly interesting in the regime

$ks_x \ll 1$, $ks_y \ll 1$ and $kp \ll 1$, which is precisely the one of relevance to sub-wavelength imaging. In this limit we have

$$\lim_{(s_x,s_y,p)\to(0,0,0)} H = \mathrm{diag}\left\{\frac{k}{2z_R}, \frac{2k}{z_R}, \frac{k}{2z_R}, \frac{2k}{z_R}, \frac{1}{4{z_R}^2}, \frac{1}{{z_R}^2}\right\}, \tag{3.50}$$

$$\lim_{(s_x,s_y,p)\to(0,0,0)} \Omega = \mathrm{diag}\left\{0,0,0,0,0,0\right\}, \tag{3.51}$$

where we find that even in the full 3-D case the estimators of the six parameters are approximately statistically independent. This means that the optimal estimators of the whole six parameters $s_x, \bar{x}, s_y, \bar{y}, p, \bar{z}$ are approximately statistically independent.

3.5 Spatial-mode demultiplexing (SPADE)

A method that could be taken in consideration to estimate the separation is based on a discrimination in terms of the Hermite-Gaussian spatial modes $\{|\Phi_{m,n}\rangle\}_{m,n=0,1,\ldots}$ [18]. To approach with this method we assume that the basis of the modes can be factorized

$$|\Phi_{m,n}\rangle = |\phi_m\rangle \otimes |\phi_n\rangle\,, \tag{3.52}$$

where

$$\begin{aligned} |\phi_m\rangle &= \int_{-\infty}^{\infty} \phi_m(x,Z)\,|x\rangle\; dx, \qquad m = 0,1,\ldots, \\ |\phi_n\rangle &= \int_{-\infty}^{\infty} \phi_n(y,Z)\,|y\rangle\; dy, \qquad n = 0,1,\ldots, \end{aligned} \tag{3.53}$$

and

$$\phi_m(x,Z) = \left(\frac{2}{\pi}\right)^{\frac{1}{4}} \sqrt{\frac{k}{2^{m+1} f! z_R}} \sqrt{\frac{i z_R}{Z + i z_R}} \left(\frac{Z - i z_R}{Z + i z_R}\right)^{\frac{m}{2}} \mathcal{H}_m\left(\sqrt{\frac{k z_R}{Z^2 + {z_R}^2}} x\right) e^{-ik\frac{x^2}{2(Z+iz_R)}}, \tag{3.54}$$

where $\mathcal{H}_m$ is the Hermite polynomial and Z is the axial distance of the filter from the screen [81]. This measurement, introduced by [18], has been shown to achieve near-optimal precision in the small angular separation regime. The basic idea is to measure the intensity of incoming light in a basis of normalized spatial modes, in this case the Hermite-Gaussian modes Eq. (3.52) and this is why this measurement take the name SPADE, from SPAtial-mode DEmultiplexing. Conditioned on detecting the incoming photons, the probability to detect the photon in the specific mode of Hermite-Gaussian basis is

$$P_{1_{m,n}}\left(s_x, s_y, p, \bar{x}, \bar{y}, \bar{z}, z_m\right) = \frac{1}{2}\left(\left|\langle \Phi_{m,n} | \psi_1 \rangle\right|^2 + \left|\langle \Phi_{m,n} | \psi_2 \rangle\right|^2\right), \tag{3.55}$$

where z_m is the distance to set filter for the measures, $\left|\langle \Phi_{m,n} | \psi_1 \rangle\right|^2$ and $\left|\langle \Phi_{m,n} | \psi_2 \rangle\right|^2$ are the probabilities to get one photon in the $m-th$ and $n-th$ modes from the

source 1 and 2, respectively

$$
\begin{aligned}
P_{1m,n}\left(s_x, s_y, p, \bar{x}, \bar{y}, \bar{z}, z_m\right) = \frac{2^{1-m-n} {z_R}^2}{\Gamma(1+m)\,\Gamma(1+n)} \Bigg\{ \Bigg[& e^{-\frac{2kz_R\left((s_x+2\bar{x})^2+(s_y+2\bar{y})^2\right)}{(p+2\bar{z}-2z_m)^2+16{z_R}^2}} \\
& \left(\frac{(p+2\bar{z}-2z_m)^2}{(p+2\bar{z}-2z_m)^2+16{z_R}^2}\right)^{\frac{m+n}{2}} \frac{4}{(p+2\bar{z}-2z_m)^2+16{z_R}^2} \\
& \mathcal{H}_m\left(-\frac{s_x+2\bar{x}}{p+2\bar{z}-2z_m}\sqrt{\frac{kz_R}{-4iz_R\,(p+2\bar{z}-2z_m)}}\right) \\
& \mathcal{H}_m\left(-\frac{s_x+2\bar{x}}{p+2\bar{z}-2z_m}\sqrt{\frac{kz_R}{4iz_R\,(p+2\bar{z}-2z_m)}}\right) \\
& \mathcal{H}_n\left(-\frac{s_y+2\bar{y}}{p+2\bar{z}-2z_m}\sqrt{\frac{kz_R}{-4iz_R\,(p+2\bar{z}-2z_m)}}\right) \\
& \mathcal{H}_n\left(-\frac{s_y+2\bar{y}}{p+2\bar{z}-2z_m}\sqrt{\frac{kz_R}{4iz_R\,(p+2\bar{z}-2z_m)}}\right)\Bigg] + \\
& + \Bigg[e^{-\frac{2kz_R\left((s_x-2\bar{x})^2+(s_y-2\bar{y})^2\right)}{(p-2\bar{z}+2z_m)^2+16{z_R}^2}} \frac{4}{(p-2\bar{z}+2z_m)^2+16{z_R}^2} \\
& \left(\frac{(p-2\bar{z}+2z_m)^2}{(p-2\bar{z}+2z_m)^2+16{z_R}^2}\right)^{\frac{m+n}{2}} \\
& \mathcal{H}_m\left(-\frac{s_x-2\bar{x}}{p-2\bar{+}2z_m}\sqrt{\frac{kz_R}{-4iz_R\,(p-2\bar{z}+2z_m)}}\right) \\
& \mathcal{H}_m\left(-\frac{s_x-2\bar{x}}{p-2\bar{z}+2z_m}\sqrt{\frac{kz_R}{4iz_R\,(p-2\bar{z}+2z_m)}}\right) \\
& \mathcal{H}_n\left(-\frac{s_y-2\bar{y}}{p-2\bar{z}+2z_m}\sqrt{\frac{kz_R}{-4iz_R\,(p-2\bar{z}+2z_m)}}\right) \\
& \mathcal{H}_n\left(-\frac{s_y-2\bar{y}}{p-2\bar{z}+2z_m}\sqrt{\frac{kz_R}{4iz_R\,(p-2\bar{z}+2z_m)}}\right)\Bigg]\Bigg\}
\end{aligned}
\quad , \qquad (3.56)
$$

where z_m is the axial distance of the filters from the screen. For small separations, the centroids $\bar{x}$ and $\bar{y}$ can be localized by direct imaging. While the axial centroid $\bar{z}$ is taken in the limit $\bar{z} \to z_m$ then we are able to know the localization of this coordinate from the position of apparatus. Thanks to this the probability Eq. 3.56 became

$$P_{1m,n}\left(s_x, s_y, p, z_m\right) = \frac{2^{4-m-n} e^{-\frac{2k\left({s_x}^2+{s_y}^2\right)z_R}{p^2+16{z_R}^2}} {z_R}^2 \left(\frac{p^2}{p^2+16{z_R}^2}\right)^{\frac{m+n}{2}}}{\left(p^2+16{z_R}^2\right)\Gamma(1+m)\Gamma(1+n)} \mathcal{H}_m\left(-\frac{1}{2}(-1)^{\frac{3}{4}}\sqrt{\frac{k}{p^3}}s_x\right)\mathcal{H}_m\left(-\frac{1}{2}(-1)^{\frac{1}{4}}\sqrt{\frac{k}{p^3}}s_x\right)\cdot \mathcal{H}_m\left(-\frac{1}{2}(-1)^{\frac{3}{4}}\sqrt{\frac{k}{p^3}}s_y\right)\mathcal{H}_m\left(-\frac{1}{2}(-1)^{\frac{1}{4}}\sqrt{\frac{k}{p^3}}s_y\right) \tag{3.57}$$

To measure in the Hermite-Gaussian basis, one needs to demultiplex the image-plane field in terms of the desired spatial modes before determining the outcome based on the mode in which the photon is detected. To do so with a high information-extraction efficiency, one should perform a one-to-one conversion of the Hermite-Gaussian modes into modes in a more accessible degree of freedom with minimal loss and measurements that capture as many photons as possible. For example, we can take advantage of the fact that the Hermite-Gaussian modes are waveguide modes of a quadratic-index waveguide. The classical Fisher information for the Hermite-Gaussian basis measurements is

$$J_{\mu\nu} = N\sum_{m,n=0}^{\infty}\frac{1}{P_{1m,n}}\frac{\partial}{\partial\lambda_\mu}P_{1m,n}\frac{\partial}{\partial\lambda_\nu}P_{1m,n}. \tag{3.58}$$

In Figures 3.3, 3.4, 3.5 is plot the classical Fisher information of Eq. (3.58) (red curve) versus the qFim (blue curve) of the relative distances s_x, s_y and p from

Eq. 3.47. The classical Fisher information plots are obtained numerically for a Gaussian beam with $k = 1$, $z_R = 2$. The vertical axes are normalized to $\mathcal{N} = \frac{1}{2}k/z_R$. For these plots we are considering the centroid coordinates $(\bar{x}, \bar{y}, \bar{z})$ in the axes origin of my reference system, and the distance to set filter for the measures $z_m \to \bar{z}$.

It is possible to observe that in the regime where the relative distances between the two light emitters $\left(s_x, s_y, p\right)$ are in small distances regime, the classical Fisher information for the Hermite-Gaussian modes coincide with the qFim beating also the Rayleigh's curse.

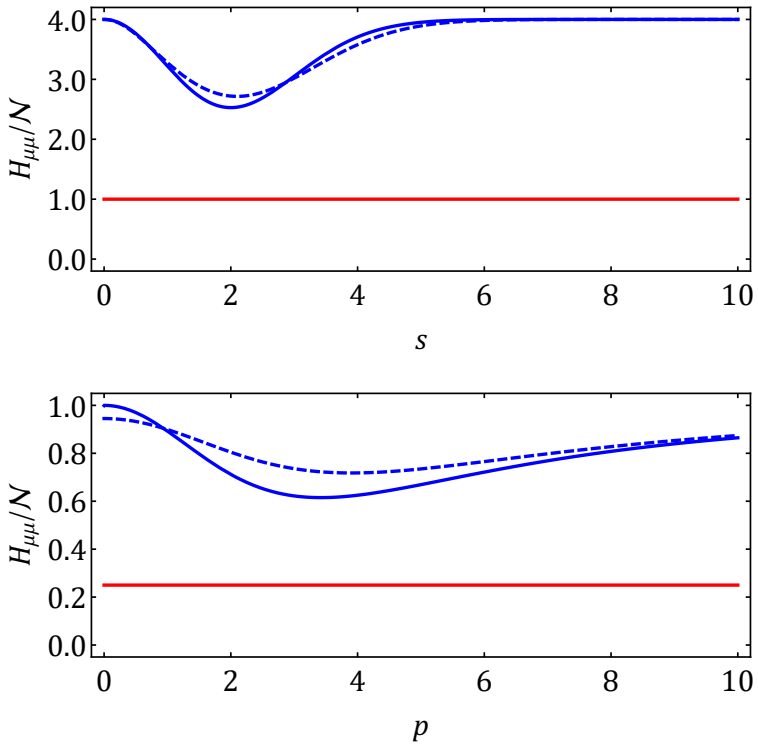

Figure 3.2: ***Top: Angular localization.*** Plots of the qFim elements H_{ss} (red, lowermost curve) and $H_{\bar{x}\bar{x}}$ (blue, uppermost curves), versus the angular separation s; continuous lines refer to $p = 0$ and dashed lines to $p = 2$. ***Bottom: Axial localization.*** Plots of the qFim elements H_{pp} (red, lowermost curve) and $H_{\bar{z}\bar{z}}$ (blue, uppermost curves), versus the axial separation p; continuous lines are for $s = 0$ and dashed lines for $s = 1$. The results are for Gaussian beams with $k = 1, z_R = 2$. The vertical axes are normalized to $\mathcal{N} = \frac{1}{2}k/z_R$.

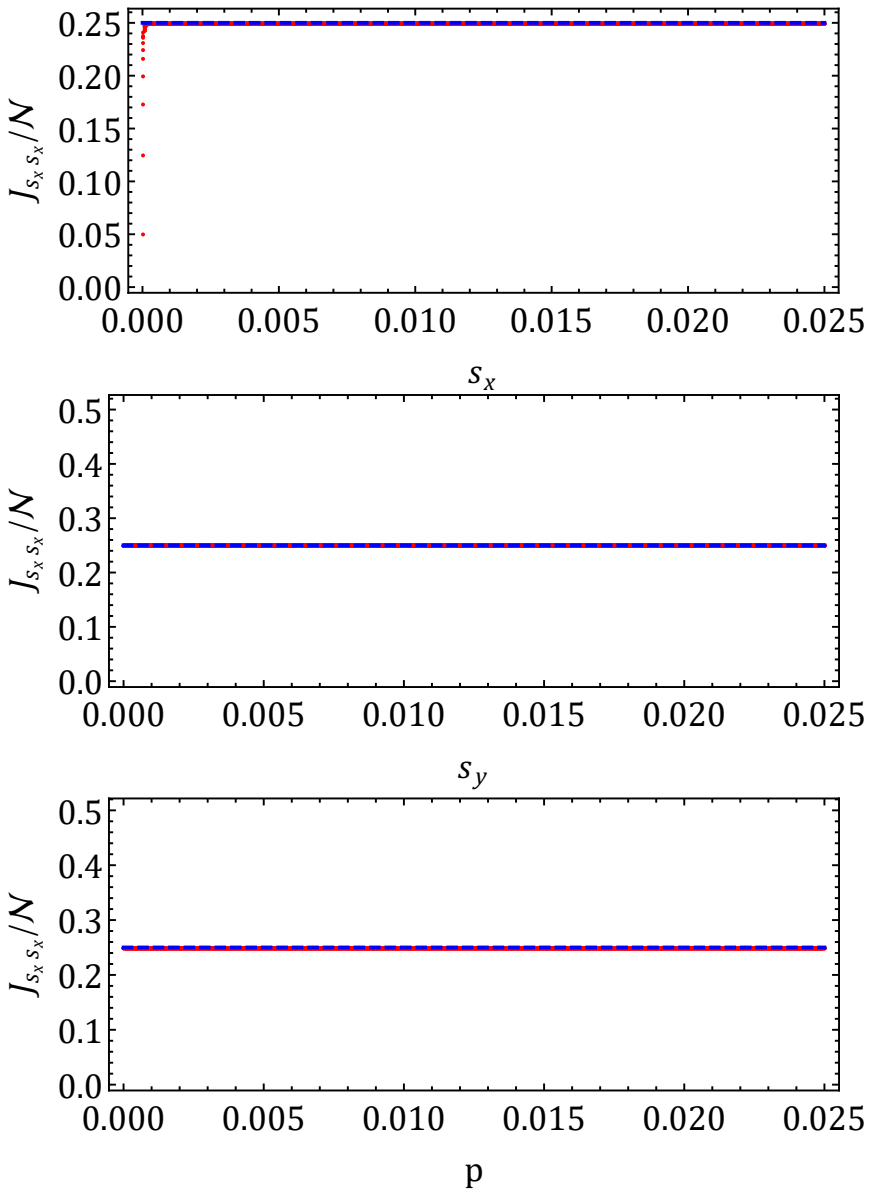

Figure 3.3: Plots of the classical Fisher information elements $J_{s_x s_x}$ (red curves) compared with the counterpart of qFim element $H_{s_x s_x}$ (blue dashed) when $p \to 0$ and $s_y \to 0$. The results are for a Gaussian beam with $k = 1$ and $z_R = 2$. The vertical axes are normalized to $\mathcal{N} = \frac{k}{2z_R}$. These graphs are made with variation of: ***top*** s_x, ***middle*** s_y, ***bottom*** p

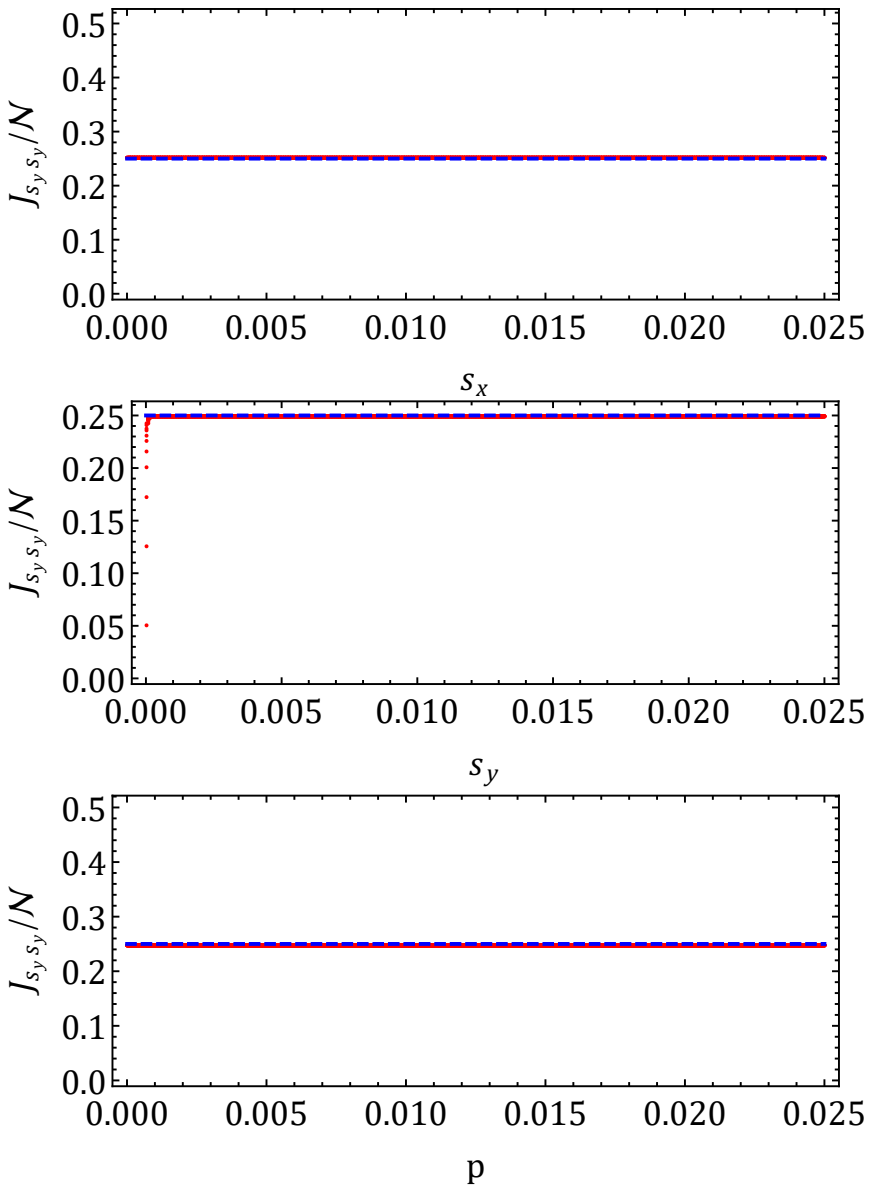

Figure 3.4: Plots of the classical Fisher information elements $J_{s_y s_y}$ (red curves) compared with the counterpart of qFim element $H_{s_y s_y}$ (blue dashed) when $p \to 0$ and $s_y \to 0$. The results are for a Gaussian beam with $k = 1$ and $z_R = 2$. The vertical axes are normalized to $\mathcal{N} = \frac{k}{2z_R}$. These graphs are made with variation of: ***top*** s_x, ***middle*** s_y, ***bottom*** p

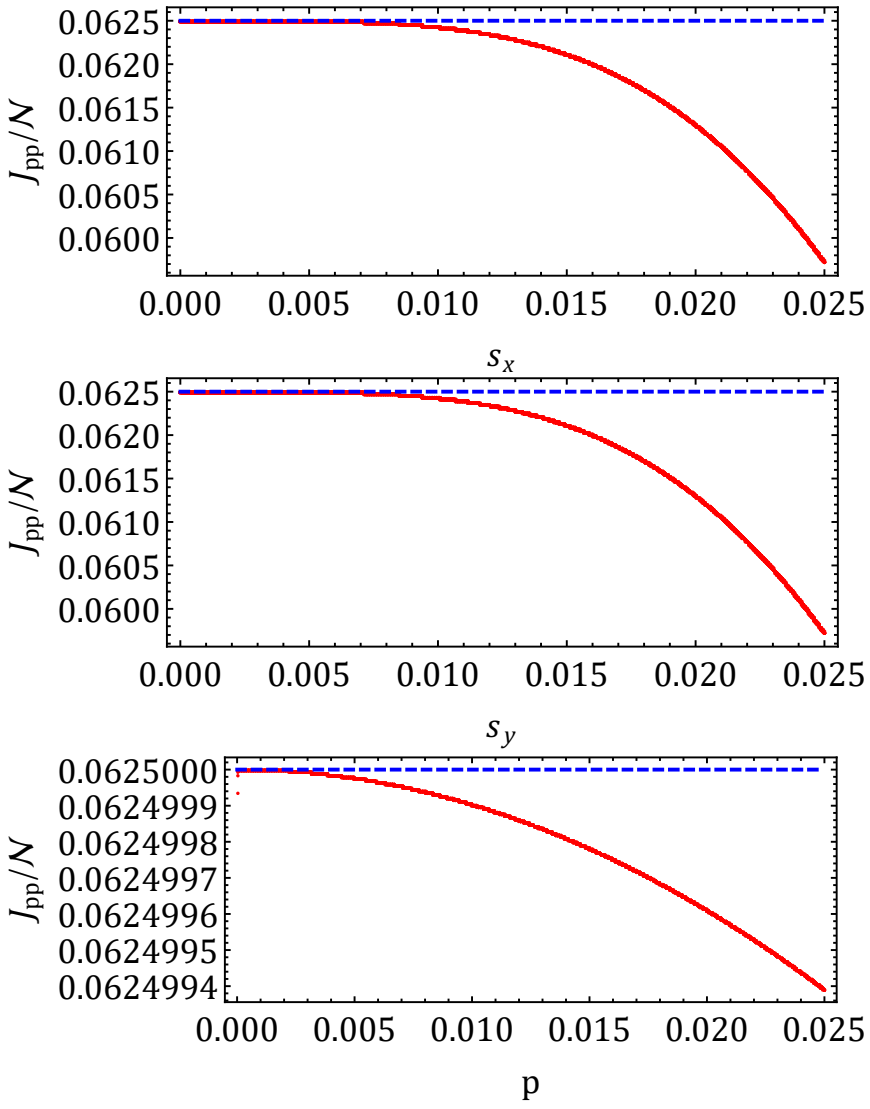

Figure 3.5: Plots of the classical Fisher information elements J_{pp} (red curves) compared with the counterpart of qFim element H_{pp} (blue dashed) when $p \to 0$ and $s_y \to 0$. The results are for a Gaussian beam with $k = 1$ and $z_R = 2$. The vertical axes are normalized to $\mathcal{N} = \frac{k}{2z_R}$. These graphs are made with variation of: ***top*** s_x, ***middle*** s_y, ***bottom*** p

Part II

4 — Quantum resource theory

Some properties of a quantum system such as quantum entanglement, coherence, athermality, asymmetry, and others, can be regarded as resources useful to perform certain operational tasks within different areas of physics including quantum optics, quantum thermodynamics, condensed matter theory, quantum biology, quantum information, and quantum metrology. The objective of any *quantum resource theory* (QRT) is to understand how we can make use of each of such quantum resources in the most efficient way. Entanglement stands probably as the paradigmatic example of QRT. It can be indeed seen as a resource for quantum teleportation[83], wherein an entangled state is consumed via *local operations and classical communication* (LOCC) and transformed into a single use of a non local quantum channel. In other words, even though one is restricted to use only local quantum operations and classical communication, entanglement can be exploited as a resource in order to circumvent such restriction. More generally, every restriction on quantum operations defines a resource theory.
Following [24, 84], we now provide a review of the general structure of a QRT.

4.1 The general structure of quantum resource theories

QRTs are constituted by the following three ingredients:

- *free states*, i.e. the states that can be implemented for free, like separable states in entanglement theory, that can be created via LOCC;
- *resource states*, i.e. the states which are not free, like entangled states in entanglement theory, that cannot be created via LOCC;
- *free operations*, i.e. the operations that can be implemented for free and that we are restricted to, like the LOCC in the case of entanglement theory.

To describe the general structure of QRTs we consider for simplicity finite dimensional quantum systems composed of distinguishable particles, whose carrier Hilbert space is thus given by $\mathcal{H}_{\mathbf{m}} \equiv \mathbb{C}^{m_1} \otimes \mathbb{C}^{m_2} \otimes \cdots \otimes \mathbb{C}^{m_s}$, where s is the number of subsystems and $\boldsymbol{m} = \{m_1, m_2, \cdots, m_s\}$ is the vector of the subsystem dimensions. We denote by $\mathcal{D}(\mathcal{H}_{\mathbf{m}})$ the set of density operators over $\mathcal{H}_{\mathbf{m}}$, i.e. the states of the particular quantum system associated with the Hilbert space $\mathcal{H}_{\mathbf{m}}$, by $\mathcal{F}$ the set of free states corresponding to all possible finite dimensional quantum systems, and by $\mathcal{F}_{\mathbf{m}} = \mathcal{F} \cap \mathcal{D}(\mathcal{H}_{\mathbf{m}})$ the set of free states pertaining only to the quantum system whose carrier Hilbert space is $\mathcal{H}_{\mathbf{m}}$.

4.1.1 The free states

We now provide five physically motivated requirements that the set of free states should fulfil, as introduced by [24]. First of all, we require that if we have a pair of free states $\rho, \sigma \in \mathcal{F}$, then we have also that $\rho \otimes \sigma \in \mathcal{F}$.

Postulate 4.1.1. The set of free states $\mathcal{F}$ is closed under tensor products.

Let us now consider a quantum system composed of two spatially separated subsystems and whose carrier Hilbert space is given by $\mathcal{H}_{\mathbf{m}\otimes\mathbf{m}'} = \mathcal{H}_{\mathbf{m}} \otimes \mathcal{H}_{\mathbf{m}'}$. If $\rho \in \mathcal{D}(\mathcal{H}_{\mathbf{m}\otimes\mathbf{m}'})$ is a free state of such system, then also the corresponding subsystem states are free, i.e. $Tr_{\mathcal{H}_{\mathbf{m}'}}(\rho) \in \mathcal{F}_{\mathbf{m}}$ and $Tr_{\mathcal{H}_{\mathbf{m}}}(\rho) \in \mathcal{F}_{\mathbf{m}'}$. This postulate is thus somehow the opposite of the previous one and can be stated formally as follows.

Postulate 4.1.2. The set of free states $\mathcal{F}$ is closed under partial trace of spatially separated subsystems.

Furthermore, if $\rho \in \mathcal{D}(\mathbb{C}^{m_1} \otimes \cdots \otimes \mathbb{C}^{m_s})$ is a free state of a quantum system composed of s spatially separated subsystems, then any permutation of these subsystems cannot generate any resource. A particular intuitive instance of this axiom arises actually from postulate 4.1.1, whereby if ρ and σ are free states, then both $\rho \otimes \sigma$ and $\sigma \otimes \rho$ are free states.

Postulate 4.1.3. The set of free states $\mathcal{F}$ is closed under permutations of spatially separated subsystems.

We now assume that a QRT is continuous. Specifically, if we consider a sequence of free states $\{\rho_n\}$ that converges to a state ρ, in the sense that $\lim_{n\to\infty} \|\rho_n - \rho\|_p = 0$ according to any p-norm $\|\cdot\|_p$, then also the state ρ is free.

Postulate 4.1.4. Each $\mathcal{F}_{\boldsymbol{m}}$ is a closed set.

Finally, suppose that $\rho, \sigma \in \mathcal{F}_{\boldsymbol{m}}$, we assume that also $t\rho + (1-t)\sigma \in \mathcal{F}_{\boldsymbol{m}}$ for any $t \in [0,1]$. Stated differently, classical mixtures of free states cannot create a resource state.

Postulate 4.1.5. Each $\mathcal{F}_{\boldsymbol{m}}$ is a convex set.

When considering entanglement theory, one can easily see that the set of separable states in all possible finite dimensions, i.e. the states of the form

$$\sigma = \sum_i p_i \rho_i^{(1)} \otimes \rho_i^{(2)} \otimes \cdots \otimes \rho_i^{(s)}, \tag{4.1}$$

with $\{p_i\}$ being a probability distribution and $\rho_i^{(j)}$ being arbitrary states of the j-th subsystem, satisfies all the above five axioms.

4.1.2 The free operations

The three ingredients of a QRT, i.e. the free states, resource states and free operations, are not independent of each other, but rather they must be compatible in the following sense: the free operations cannot generate resource states out of free states. This should be the case in order for the corresponding QRT to have an operational meaning. Indeed, it would not make sense if through operations that can be implemented for free it was possible to create something costly from something which is free.

Postulate 4.1.6. The set of free operations cannot convert free states into resource states.

When considering entanglement theory again, one can easily see that trace-preserving LOCC [24], i.e. operations such that each party is allowed to perform quantum operations only locally on his own particle and then to communicate the result to the other parties via classical means[85], satisfy such postulate, i.e. they cannot transform a separable state into an entangled state.

4.2 Measures of a resource

Actually, in order for a QRT to be operationally meaningful, it is reasonable to require something stronger than postulate 4.1.6, i.e. that any valid quantifier of a resource cannot increase under the action of free operators.

Postulate 4.2.1. The free operations cannot convert a state into a more resourceful state.

In the following we provide two main approaches whereby it is possible to faithfully quantify the amount of resource contained into a state.

4.2.1 Geometric measures

Thanks to the closure of the set of free states $\mathcal{F}_m$, we can define an infinite class of geometric resource quantifiers that are monotonically non increasing under any possible free operation. Quite intuitively, we just need to consider the distance D of the given state $\rho \in \mathcal{D}(\mathcal{H}_m)$ from the set of free states, i.e.

$$M_D(\rho) = \inf_{\sigma \in \mathcal{F}_m} D(\rho, \sigma). \tag{4.2}$$

However, an obvious question arises: what are the requirements on the distance D in order for the corresponding measure of resource M_D to faithfully quantify the degree of resource of ρ? A sufficient requirement is the contractivity of such distance under CPTP maps[24], i.e.

$$D\left(\Lambda\left(\rho\right), \Lambda\left(\sigma\right)\right) \leq D\left(\rho, \sigma\right), \tag{4.3}$$

for any CPTP map Λ and any pair of states ρ and σ.
A notable example of such kind of distance is the relative entropy S, which is defined as follows:

$$S\left(\rho \| \sigma\right) = \mathrm{Tr}\left[\rho \log \rho\right] - \mathrm{Tr}\left[\rho \log \sigma\right]. \tag{4.4}$$

Other examples are the trace distance, Hellinger distance, and Bures distance[86]. Quite remarkably, the euclidean Hilbert-Schmidt distance is not contractive under CPTP maps[86].
In the case of entanglement theory, we can thus quantify the entanglement of a given state ρ by considering its distance from the set $\mathcal{S}$ of separable states:

$$\mathcal{E}_D\left(\rho\right) = \inf_{\sigma \in \mathcal{S}} D\left(\rho, \sigma\right). \tag{4.5}$$

In particular, when D is the relative entropy we recover the celebrated relative entropy of entanglement[87].
However, there are also other requirements that are usually imposed on a measure of a resource in order to make it a fully bona fide quantifier. These include monotonicity on average under selective free operations and convexity. Overall, when considering for example an entanglement quantifier, all the requirements that a real positive function E defined on the set of states needs to satisfy in order to be a fully bona fide quantifier of entanglement can thus be summarised as follows[88, 89, 90]:

- $E(\rho) = 0$ if ρ is separable;
- $E(\Lambda_{LOCC}(\rho)) \leq E(\rho)$ for any trace-preserving LOCC Λ_{LOCC}, that implies in particular invariance of entanglement under local unitaries;
- $\sum_i p_i E(\rho_i) \leq E(\rho)$, where $p_i = Tr(V_i \rho V_i^\dagger)$ and $\rho_i = V_i \rho V_i^\dagger / p_i$, for any local operators V_i such that $\sum_i V_i^\dagger V_i = \mathbb{1}$, which is the monotonicity under selective measurements on average;
- $E(\sum_i p_i \rho_i) \leq \sum_i p_i E(\rho_i)$, for any probability distribution $\{p_i\}$ and states ρ_i.

Again, one can ask what are the properties that a distance D needs to satisfy in order for the corresponding measure of a resource to be fully bona fide. Apart from the contractivity of the distance under CPTP maps, there are other properties of D that are sufficient for this purpose[91]:

- $\sum_i p_i D\left(\frac{\rho_i}{p_i}, \frac{\sigma_i}{q_i}\right) \leq \sum_i D(\rho_i, \sigma_i)$, where $p_i = \mathrm{Tr}[\rho_i]$, $q_i = \mathrm{Tr}[\sigma_i]$ and $\rho_i = V_i \rho V_i^\dagger$ and $\sigma_i = V_i \sigma V_i^\dagger$, with V_i not necessarily local;
- $D(\sum_i P_i \rho P_i, \sum_i P_i \sigma P_i) = \sum_i D(P_i \rho P_i, P_i \sigma P_i)$, where P_i is any set of orthogonal projectors such that $P_i P_j = \delta_{ij} P_i$;
- $D(\rho \otimes P_\alpha, \rho \otimes P_\alpha) = D(\rho, \sigma)$ where P_α is any projector.

- $D(\sum_i p_i\rho_i, \sum_i p_i\sigma_i) \leq \sum_i p_i D(\rho_i, \sigma_i)$, for any probability distribution $\{p_i\}$ and any set of states ρ_i and σ_i.

Again, the relative entropy distance satisfies all the aforementioned properties, so that the relative entropy of entanglement can be regarded as a fully fledged quantifier[91].

4.2.2 Robustness of a resource

The convexity of the set of free states allows us to introduce another quantifier of a resource, the so-called robustness. The robustness of a state ρ quantifies the minimal amount of classical mixing s with a free state σ required to wash out all the resource of ρ:

$$\mathcal{R}_{sp}(\rho) = \inf_{\sigma\in\mathcal{F}_{\mathbf{m}}} \min_{s} \left\{ s \geq 0 : \frac{\rho + s\sigma}{1+s} \in \mathcal{F}_{\mathbf{m}} \right\}. \tag{4.6}$$

Quite intuitively, this quantity measures how much the quantum resource of a given state ρ is robust against classical mixtures with free states.
Again, this sort of resource quantifier arose within entanglement theory. More precisely, it was introduced in a seminal paper by Vidal and Tarrach[92], where it was defined as follows:

$$\mathcal{E}_{\mathcal{R}_{sp}}(\rho) = \inf_{\sigma\in\mathcal{S}} \min_{s} \left\{ s \geq 0 : \frac{\rho + s\sigma}{1+s} \in \mathcal{S} \right\}, \tag{4.7}$$

i.e. as the minimal amount of mixing s with a separable state σ required to get a separable state out of ρ. The robustness of entanglement is well defined since for any state ρ there always exist a positive number s and a separable state $\sigma \in \mathcal{S}$ such that $\rho_s = \frac{\rho+s\sigma}{1+s}$ is also a separable state. This entails that we can always decompose a state ρ in terms of separable states as follows

$$\rho = (1+s)\rho_s - s\sigma. \tag{4.8}$$

Such decomposition is denoted by local pseudomixture for the state ρ (see Fig.4.1). A local pseudomixture for ρ is said to be optimal if the separable states ρ_s and σ appearing in Eq. (4.8) achieve both the optimisations in the definition of the robustness of entanglement of ρ in Eq. 4.7, so that $s = \mathcal{E}_{\mathcal{R}_{sp}}(\rho)$.
We now show that the robustness of entanglement is a fully bona fide quantifier. First of all, due to the convexity of the set of separable states, the robustness of entanglement is zero for all, and only, separable states. Second, we now show that

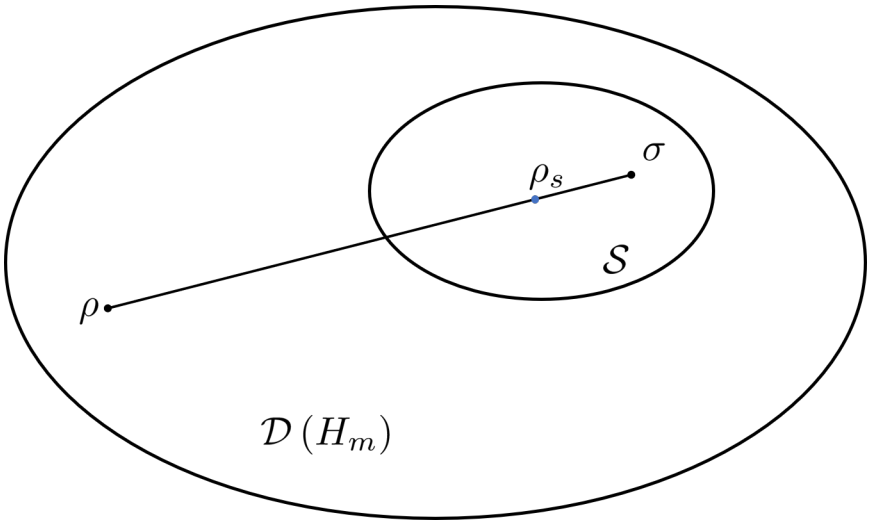

Figure 4.1: Local pseudomixture for the entangled state ρ. Since there always exist a $\sigma \in \mathcal{S}$ and a finite $s > 0$ such that $\rho_s = \frac{\rho + s\sigma}{1+s}$ is in $\mathcal{S}$, we are able to express ρ in terms of two separable states and the weight s as $\rho = (1+s)\,\rho_s - s\sigma$.

the robustness of entanglement is monotonically non-increasing on average under selective local measurements, i.e.

$$\mathcal{E}_{\mathcal{R}_{sp}}(\rho) \geq \sum_n p_n \mathcal{E}_{\mathcal{R}_{sp}}(\rho_n) \tag{4.9}$$

with $\rho_n = \frac{K_n \rho K_n^\dagger}{p_n}$ and $p_n = \mathrm{Tr}\left[K_n \rho K_n^\dagger\right]$, $\forall K_n$ such that $\sum_n K_n^\dagger K_n = \mathbb{1}$ and K_n being local operators.

Let us recall that any optimal local pseudomixture ρ_s of ρ is such that:

$$\rho = \left(1 + \mathcal{E}_{\mathcal{R}_{sp}}(\rho)\right)\rho_s - \mathcal{E}_{\mathcal{R}_{sp}}(\rho)\,\sigma, \tag{4.10}$$

where σ is a separable state. Consequently, we get that:

$$\rho_n = \frac{K_n \rho K_n^\dagger}{p_n} = \frac{1}{p_n}\left\{\left(1 + \mathcal{E}_{\mathcal{R}_{sp}}(\rho)\right) K_n \rho_s K_n^\dagger - \mathcal{E}_{\mathcal{R}_{sp}}(\rho)\, K_n \sigma K_n^\dagger\right\}. \tag{4.11}$$

Introducing

$$\begin{aligned} \rho_{s_n} &= \frac{1}{1+t}\frac{1}{p_n}\left(1 + \mathcal{E}_{\mathcal{R}_{sp}}(\rho)\right) K_n \rho_s K_n^\dagger \in \mathcal{S} \\ \sigma_n &= \frac{1}{t}\frac{1}{p_n}\mathcal{E}_{\mathcal{R}_{sp}}(\rho)\, K_n \sigma K_n^\dagger \in \mathcal{S} \\ t &= \frac{1}{p_n}\mathcal{E}_{\mathcal{R}_{sp}}(\rho)\,\mathrm{Tr}\left[K_n \sigma K_n^\dagger\right], \end{aligned} \tag{4.12}$$

we obtain:

$$\rho_n = (1+t)\,\rho_{s_n} - t\sigma_n. \tag{4.13}$$

Since the above local pseudomixture of ρ_n is not necessarily optimal, by using the definition of robustness of entanglement for the state ρ_n we immediately get:

$$\mathcal{E}_{\mathcal{R}_{sp}}(\rho_n) \leq t. \tag{4.14}$$

We thus obtain the following sequence of inequalities:

$$\begin{aligned}\sum_n p_n \mathcal{E}_{\mathcal{R}_{sp}}(\rho_n) \leq \sum_n p_n \mathcal{E}_{\mathcal{R}_{sp}}(\rho) \frac{\mathrm{Tr}\left[K_n \sigma K_n^\dagger\right]}{p_n} = \\ = \sum_n \mathcal{E}_{\mathcal{R}_{sp}}(\rho) \mathrm{Tr}\left[K_n \sigma K_n^\dagger\right] = \\ = \sum_n \mathcal{E}_{\mathcal{R}_{sp}}(\rho) \mathrm{Tr}\left[K_n^\dagger K_n \sigma\right] = \\ = \mathcal{E}_{\mathcal{R}_{sp}}(\rho) \mathrm{Tr}\left[\sum_n \left(K_n^\dagger K_n\right)\sigma\right] = \\ = \mathcal{E}_{\mathcal{R}_{sp}}(\rho) \mathrm{Tr}[\sigma] = \mathcal{E}_{\mathcal{R}_{sp}}(\rho),\end{aligned} \tag{4.15}$$

which lead to the desired monotonicity under selective local measurements of the robustness of entanglement. Third, the robustness of entanglement is convex, i.e. it satisfies the following inequality

$$\mathcal{E}_{\mathcal{R}_{sp}}(\rho) \leq \sum_{k=1}^{l} p_k \mathcal{E}_{\mathcal{R}_{sp}}(\rho_k), \tag{4.16}$$

for any probability distribution $\{p_k\}$, any set of states $\{\rho_k\}$ and any l. To prove the above inequality, it suffices to restrict to the case of $l = 2$, since the latter implies any other case with $l > 2$, as it can be easily seen by iteration. In other words, we just need to prove the following:

$$\mathcal{E}_{\mathcal{R}_{sp}}(p\rho_1 + (1-p)\rho_2) \leq p\mathcal{E}_{\mathcal{R}_{sp}}(\rho_1) + (1-p)\mathcal{E}_{\mathcal{R}_{sp}}(\rho_2), \tag{4.17}$$

for any $p \in [0,1]$. For each ρ_k, $k = 1,2$, let us consider an optimal local pseudomixture ρ_{s_k}, which is thus such that:

$$\rho_k = \left(1 + \mathcal{E}_{\mathcal{R}_{sp}}(\rho_k)\right)\rho_{s_k} - \mathcal{E}_{\mathcal{R}_{sp}}(\rho_k)\sigma_k, \tag{4.18}$$

where σ_k, $k = 1, 2$, is a separable state. Consequently, the convex combination $\rho = p\rho_1 + (1-p)\rho_2$ can be written as:

$$\rho = (1+t)\rho_s - t\sigma, \tag{4.19}$$

which is a local pseudomixture with:

$$\begin{aligned} \rho_s &= \frac{1}{1+t}\left[p\left(1+\mathcal{E}_{\mathcal{R}_{sp}}(\rho_1)\right)\rho_{s_1} + (1-p)\left(1+\mathcal{E}_{\mathcal{R}_{sp}}(\rho_2)\right)\rho_{s_2}\right] \in \mathcal{S} \\ \sigma &= \frac{1}{t}\left[p\mathcal{E}_{\mathcal{R}_{sp}}(\rho_1)\,\sigma_1 + (1-p)\,\mathcal{E}_{\mathcal{R}_{sp}}(\rho_2)\,\sigma_2\right] \in \mathcal{S} \\ t &= p\mathcal{E}_{\mathcal{R}_{sp}}(\rho_1) + (1-p)\,\mathcal{E}_{\mathcal{R}_{sp}}(\rho_2)\,. \end{aligned} \tag{4.20}$$

Since the local pseudomixture in Eq. (4.19) is not necessarily optimal, then by the definition of $\mathcal{R}_{sp}(\rho)$ we have that $\mathcal{E}_{\mathcal{R}_{sp}}(\rho = p\rho_1 + (1-p)\rho_2) \leq t$, i.e. we get the desired convexity inequality.

Finally, the robustness of entanglement is monotonically non-increasing under LOCC [93]. One can easily see that this simply arises from its convexity and monotonicity on average under selective local measurements [92, 94].

An interesting example regards generic pure states of quantum systems composed of two identical yet distinguishable m-dimensional particles. The Schmidt theorem states that any pure state $|\psi\rangle$ of such quantum system can be decomposed as follows:

$$|\psi\rangle = \sum_{i=1}^{m} a_i\,|i\rangle \otimes |i\rangle\,, \quad 0 \leq a_{i+1} \leq a_i, \quad \sum_{i=1}^{m} a_i^2 = 1, \tag{4.21}$$

where $\{|i\rangle\}_{i=1}^{m}$ is an orthonormal basis of $\mathbb{C}^m$. In terms of the positive coefficients $\{a_i\}$, the robustness $\mathcal{E}_{\mathcal{R}_{sp}}$ of the pure state $|\psi\rangle$ is given by:

$$\mathcal{E}_{\mathcal{R}_{sp}}(|\psi\rangle) = \left(\sum_{i=1}^{m} a_i\right)^2 - 1. \tag{4.22}$$

This result confirms how for bipartite pure states the entanglement depends only

on the eigenvalues of the marginal states[92, 94, 93]. Indeed, given the projector onto the pure state $|\psi\rangle$, i.e. $|\psi\rangle\langle\psi|$, we can immediately see that the eigenvalues of the marginal states $\rho_A = Tr_B(|\psi\rangle\langle\psi|) = \rho_B = Tr_A(|\psi\rangle\langle\psi|)$ are given exactly by the a_i^2 so that the sum of their square roots will lead to $\mathcal{E}_{\mathcal{R}_{sp}}(|\psi\rangle)$.
The robustness of a resource can be readily generalised, when realising that also a convex mixture between two resourceful states can very well be a free state. This gives rise to the generalised robustness of a resource, which is defined as follows:

$$\mathcal{R}_g(\rho) = \min_{\tau\in\mathcal{D}(\mathcal{H}_m)} \left\{ s \geq 0 : \frac{\rho + s\tau}{1+s} \in \mathcal{F}_m \right\}, \tag{4.23}$$

i.e. as the minimal amount of mixing s with an arbitrary state τ required to erase all the resource of ρ. Consequently, the generalised robustness of a state quantifies how much its resource is robust against general classical mixtures. In the following, to distinguish between the two robustness measures, we will denote the original one by specialised robustness. Steiner gave birth to this generalisation again within entanglement theory, in Ref.[94], when considering the problem whereby also by convex combinations between entangled states it is possible to create a separable state. Specifically, he defined the generalised robustness of entanglement of a state ρ as follows:

$$\mathcal{E}_{\mathcal{R}_g}(\rho) = \min_{\tau\in\mathcal{D}(\mathcal{H}_m)} \min_{s} \left\{ s : \frac{\rho + s\tau}{1+s} \in \mathcal{S} \right\}. \tag{4.24}$$

i.e. as the minimal amount of mixing s with any state τ required to have a separable state out of ρ. Again, this generalised definition of the robustness of entanglement is well posed since there always exist a positive number s and a state τ such that $\rho_s = \frac{\rho+s\tau}{1+s}$ is a separable state (see Figure 4.2). Moreover, via a simple generalisation of the arguments used in the case of the specialised robustness, one can easily see that also the generalised robustness is a fully bona fide quantifier of entanglement. Resorting to entanglement witnesses, it is possible to provide the generalised robustness with an operational meaning. Entanglement witnesses

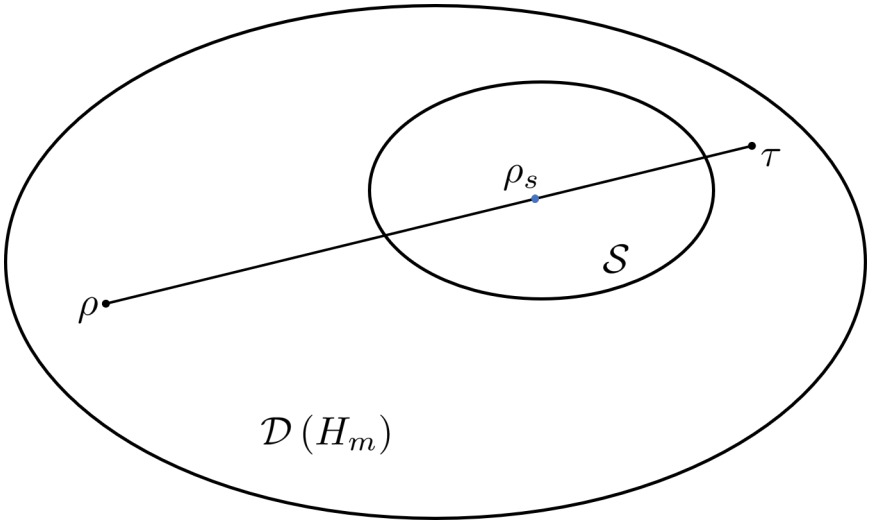

Figure 4.2: Generalised pseudomixture for the entangled state ρ. Since there always exist a $\tau \in \mathcal{D}(\mathcal{H}_{\mathbf{m}})$ and a finite $s > 0$ such that $\rho_s = \frac{\rho + s\tau}{1+s}$ is in $\mathcal{S}$, we are able to express ρ in terms of a separable state, an arbitrary state and the weight s as $\rho = (1 + s)\,\rho_s - s\tau$.

stand as fundamental tools in quantum information theory, since they are observables that allow to detect entanglement in an experimentally friendly way[88, 95, 96]. Specifically, an entanglement witness is an Hermitian operator W such that

$$\mathrm{Tr}\left[W\sigma\right] \geq 0, \tag{4.25}$$

for any separable state σ. Consequently, if we have a state ρ such that:

$$\mathrm{Tr}\left[W\rho\right] < 0, \tag{4.26}$$

then we can conclude that ρ is entangled and we say that W detects ρ. However, the fact that $\mathrm{Tr}\left[W\rho\right] \geq 0$ does not imply that ρ is separable, so that given a state ρ there are only some witnesses that are particularly tailored to it and can detect its entanglement. In particular, given a state ρ, we can define an optimal

entanglement witness W_ρ for ρ as any entanglement witness such that

$$\mathrm{Tr}\left[W_\rho \rho\right] = \min_{W \in \mathcal{W}} \mathrm{Tr}\left[W\rho\right], \tag{4.27}$$

where $\mathcal{W}$ is the intersection of the sets of entanglement witnesses with some other set (e.g., the set $W \leq \mathbb{1}$). Entanglement witnesses enjoy a nice geometric interpretation, wherein they are represented by hyperplanes in the set of states such that all states located into one side of the hyperplane or belonging to it provide non-negative mean value of the witness, such as the entire convex set of separable states, whereas those located into the other side are entangled states detected by the witness (see Figure 4.3).

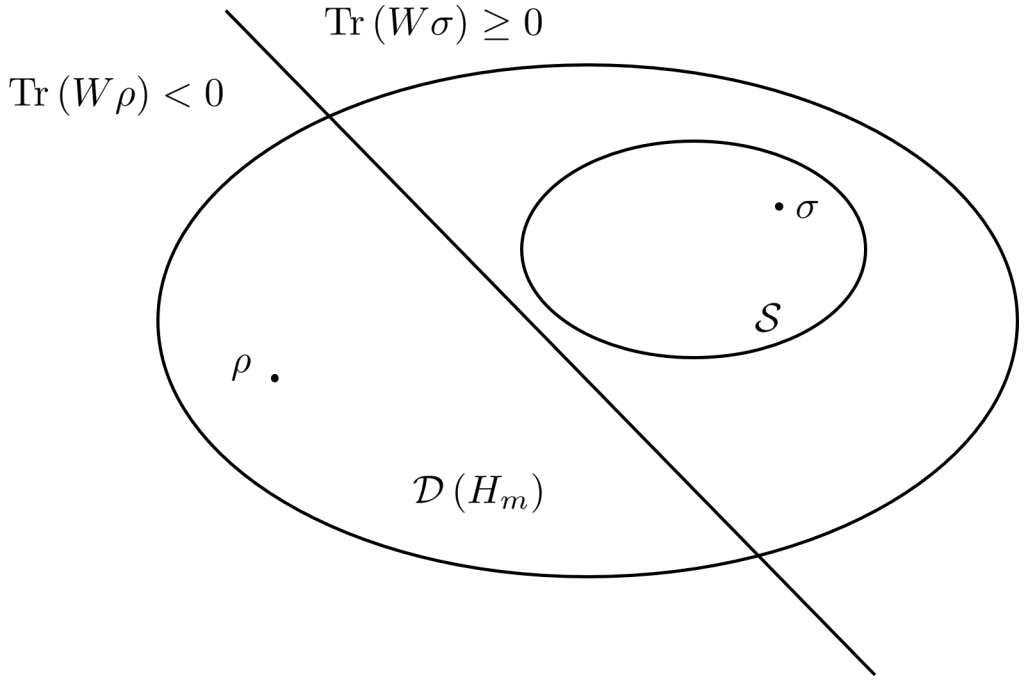

Figure 4.3: The line represents a hyperplane corresponding to the entanglement witness W. All states located to the right of the hyperplane or belonging to it provide non-negative mean value of the witness, while those located to the left are entangled states detected by the witness.

Interestingly, by adopting optimal witnesses, we can turn the qualitative statement provided by an entanglement witness into a quantitative evaluation of the entanglement of ρ. Indeed, it turns out that the following quantity

$$\mathcal{E}_W(\rho) = \max\left\{0, -\min_{W\in\mathcal{W}} \mathrm{Tr}\left[W\rho\right]\right\}. \tag{4.28}$$

faithfully quantifies the entanglement of ρ[97].

5 — Coherence as a resource

Quantum coherence constitute the underlying structure of quantum correlations and is one of the most fundamental features that depart from the classical world [98, 99]. Fundamental experiments‘ have just been able to demonstrate, beyond any major loophole, that quantum correlations are incompatible with a local realistic interpretation [100, 101, 102, 103, 104, 105, 106]. On the other hand, the realization that quantum properties can be harnessed for practical applications [25] is presently fuelling a heated international race [107] to develop and deploy quantum technologies [108]. This is no coincidence: the improved study and test of fundamental quantum properties and our increased ability to exploit them go hand in hand.

The most essential feature signifying quantumness in a single system and underpinning all forms of quantum correlations in composite systems [109, 110, 111] is *quantum coherence*, namely the possibility of creating superpositions of a set of orthogonal states. Revealing quantum coherence in the state of a natural complex or man-made device earmarks its behaviour as genuinely nonclassical [98, 99]. Its degree of coherence often quantifies the ability of such an object to be an effective medium for quantum-enhanced applications [103, 112], ranging from cryptography [105] to metrology [106] and thermodynamics [113, 114]. Thus, it has become imperative to accomplish a rigorous operational characterization of quantum coherence.

5.1 Quantum coherence and quantum interference

Consider an observable K on the carrier Hilbert space $\mathcal{H}$, and $\{|k_i\rangle, k_i\}$ respectively the eigenstates and eigenvalues of K[1]. From Eq. 1.6 we know that the quantum measurement of the observable K in general perturbs the physical system. Supposing that the system is described by the state $|\psi\rangle$, the measurement of the observable changes the system transforming its state $|\psi\rangle$ into one of the eigenstates $|k_i\rangle$, with probability:

$$p_\psi(k_i) = |\langle k_i|\psi\rangle|^2 = \langle\psi|k_i\rangle\langle k_i|\psi\rangle = \langle\psi|\Pi_{k_i}|\psi\rangle = \langle\Pi_{k_i}\rangle_\psi , \tag{5.1}$$

where Π_{k_i} is the projector onto the eigenspace of k_i.
We can represent the state $|\psi\rangle$ as a coherent superposition of the above eigenstates

$$|\psi\rangle = \sum_i d_i |k_i\rangle , \tag{5.2}$$

and then we can consider the corresponding classical mixture of such eigenstates

$$\rho = \sum_i c_i |k_i\rangle\langle k_i| , \quad c_i = |d_i|^2 . \tag{5.3}$$

Let us consider a second observable L, having eigenvalues and eigenstates, respectively: $\{|l_m\rangle, l_m\}$, which does not commute with K. In the case of the classical mixture ρ in Eq. 5.3, the probability to have the eigenvalue l_m as the result of a measurement of L is, from Eq. 1.12:

$$p_\rho(l_m) = \mathrm{Tr}\left[\rho\Pi_{l_m}\right] = \sum_i c_i |\langle l_m|k_i\rangle|^2 , \tag{5.4}$$

[1] We suppose to measure the value of the physical quantity K in this state by projective measurement: $K = \sum_i k_i |k_i\rangle\langle k_i| = \sum_i k_i \Pi_{k_i}$

while in the case of the coherent superposition in Eq. 5.2 one has, from Eq. 5.1:

$$\begin{aligned} p_\psi(l_m) = |\langle l_m|\psi\rangle|^2 &= \sum_j d_j^* \langle k_j|l_m\rangle \sum_i d_i \langle l_m|k_i\rangle = \\ &= \sum_i |d_i|^2 |\langle l_m|k_i\rangle|^2 + 2\sum_{i\neq j} d_j^* d_i \langle k_j|l_m\rangle \langle l_m|k_i\rangle = \\ &= p_\rho(l_m) + 2\sum_{i>j} \Re\left\{d_j^* d_i \langle k_j|l_m\rangle \langle l_m|k_i\rangle\right\}. \end{aligned} \tag{5.5}$$

The information about quantum coherent superposition is stored in the off-diagonal elements of the matrix representing the projector $|\psi\rangle\langle\psi|$ in the basis $\{|k_i\rangle\}$. These terms are exactly those that give rise to quantum interference. In the classical mixture, the information about the relative phase β in the product $d_i d_j^* = |\alpha| e^{i\beta}$ is lost, as only the square modules $|d_i|^2 = c_i$ appear. This prevent such classical mixture to allow for quantum interference. Classically we can imagine neither a coin that is in a superposition of the states "head" and "tail" nor a Schrödinger's cat that is both "dead" and "alive" at the same time, while in the microscopic world quantum coherence is not only relevant but also necessary to provide a satisfactory description of physical phenomena.

5.2 The resource theory of quantum coherence

Following the general structure of QRTs, we can describe quantum coherence as a resource [115].

In the resource theory of quantum coherence, the first step is to identify the free states. A natural definition arises by fixing a particular basis $\{|i\rangle\}_{i=1}^m$ of the carrier Hilbert space $\mathcal{H}_m$. We call all density matrices that are diagonal in this basis *incoherent states* and label the set of all quantum incoherent states with all possible finite dimensions by $\mathcal{I}$, then the incoherent set of all states pertaining specifically to the system with carrier Hilbert space $\mathcal{H}_m$ is: $\mathcal{I}_m = \mathcal{I} \cap \mathcal{D}(\mathcal{H}_m)$. Hence, all

density operator $\sigma \in \mathcal{I}$ are of the form:

$$\sigma = \sum_i p_i |i\rangle \langle i| , \tag{5.6}$$

with $\{p_i\}$ being a probability distribution. It is easy to see that this set satisfies all the five axioms that free states should satisfy, and have been outlined in section 4.1.1.

The free operations of the resource theory of quantum coherence, according to Baumgratz et al [104], are given by the so-called incoherent completely positive trace preserving (ICPTP) maps, even if the discussion about it is still open [115]. By definition, the Kraus operators $\{K_n\}$ of any ICPTP map satisfy not only the trace preserving condition $\sum_n K_n^\dagger K_n = \mathbb{1}$ but also $K_n \mathcal{I} K_n^\dagger \subset \mathcal{I}$ for all n. This definition guarantees that in an overall incoherent quantum operation $\rho \to \sum_n K_n \rho K_n^\dagger$, even if one has access to individual outcomes n, no observer would conclude that coherence has been generated from an incoherent state.

5.3 Measures of coherence

Following [104] we can give a collection of physically motivated properties that any functional $\mathscr{C}$ mapping the states to the non-negative real numbers should satisfy in order to be regarded as a proper coherence measure.

First of all it is required that the measure is zero if and only if the state is an incoherent state

C1

$$\mathscr{C}(\rho) = 0 \iff \rho \in \mathcal{I}. \tag{5.7}$$

It is also required that the functional must be monotonically non-increasing under incoherent completely positive trace preserving (ICPTP) maps

C2a

$$\mathscr{C}(\rho) \geq \mathscr{C}(\Phi_{ICPTP}(\rho)). \tag{5.8}$$

The above condition has the same physical meaning of **Postulate** 4.2.1.
It is also required a further condition of monotonicity, that is non-increasing on average under selective incoherent measurements

C2b

$$\mathscr{C}(\rho) \geq \sum_n p_n \mathscr{C}(\rho_n), \tag{5.9}$$

with $\rho_n = \frac{K_n \rho K_n^\dagger}{p_n}$, $p_n = \mathrm{Tr}\left[K_n \rho K_n^\dagger\right]$ for all $\{K_n\}$ such that $\sum_n K_n^\dagger K_n = \mathbb{1}$ and $K_n \mathcal{I} K_n^\dagger \subset \mathcal{I}$.

This condition is more important as it allows for sub-selection, a process available in well controlled quantum experiments, indeed this condition is the monotonicity under selective measurements on average.
In the end it is required that the measure can not increase under classical mixing.

C3

$$\mathscr{C}\left(\sum_n p_n \rho_n\right) \leq \sum_n p_n \mathscr{C}(\rho_n), \tag{5.10}$$

for any set of states $\{\rho_n\}$ and any $p_n \geq 0$ with $\sum_n p_n = 1$ **Postulate** 4.1.5.

As pointed out [104], any coherence measure that satisfies conditions (**C2b**) and (**C3**) necessarily satisfies also condition (**C2a**), indeed:

$$\mathscr{C}(\Phi_{ICPTP}(\rho)) = \mathscr{C}\left(\sum_n p_n \rho_n\right) \overset{\mathbf{C3}}{\leq} \sum_n \mathscr{C}(p_n \rho_n) \overset{\mathbf{C2b}}{\leq} \mathscr{C}(\rho). \tag{5.11}$$

5.4 Geometric measures

Also for the coherence, the most intuitive kind of measure is the class of measure based on the distance between the given state $\rho \in \mathcal{D}(\mathcal{H}_m)$ and the closest state

$\sigma \in \mathcal{I}_m$:

$$\mathscr{C}_D(\rho) = \min_{\sigma \in \mathcal{I}_m} D(\rho, \sigma). \tag{5.12}$$

All conditions are immediately satisfied for this class of measures, provided that D is contractive under CPTP maps, except for the (**C2b**). This condition needs to be proven on a case by case basis considering specific instances of distance.

5.4.1 Relative entropy of coherence

Like for the entanglement theory, and more generally in QRTs, the relative entropy is a very useful example of distance-based measure:

$$\begin{aligned} \mathscr{C}_{relent}(\rho) &= \min_{\sigma \in \mathcal{I}_m} S(\rho \| \sigma) = \min_{\sigma \in \mathcal{I}_m} \mathrm{Tr}[\rho \log \rho] - \mathrm{Tr}[\rho \log \sigma] = \\ &= \min_{\sigma \in \mathcal{I}_m} S\left(\rho_{diag}\right) - S(\rho) + S\left(\rho_{diag} \| \sigma\right) = \\ &= S\left(\rho_{diag}\right) - S(\rho), \end{aligned} \tag{5.13}$$

where $\rho_{diag.} = \sum_i \rho_{i,i} |i\rangle\langle i|$, and $\rho_{ii} = \langle i|\rho|i\rangle$ is the matrix representing ρ in the basis $\{|i\rangle\}$.

5.5 lp-norms measures

Another intuitive coherence quantifier is the class of measures based on the off-diagonal elements, using the $l_p - norms$:

$$\|\rho\|_p = \left(\sum_{i \neq j} \left|\rho_{i,j}\right|^p \right)^{\frac{1}{p}}, \tag{5.14}$$

where $\rho_{i,j} = \langle i|\rho|j\rangle$.
In this class, the proper measure, in sense of the conditions by [104, 116], is the

$l_1 - norm$:

$$\mathscr{C}_{l_1}(\rho) = \sum_{i \neq j} \left|\rho_{i,j}\right|. \tag{5.15}$$

5.6 Robustness of coherence

In the same vein with the entanglement theory, we can introduce the robustness resource quantifier for the coherence theory. More precisely, we define the *robustness of coherence* as:

$$\mathscr{C}_{\mathcal{R}}(\rho) = \inf_{\tau \in \mathcal{D}(\mathcal{H}_m)} \min_{s} \left\{ s \geq 0 : \delta = \frac{\rho + s\tau}{1+s} \in \mathcal{I} \right\} \tag{5.16}$$

i.e. as the minimal amount of mixing s with any state τ to get an incoherent state out of ρ. As in the entanglement theory, also the robustness of coherence is well defined since for any state ρ there always exist a positive number s and a state $\tau \in \mathcal{D}(\mathcal{H}_m)$ such that $\delta = \frac{\rho+s\tau}{1+s}$ is an incoherent state.
As in the entanglement theory, it is possible to provide also for robustness of coherence an operational meaning using the witnesses operators for coherence.
The coherence witnesses are hermitian operators W with following this properties:

- $\mathrm{diag}(W) = 0$;

- $\lambda_{min}(W) \geq -1$, where λ_{min} is the minimum eigenvalue of W.

Then given such an operator W, it is true that

$$\mathscr{C}_{\mathcal{R}}(\rho) \geq \max\{0, -\mathrm{Tr}[W\rho]\}, \tag{5.17}$$

so W witnesses the coherence in ρ.
There is always an "*optimal*" witness, that is a witness W satisfying the two prop-

erties above and for which

$$\mathscr{C}(\rho) = -\mathrm{Tr}\left[W\rho\right], \tag{5.18}$$

and this optimal W can be found by semidefinite programming. We also report an alternative form of the dual of the semidefinite programming in Eq. 5.18 as

$$\mathscr{C}(\rho) = \mathrm{Tr}\left[X\rho\right] - 1, \tag{5.19}$$

where $X \geq 0$ and X came from the substitution made for the semidefinite programming variable $X = \mathbb{1} - W$.

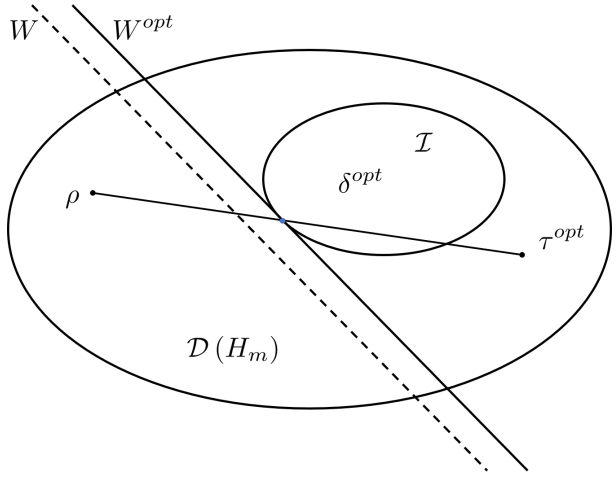

Figure 5.1: The line represents a hyperplane corresponding to the lower bound for witness of coherence W^{opt}. All states located to the right of the hyperplane or belonging to it provide non-negative mean value of the witness.

5.6.1 Is the robustness of coherence bona fide?

We now prove that our definition of robustness of coherence satisfies all the conditions to be a proper measure of coherence [87].

Faithful

In the beginning we start to prove the faithfulness condition (**C1**) 5.7

$$\mathscr{C}_{\mathcal{R}}(\rho) = 0 \iff \rho \in \mathcal{I}. \tag{5.20}$$

Proof. The proof of this condition is trivial because the robustness of coherence quantifies the minimal amount of mixing with any state τ required to have an incoherent state out ρ, and if ρ is exactly an incoherent state the minimal amount of mixing is exactly 0 because we do not need to mix ρ with another state, if $\mathscr{C}_{\mathcal{R}}(\rho) = 0$ this means that the minimal amount of mixing is 0 then we have that $\delta = \rho$, but $\delta \in \mathcal{I}$ then also $\rho \in \mathcal{I}$. □

Convexity

Now we set out the convexity criterion for the robustness of coherence Eq. 5.16 under the condition Eq. 5.10:

$$\sum_n p_n \mathscr{C}_{\mathcal{R}}(\rho_n) \geq \mathscr{C}_{\mathcal{R}}\left(\sum_n p_n \rho_n\right) \quad \forall \{\rho_n\} \tag{5.21}$$

with any $p_n \geq 0$ such that $\sum_n p_n = 1$.

Proof. This condition requires that the robustness of any realization of ρ: $\{p_n, \rho_n\}_{n=1\ldots N}$ is not smaller than ρ. To prove it, it suffices to prove for $N = 2$, since $N > 2$ can be realized by iterating of this case.
In this case we have that $\rho = p_1\rho_1 + p_2\rho_2$ with $p_1 + p_2 = 1$ then we can write $p_2 = 1 - p_1$ and then, recalling $p_1 = p$, we have $p_2 = 1 - p$ and then in this case we have that:

$$\rho = p\rho_1 + (1 - p)\rho_2. \tag{5.22}$$

Then prove the condition:

$$p\mathscr{C}_{\mathcal{R}}(\rho_1) + (1-p)\,\mathscr{C}_{\mathcal{R}}(\rho_2) \geq \mathscr{C}_{\mathcal{R}}(p\rho_1 + (1-p)\,\rho_2)\,. \tag{5.23}$$

For each ρ_k $(k = 1, 2)$ considering the *optimal* mixture, we can say:

$$\rho_k = (1 + \mathscr{C}_{\mathcal{R}}(\rho_k))\,\delta_k^{opt} - \mathscr{C}_{\mathcal{R}}(\rho_k)\,\tau_k^{opt}, \tag{5.24}$$

with δ_k^{opt} and τ_k^{opt} such that:

$$\begin{aligned} \mathscr{C}_{\mathcal{R}}(\rho_k) &= \inf_{\tau_k \in \mathcal{D}(\mathcal{H}_m)} \min_{s} \left\{ s : \delta_k = \frac{\rho_k + s\tau_k}{1+s} \in \mathcal{I} \right\}; \\ \delta_k^{opt} &= \frac{\rho_k + \mathscr{C}_{\mathcal{R}}(\rho_k)\,\tau_k^{opt}}{1 + \mathscr{C}_{\mathcal{R}}(\rho_k)}. \end{aligned} \tag{5.25}$$

Substituting Eq. 5.24 in the Eq. 5.22 we obtain:

$$\begin{aligned} \rho = p\rho_1 + (1-p)\,\rho_2 = p\,(1 + \mathscr{C}_{\mathcal{R}}(\rho_1))\,\delta_1^{opt} + p\mathscr{C}_{\mathcal{R}}(\rho_1)\,\tau_1^{opt} + \\ + (1-p)\,(1 + \mathscr{C}_{\mathcal{R}}(\rho_2))\,\delta_2^{opt} + (1-p)\,\mathscr{C}_{\mathcal{R}}(\rho_2)\,\tau_2^{opt}. \end{aligned} \tag{5.26}$$

Calling

$$\begin{aligned} \delta &= \frac{1}{1+s}\left\{ p\,(1 + \mathscr{C}_{\mathcal{R}}(\rho_1))\,\delta_1^{opt} + (1-p)\,(1 + \mathscr{C}_{\mathcal{R}}(\rho_2))\,\delta_2^{opt} \right\} \\ \tau &= \frac{1}{s}\left\{ p\mathscr{C}_{\mathcal{R}}(\rho_1)\,\tau_1^{opt} + (1-p)\,\mathscr{C}_{\mathcal{R}}(\rho_2)\,\tau_2^{opt} \right\} \\ s &= p\mathscr{C}_{\mathcal{R}}(\rho_1) + (1-p)\,\mathscr{C}_{\mathcal{R}}(\rho_2)\,. \end{aligned} \tag{5.27}$$

Substituting in the Eq. 5.26 we have:

$$\rho = (1+s)\,\delta - s\tau. \tag{5.28}$$

Then we have that:

$$\mathscr{C}_{\mathcal{R}}(p\rho_1 + (1-p)\,\rho_2) \leq s, \tag{5.29}$$

by definition of $\mathscr{C}_{\mathcal{R}}(\rho)$. □

Monotonicity under selective measurements on average

We show monotonicity for the robustness of coherence according to (**C2b**) 5.9:

$$\mathscr{C}_{\mathcal{R}}(\rho) \geq \sum_n p_n \mathscr{C}_{\mathcal{R}}(\rho_n) \tag{5.30}$$

with $\rho_n = \frac{K_n \rho K_n^\dagger}{p_n}$ and $p_n = \mathrm{Tr}\left[K_n \rho K_n^\dagger\right]$, $\forall K_n$ such that $\sum_n K_n^\dagger K_n = \mathbb{1}$ and $K_n \mathcal{I} K_n^\dagger \subset \mathcal{I}$.

Proof. The **optimal** mixture of ρ is:

$$\rho = (1 + \mathscr{C}_{\mathcal{R}}(\rho))\,\delta^{opt} - \mathscr{C}_{\mathcal{R}}(\rho)\,\tau^{opt}, \tag{5.31}$$

where δ^{opt} and τ^{opt} are such that:

$$\begin{aligned} \mathscr{C}_{\mathcal{R}}(\rho) &= \inf_{\tau \in \mathcal{D}(\mathcal{H}_m)} \min_s \left\{ s : \delta = \frac{\rho + s\tau}{1+s} \in \mathcal{I} \right\}; \\ \delta^{opt} &= \frac{\rho + \mathscr{C}_{\mathcal{R}}(\rho)\,\tau^{opt}}{1 + \mathscr{C}_{\mathcal{R}}(\rho)}. \end{aligned} \tag{5.32}$$

Then substituting Eq. 5.31 we have:

$$\rho_n = \frac{K_n \rho K_n^\dagger}{p_n} = \frac{1}{p_n}\left\{(1 + \mathscr{C}_{\mathcal{R}}(\rho))\,K_n \delta^{opt} K_n^\dagger - \mathscr{C}_{\mathcal{R}}(\rho)\,K_n \tau^{opt} K_n^\dagger\right\}. \tag{5.33}$$

Calling

$$\begin{aligned} \delta_n &= \frac{1}{1+t}\frac{1}{p_n}(1 + \mathscr{C}_{\mathcal{R}}(\rho))\,K_n \delta^{opt} K_n^\dagger \\ \tau_n &= \frac{1}{t}\frac{1}{p_n}\mathscr{C}_{\mathcal{R}}(\rho)\,K_n \tau^{opt} K_n^\dagger \\ t &= \frac{1}{p_n}\mathscr{C}_{\mathcal{R}}(\rho)\,\mathrm{Tr}\left[K_n \tau^{opt} K_n^\dagger\right], \end{aligned} \tag{5.34}$$

we obtain:

$$\rho_n = (1+t)\,\delta_n - t\tau_n. \tag{5.35}$$

Then using the robustness of coherence for the state ρ_n we have:

$$\mathscr{C}_{\mathcal{R}}(\rho_n) = \inf_{\tau_n \in \mathcal{D}(\mathcal{H}_m)} \min_t \left\{ t : \delta_n = \frac{\rho_n + t\tau_n}{1+t} \in \mathcal{I} \right\} \leq t, \tag{5.36}$$

by definition.
Then substituting in Eq. 5.30 we have:

$$\begin{aligned}
\sum_n p_n \mathscr{C}_{\mathcal{R}}(\rho_n) &\leq \sum_n p_n \mathscr{C}_{\mathcal{R}}(\rho)\, \frac{\mathrm{Tr}\left[K_n \tau^{opt} K_n^\dagger\right]}{p_n} = \\
&= \sum_n \mathscr{C}_{\mathcal{R}}(\rho)\, \mathrm{Tr}\left[K_n \tau^{opt} K_n^\dagger\right] = \\
&= \sum_n \mathscr{C}_{\mathcal{R}}(\rho)\, \mathrm{Tr}\left[K_n^\dagger K_n \tau^{opt}\right] = \\
&= \mathscr{C}_{\mathcal{R}}(\rho)\, \mathrm{Tr}\left[\sum_n \left(K_n^\dagger K_n\right) \tau^{opt}\right] = \\
&= \mathscr{C}_{\mathcal{R}}(\rho)\, \mathrm{Tr}\left[\tau^{opt}\right] = \mathscr{C}_{\mathcal{R}}(\rho)\,.
\end{aligned} \tag{5.37}$$

□

Monotonicity under ICPTP maps

$$\mathscr{C}_{\mathcal{R}}(\rho) \geq \mathscr{C}_{\mathcal{R}}(\Phi_{ICPTP}(\rho))\,; \tag{5.38}$$

as verified in Eq. 5.11 the coherence measure satisfies the condition (**C2b**)
Eq. 5.30 and condition (**C3**) Eq. 5.21, this imply the condition (**C2a**), which proves the monotonicity of the robustness of coherence respect to all possible formulation of the theory of coherence[23].

□

5.7 Robustness of coherence as advantage in discrimination games

Here, we provide a direct operational interpretation for the robustness of coherence in quantum metrology. We consider the following phase discrimination game: Alice prepares a quantum state $\rho \in \mathcal{D}(\mathcal{H}_m)$, which then enters a black box. The black box encodes a phase on ρ by implementing a unitary

$$U_\phi = e^{iN\phi}, \tag{5.39}$$

with $N = \sum_{j=0}^{m-1} j\,|j\rangle\langle j|$ and $\phi \in \mathbb{R}$, so that the output state is determined by the action of the unitary channel

$$\mathcal{U}_\phi(\rho) \coloneqq U_\phi \rho {U_\phi}^\dagger. \tag{5.40}$$

We can think of N as a Hamiltonian for the system with an equispaced spectrum, assuming unit spacing without loss of generality. In this way, the reference basis $\{|j\rangle\}$, with respect to which coherence is defined and measured, is physically identified by the choice of the Hamiltonian. Suppose one of n phases $\{\phi_k\}_{k=0}^{n-1}$ can be applied, each with a probability p_k. Any collection of pairs

$$\{(p_k, \phi_k)\}_{k=0}^{n-1} \coloneqq \Theta \tag{5.41}$$

defines a phase discrimination game, where Alice's goal is that of guessing correctly the phase that was actually imprinted on the state as shown in Figure 5.2. To this end, she performs a generalized measurement with elements $\{M_k\}$ (satisfying $M_k \geq 0$, $\sum_k M_k = \mathbb{1}$) on the output state $\mathcal{U}_\phi(\rho)$ after the black box. Optimizing over all measurements, the maximal probability of success depend on the game Θ

and the input state ρ, and is given

$$p_{\Theta}^{succ}(\rho) = \max_{M_k} \sum_{k=0}^{n-1} p_k \mathrm{Tr}\left[U_{\phi_k} \rho {U_{\phi_k}}^{\dagger} M_k\right]. \tag{5.42}$$

Supposing now Alice's input state is incoherent, $\rho \equiv \delta \in \mathcal{I}$. Since every unitary channel $\mathcal{U}_\phi$ leaves any such state invariant, $\mathcal{U}_\phi(\delta) = \delta$, the best strategy for Alice is always to cast the guess k^{max} corresponding to the phase with the highest prior probability

$$p_{k^{max}} := \max_k p_k. \tag{5.43}$$

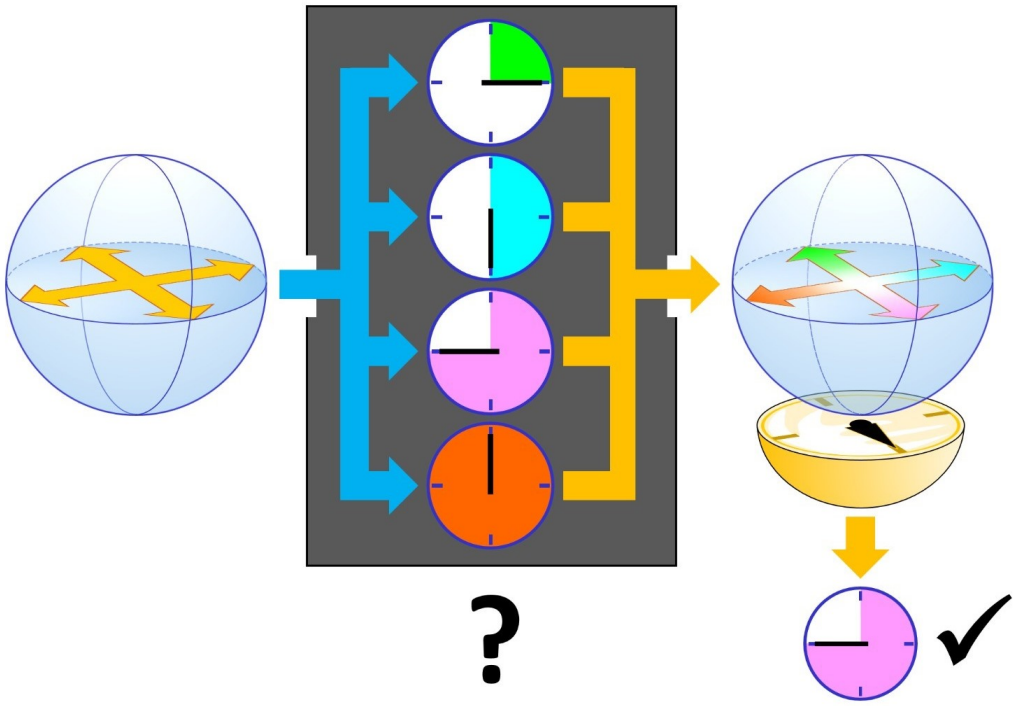

Figure 5.2: The probe state is entering in a black box, where is implemented a random phase shift sampled from a finite set of unknown phases. At the output Alice perform an measure in order to guess which specific phase was applied in the process.

This results in an optimal probability of success for any incoherent state given by

$$p_{\Theta}^{succ}(\mathcal{I}) \coloneqq p_{k^{max}}, \tag{5.44}$$

which can be achieved even without actually probing the channel, just by a fixed guess.

It is clear that, by preparing a coherent state $\rho \notin \mathcal{I}$, Alice can expect to do better. What it less obvious yet more remarkable is that the maximum advantage achievable by using ρ as opposed to any incoherent probe δ in all possible phase discrimination games. Now we face this problem showing that the robustness of coherence of ρ is who determines the advantage enabled by choosing ρ as a probe in the above channel discrimination game, as opposed to any incoherent probe δ.

Theorem 5.7.1. $\forall$ *state* $\rho \in \mathcal{D}(\mathcal{H}_m)$ *and any prior probability distribution* p_Θ *it holds that*

$$\max\left\{\frac{1}{n}\left(1+\mathscr{C}_{\mathcal{R}}(\rho)\right), p_{\Theta}^{succ}(\mathcal{I})\right\} \leq p_{\Theta}^{succ}(\rho) \leq \left(1+\mathscr{C}_{\mathcal{R}}(\rho)\right) p_{\Theta}^{succ}(\mathcal{I}). \tag{5.45}$$

Proof. The second inequality comes from the definition of $\mathscr{C}_{\mathcal{R}}(\rho)$ Eq. 5.16, which implies that there is an incoherent δ such that $\rho \leq (1+\mathscr{C}_{\mathcal{R}}(\rho))\,\delta$, so

$$\begin{aligned}\sum_{k=0}^{n-1} p_k \mathrm{Tr}\left[U_{\phi_k}\rho {U_{\phi_k}}^{\dagger} M_k\right] &\leq \left(1+\mathscr{C}_{\mathcal{R}}(\rho)\right)\sum_{k=0}^{n-1} p_k \mathrm{Tr}\left[\delta M_k\right] \\ &\leq \left(1+\mathscr{C}_{\mathcal{R}}(\rho)\right) p_{\Theta}^{succ}(\mathcal{I}),\end{aligned} \tag{5.46}$$

this because $\mathcal{U}_\phi(\delta) = \delta$ for any $\delta \in \mathcal{I}$. On the other hand, to prove the first inequality, we consider the optimal X for the semidefinite programming Eq. 5.19, such that

$$\mathrm{Tr}\left[X\rho\right] = 1+\mathscr{C}_{\mathcal{R}}(\rho), \tag{5.47}$$

with $X = \mathbb{1} - W$, and since $X \geq 0$ also $\mathcal{U}_{\phi_k}(X) \geq 0$ we can write

$$M_k = \frac{1}{n} U_{\phi_k} X {U_{\phi_k}}^{\dagger}. \tag{5.48}$$

Then we have

$$\begin{aligned} \sum_{k_0}^{n-1} p_k \mathrm{Tr}\left[M_k U_{\phi_k} \rho {U_{\phi_k}}^{\dagger}\right] &= \sum_{k_0}^{n-1} \frac{p_k}{n} \mathrm{Tr}\left[U_{\phi_k} X {U_{\phi_k}}^{\dagger} U_{\phi_k} \rho {U_{\phi_k}}^{\dagger}\right] \\ &= \sum_{k_0}^{n-1} \frac{p_k}{n} \mathrm{Tr}\left[X\rho\right] \\ &= \frac{1}{n} \mathrm{Tr}\left[X\rho\right] \\ &= \frac{1}{n}\left(1 + \mathscr{C}_{\mathcal{R}}(\rho)\right). \end{aligned} \tag{5.49}$$

This prove that

$$p_{\Theta}^{succ}(\rho) \geq \frac{1}{n}\left(1 + \mathscr{C}_{\mathcal{R}}(\rho)\right). \tag{5.50}$$

The other possibility in the lower bound follows from the fact that simply guessing k^{max} is always a potentially valid strategy. □

As a consequence of the previous theorem, we can write the following result.

Corollary. ∀ *state* $\rho \in \mathcal{D}(\mathcal{H}_m)$ *and any prior probability distribution* p_Θ *it holds that*

$$\max_{\Theta} \frac{p_{\Theta}^{succ}(\rho)}{p_{\Theta}^{succ}(\mathcal{I})} = 1 + \mathscr{C}_{\mathcal{R}}(\rho). \tag{5.51}$$

Proof. Dividing Eq. 5.45 by $p_{\Theta}^{succ}(\mathcal{I})$ we have

$$\max\left\{\frac{1}{n}\frac{1}{p_{\Theta}^{succ}(\mathcal{I})}\left(1 + \mathscr{C}_{\mathcal{R}}(\rho)\right), 1\right\} \leq \frac{p_{\Theta}^{succ}(\rho)}{p_{\Theta}^{succ}(\mathcal{I})} \leq \left(1 + \mathscr{C}_{\mathcal{R}}(\rho)\right). \tag{5.52}$$

the lower bound matches the upper bound in the case $p_{\Theta}^{succ}(\mathcal{I}) = p_{k^{max}} = \frac{1}{n}$, that is, for a flat prior probability distribution over all $\{\phi_k\}_{k=0}^{n-1}$. □

The maximum is achieved for the phase discrimination game

$$\Theta^{*} \equiv \left\{ \frac{1}{d}, \frac{2\pi k}{d} \right\}_{k=0}^{m-1} . \tag{5.53}$$

Therefore, $\mathscr{C}_{\mathcal{R}}(\rho)$ exactly quantifies, in particular, how useful the state ρ is for reliable decoding and transmission of messages enceded be generalized phase channels $\rho \mapsto Z^{k} \rho Z^{k^{\dagger}}$ with $Z|j\rangle = \exp\left[i\,(2\pi/d)\,j\right]|j\rangle$. These channels features in several quantum information tasks suchas quantum error correction [117], cloning [118], dense coding [119, 120] and discriminating coherent and multicopy quantum states .

Conclusion

In this thesis we have studied the three-dimensional superlocalization problem. From the multiparametric estimation we have determined that the Rayleigh's curse is beaten even in the case where we relax the one dimension hypothesis as shown in many works [18, 17]. Moreover, we found that, for the relative distances of the two point light sources s_x, s_y, p, the estimation of one of them is statistically independent from the other and *vice versa*. It is thus possible to build a physical measurement and estimation strategies for those parameters that saturate Eq. 3.9 asymptotically. Furthermore we have analyzed even a case of light beam when the statistical independence is verified for the whole set of parameters in the limit of $ks_x \ll 1$, $ks_y \ll 1$, $kp \ll 1$. Then we adapt an experimental setup known as SPADE [18] where we show numerically that the measure performed in this implementation can extract the full information offered by quantum mechanics concerning the separations parameters via linear photonics. This scheme works well for close sources, in other words with a relevant overlap function in their wave function, avoiding Rayleigh's curse that plagues direct imaging.

In the second part we have investigated quantum coherence by adopting a resource perspective [24, 121]. In this scenario, and inspired by Vidal and Tarrach [92] and by [94], we have proposed a new quantum coherence quantifier, the so-called robustness of coherence defined in Eq. 5.16, showing that it is a proper measure. Furthermore, we have shown that the evaluation of robustness of coherence can be recast as a semidefinite program to reach an efficient numerical computability and

we give an operational interpretation of the robustness of coherence as quantifier of the advantage enabled by a quantum state in a discrimination task.

Bibliography

[1] Richard Leach. *Fundamental principles of engineering nanometrology*. Elsevier, 2014.

[2] Samanta Piano, Rong Su, and Richard Leach. "Micro-scale geometry measurement". In: *Micro-Manufacturing Technologies and Their Applications*. Springer, 2017, pp. 197–221.

[3] Vittorio Giovannetti, Seth Lloyd, and Lorenzo Maccone. "Advances in quantum metrology". In: *Nature Photonics* 5.4 (2011), p. 222.

[4] Vittorio Giovannetti, Seth Lloyd, and Lorenzo Maccone. "Quantum-enhanced measurements: beating the standard quantum limit". In: *Science* 306.5700 (2004), pp. 1330–1336.

[5] Max Born and Emil Wolf. *Principles of optics: electromagnetic theory of propagation, interference and diffraction of light*. CUP Archive, 2000.

[6] Ariel Lipson, Stephen G Lipson, and Henry Lipson. *Optical physics*. Cambridge University Press, 2010.

[7] Lord Rayleigh. "XXXI. Investigations in optics, with special reference to the spectroscope". In: *The London, Edinburgh, and Dublin Philosophical Magazine and Journal of Science* 8.49 (1879), pp. 261–274.

[8] Lord Rayleigh. "XV. On the theory of optical images, with special reference to the microscope". In: *The London, Edinburgh, and Dublin Philosophical Magazine and Journal of Science* 42.255 (1896), pp. 167–195.

[9] Ernst Abbe. “A contribution to the theory of the microscope and the nature of microscopic vision”. In: *Proceedings of the Bristol Naturalists’ Society*. Vol. 1. 1874, pp. 200–261.

[10] Ernst Abbe. “VII.—On the Estimation of Aperture in the Microscope.” In: *Journal of the Royal Microscopical Society* 1.3 (1881), pp. 388–423.

[11] Ernst Abbe. “XV.—The Relation of Aperture and Power in the Microscope (continued)”. In: *Journal of the Royal Microscopical Society* 3.6 (1883), pp. 790–812.

[12] Herbert A Hauptman. “The phase problem of x-ray crystallography”. In: *Reports on Progress in Physics* 54.11 (1991), p. 1427.

[13] Michael Mark Woolfson. “Direct methods in crystallography”. In: *Reports on Progress in Physics* 34.2 (1971), p. 369.

[14] C. W. Helstrom. *Quantum Detection and Estimation Theory*. New York: Academic Press, 1976.

[15] Samuel L. Braunstein and Carlton M. Caves. “Statistical distance and the geometry of quantum states”. In: *Physical Review Letters* 72 (22 1994), pp. 3439–3443. DOI: 10.1103/PhysRevLett.72.3439. URL: https://link.aps.org/doi/10.1103/PhysRevLett.72.3439.

[16] Matteo GA Paris. “Quantum estimation for quantum technology”. In: *International Journal of Quantum Information* 7.supp01 (2009), pp. 125–137.

[17] Stefano Pirandola and Cosmo Lupo. “Ultimate precision of adaptive noise estimation”. In: *Physical review letters* 118.10 (2017), p. 100502.

[18] Mankei Tsang, Ranjith Nair, and Xiao-Ming Lu. “Quantum theory of superresolution for two incoherent optical point sources”. In: *Physical Review X* 6.3 (2016), p. 031033.

[19] Ranjith Nair and Mankei Tsang. “Far-Field Superresolution of Thermal Electromagnetic Sources at the Quantum Limit”. In: *Physical Review Letters* 117.19 (2016), p. 190801.

[20] Cosmo Lupo and Stefano Pirandola. “Ultimate Precision Bound of Quantum and Subwavelength Imaging”. In: *Physical Review Letters* 117.19 (2016), p. 190802.

[21] Carmine Napoli et al. “Towards superresolution surface metrology: Quantum estimation of angular and axial separations”. In: *Physical review letters* 122.14 (2019), p. 140505.

[22] Andreas Winter and Dong Yang. “Operational resource theory of coherence”. In: *Physical review letters* 116.12 (2016), p. 120404.

[23] Carmine Napoli et al. “Robustness of coherence: an operational and observable measure of quantum coherence”. In: *Physical review letters* 116.15 (2016), p. 150502.

[24] Fernando GSL Brandao and Gilad Gour. “Reversible framework for quantum resource theories”. In: *Physical review letters* 115.7 (2015), p. 070503.

[25] Michael A Nielsen and Isaac L Chuang. *Quantum computation and quantum information*. Cambridge university press, 2010.

[26] Michael A Nielsen and Isaac Chuang. *Quantum computation and quantum information*. 2002.

[27] Mario Bertero and Christine De Mol. “III Super-resolution by data inversion”. In: *Progress in Optics* 36 (1996), pp. 129–178.

[28] Ernst Mach. *The principles of physical optics: an historical and philosophical treatment*. Courier Corporation, 2013.

[29] OS Heavens. “Optical properties of thin films”. In: *Reports on Progress in Physics* 23.1 (1960), p. 1.

[30] Joseph W Goodman. *Introduction to Fourier optics*. Roberts and Company Publishers, 2005.

[31] G Kirchhoff and Berliner Sitzungsberichte. "Vorlesungen über mathematische". In: *Armalen der Physic* 18 (1883), p. 663.

[32] Francis Weston Sears. *Principles of Physics Series: Optics*. Addison-Wesley Press, 1949.

[33] MV Berry et al. *Progress in Optics*. Vol. 50. Elsevier, 2007.

[34] Milton Abramowitz and Irene A Stegun. *Handbook of mathematical functions: with formulas, graphs, and mathematical tables*. Vol. 55. Courier Corporation, 1964.

[35] George Biddell Airy. "On the diffraction of an object-glass with circular aperture". In: *Transactions of the Cambridge Philosophical Society* 5 (1835), p. 283.

[36] John Frederick William Herschel. *On the theory of light*. 1828.

[37] Thomas D Cope. "The Rittenhouse diffraction grating". In: *Journal of the Franklin Institute* 214.1 (1932), pp. 99–104.

[38] Eugene Hecht. "Hecht optics". In: *Addison Wesley* 997 (1998), pp. 213–214.

[39] Rainer Heintzmann and Gabriella Ficz. "Breaking the resolution limit in light microscopy". In: *Briefings in functional genomics & proteomics* 5.4 (2006), pp. 289–301.

[40] Carroll Mason Sparrow. "On spectroscopic resolving power". In: *The Astrophysical Journal* 44 (1916), p. 76.

[41] Diana Nyvssonen Grimes and Brian J Thompson. "Two-point resolution with partially coherent light". In: *JOSA* 57.11 (1967), pp. 1330–1334.

[42] George W Stroke. *Coherent optics and holography*. Vol. 98. Academic Press Inc., New York, 1966.

[43] VP Nayyar and NK Verma. “Two-point resolution of Gaussian aperture operating in partially coherent light using various resolution criteria”. In: *Applied optics* 17.14 (1978), pp. 2176–2180.

[44] Toshimitsu Asakura. “Resolution of two unequally bright points with partially coherent light”. In: *Nouvelle Revue d’Optique* 5.3 (1974), p. 169.

[45] Mikhail I Kolobov and Claude Fabre. “Quantum limits on optical resolution”. In: *Physical review letters* 85.18 (2000), p. 3789.

[46] Vladislav N Beskrovnyy and Mikhail I Kolobov. “Quantum limits of superresolution in reconstruction of optical objects”. In: *Physical Review A* 71.4 (2005), p. 043802.

[47] Bahaa EA Saleh, Malvin Carl Teich, and Bahaa E Saleh. *Fundamentals of photonics*. Vol. 22. Wiley New York, 1991.

[48] David Slepian and Henry O Pollak. “Prolate spheroidal wave functions, Fourier analysis and uncertainty—I”. In: *Bell System Technical Journal* 40.1 (1961), pp. 43–63.

[49] Leonhard Möckl, Don C. Lamb, and Christoph Bräuchle. “Super-resolved Fluorescence Microscopy: Nobel Prize in Chemistry 2014 for Eric Betzig, Stefan Hell, and William E. Moerner”. In: *Angewandte Chemie International Edition* 53.51 (), pp. 13972–13977. DOI: 10.1002/anie.201410265. URL: https://onlinelibrary.wiley.com/doi/abs/10.1002/anie.201410265.

[50] W. E. Moerner. “New directions in single-molecule imaging and analysis”. In: *Proceedings of the National Academy of Sciences* 104.31 (2007), pp. 12596–12602. ISSN: 0027-8424. DOI: 10.1073/pnas.0610081104.

eprint: http://www.pnas.org/content/104/31/12596.full.pdf. URL: http://www.pnas.org/content/104/31/12596.

[51] Richard Leach and Ben Sherlock. "Applications of super-resolution imaging in the field of surface topography measurement". In: *Surface Topography: Metrology and Properties* 2.2 (2014), p. 023001. DOI: 10.1088/2051-672X/2/2/023001. URL: http://stacks.iop.org/2051-672X/2/i=2/a=023001.

[52] Marco Genovese. "Real applications of quantum imaging". In: *Journal of Optics* 18.7 (2016), p. 073002. DOI: 10.1088/2040-8978/18/7/073002. URL: http://stacks.iop.org/2040-8986/18/i=7/a=073002.

[53] Fan Yang et al. "Far-field linear optical superresolution via heterodyne detection in a higher-order local oscillator mode". In: *Optica* 3.10 (2016), pp. 1148–1152. DOI: 10.1364/OPTICA.3.001148. URL: http://www.osapublishing.org/optica/abstract.cfm?URI=optica-3-10-1148.

[54] Martin Paúr et al. "Achieving the ultimate optical resolution". In: *Optica* 3.10 (2016), pp. 1144–1147. DOI: 10.1364/OPTICA.3.001144. URL: http://www.osapublishing.org/optica/abstract.cfm?URI=optica-3-10-1144.

[55] Zong Sheng Tang, Kadir Durak, and Alexander Ling. "Fault-tolerant and finite-error localization for point emitters within the diffraction limit". In: *Frontiers in Optics 2016*. Optical Society of America, 2016, FTu2F.6. DOI: 10.1364/FIO.2016.FTu2F.6. URL: http://www.osapublishing.org/abstract.cfm?URI=FiO-2016-FTu2F.6.

[56] Weng-Kian Tham, Hugo Ferretti, and Aephraim M. Steinberg. "Beating Rayleigh's Curse by Imaging Using Phase Information". In: *Physical Review Letters* 118 (7 2017), p. 070801. DOI: 10.1103/PhysRevLett.118.

070801. URL: https://link.aps.org/doi/10.1103/PhysRevLett.118.070801.

[57] Ranjith Nair and Mankei Tsang. “Interferometric superlocalization of two incoherent optical point sources”. In: *Optics express* 24.4 (2016), pp. 3684–3701.

[58] Mankei Tsang. “Subdiffraction incoherent optical imaging via spatial-mode demultiplexing”. In: *New Journal of Physics* 19.2 (2017), p. 023054.

[59] Ronan Kerviche, Saikat Guha, and Amit Ashok. “Fundamental limit of resolving two point sources limited by an arbitrary point spread function”. In: *Information Theory (ISIT), 2017 IEEE International Symposium on*. IEEE. 2017, pp. 441–445.

[60] Shan Zheng Ang, Ranjith Nair, and Mankei Tsang. “Quantum limit for two-dimensional resolution of two incoherent optical point sources”. In: *Physical Review A* 95.6 (2017), p. 063847.

[61] Andrzej Chrostowski et al. “On super-resolution imaging as a multiparameter estimation problem”. In: *International Journal of Quantum Information* (2017), p. 1740005.

[62] J Řehaček et al. “Multiparameter quantum metrology of incoherent point sources: towards realistic superresolution”. In: *Physical Review A* 96.6 (2017), p. 062107.

[63] J Řehaček et al. “Optimal measurements for resolution beyond the Rayleigh limit”. In: *Optics Letters* 42.2 (2017), pp. 231–234.

[64] J. Řeháček et al. “Optimal measurements for quantum spatial superresolution”. In: *Physical Review A* 98 (1 2018), p. 012103.

[65] Sisi Zhou and Liang Jiang. “Modern description of Rayleigh’s criterion”. In: *Physical Review A* 99 (1 2019), p. 013808.

[66] Mankei Tsang. “Quantum limit to subdiffraction incoherent optical imaging”. In: *Physical Review A* 99 (1 2019), p. 012305.

[67] Keiji Matsumoto. “A new approach to the Cramér-Rao-type bound of the pure-state model”. In: *Journal of Physics A: Mathematical and General* 35.13 (2002), p. 3111.

[68] Sammy Ragy, Marcin Jarzyna, and Rafał Demkowicz-Dobrzański. “Compatibility in multiparameter quantum metrology”. In: *Physical Review A* 94.5 (2016), p. 052108.

[69] Antoine Labeyrie, Stephen G Lipson, and Peter Nisenson. *An introduction to optical stellar interferometry*. Cambridge University Press, 2006.

[70] Jonas Zmuidzinas. “Cramer–Rao sensitivity limits for astronomical instruments: implications for interferometer design”. In: *JOSA A* 20.2 (2003), pp. 218–233.

[71] Joseph W Goodman. *Statistical optics*. John Wiley & Sons, 2015.

[72] Leonard Mandel and Emil Wolf. *Optical coherence and quantum optics*. Cambridge University Press, 1995.

[73] Leonard Mandel. “Fluctuations of photon beams: the distribution of the photo-electrons”. In: *Proceedings of the Physical Society* 74.3 (1959), p. 233.

[74] Daniel Gottesman, Thomas Jennewein, and Sarah Croke. “Longer-baseline telescopes using quantum repeaters”. In: *Physical Review Letters* 109.7 (2012), p. 070503.

[75] Mankei Tsang. “Quantum nonlocality in weak-thermal-light interferometry”. In: *Physical Review Letters* 107.27 (2011), p. 270402.

[76] Jeffrey H Shapiro. “The quantum theory of optical communications”. In: *IEEE journal of selected topics in Quantum Electronics* 15.6 (2009), pp. 1547–1569.

[77] Horace Yuen and J Shapiro. “Optical communication with two-photon coherent states–Part I: Quantum-state propagation and quantum-noise”. In: *IEEE Transactions on Information Theory* 24.6 (1978), pp. 657–668.

[78] Mankei Tsang. “Quantum limits to optical point-source localization”. In: *Optica* 2.7 (2015), pp. 646–653.

[79] Marco G Genoni and Tommaso Tufarelli. “Non-orthogonal bases for quantum metrology”. In: *Journal of Physics A: Mathematical and Theoretical* 52.43 (2019), p. 434002.

[80] Magdalena Szczykulska, Tillmann Baumgratz, and Animesh Datta. “Multi-parameter quantum metrology”. In: *Advances in Physics: X* 1.4 (2016), pp. 621–639.

[81] Anthony E Siegman. “Lasers university science books”. In: *Mill Valley, CA* 37.208 (1986), p. 169.

[82] Orazio Svelto and David C Hanna. *Principles of lasers*. Springer, 1998.

[83] Charles H Bennett et al. “Teleporting an unknown quantum state via dual classical and Einstein-Podolsky-Rosen channels”. In: *Physical review letters* 70.13 (1993), p. 1895.

[84] Eric Chitambar and Gilad Gour. “Quantum resource theories”. In: *Reviews of Modern Physics* 91.2 (2019), p. 025001.

[85] Eric Chitambar et al. “Everything you always wanted to know about LOCC (but were afraid to ask)”. In: *Communications in Mathematical Physics* 328.1 (2014), pp. 303–326.

[86] Ingemar Bengtsson and Karol Życzkowski. *Geometry of quantum states: an introduction to quantum entanglement*. Cambridge university press, 2017.

[87] Vlatko Vedral et al. “Quantifying entanglement”. In: *Physical Review Letters* 78.12 (1997), p. 2275.

[88] Ryszard Horodecki et al. “Quantum entanglement”. In: *Reviews of modern physics* 81.2 (2009), p. 865.

[89] Charles H Bennett et al. “Mixed-state entanglement and quantum error correction”. In: *Physical Review A* 54.5 (1996), p. 3824.

[90] Wolfgang Dür, Guifre Vidal, and J Ignacio Cirac. “Three qubits can be entangled in two inequivalent ways”. In: *Physical Review A* 62.6 (2000), p. 062314.

[91] Vlatko Vedral and Martin B Plenio. “Entanglement measures and purification procedures”. In: *Physical Review A* 57.3 (1998), p. 1619.

[92] Guifré Vidal Bonafont and Rolf Tarrach. “Robustness of entanglement”. In: *Physical Review A, 1999, vol. 59, núm. 1, p. 141-155.* (1999).

[93] Rafael Chaves and Luiz Davidovich. “Robustness of entanglement as a resource”. In: *Physical Review A* 82.5 (2010), p. 052308.

[94] Michael Steiner. “Generalized robustness of entanglement”. In: *Physical Review A* 67.5 (2003), p. 054305.

[95] Jens Eisert, Fernando GSL Brandao, and Koenraad MR Audenaert. “Quantitative entanglement witnesses”. In: *New Journal of Physics* 9.3 (2007), p. 46.

[96] Otfried Gühne and Géza Tóth. “Entanglement detection”. In: *Physics Reports* 474.1-6 (2009), pp. 1–75.

[97] Fernando GSL Brandao. “Quantifying entanglement with witness operators”. In: *Physical Review A* 72.2 (2005), p. 022310.

[98] Seth Lloyd. “Quantum coherence in biological systems”. In: *J. Phys.: Conf. Ser.* 302.1 (2011), p. 012037.

[99] S. F. Huelga and M. B. Plenio. “Vibrations, Quanta and Biology”. In: *Contemp. Phys.* 54 (2013), p. 181.

[100] B. Hensen et al. “Experimental loophole-free violation of a Bell inequality using entangled electron spins separated by 1.3 km”. In: *Nature* 526 (2015), p. 682.

[101] Marissa Giustina et al. “Significant-Loophole-Free Test of Bell’s Theorem with Entangled Photons”. In: *Phys. Rev. Lett.* 115 (25 2015), p. 250401. DOI: 10.1103/PhysRevLett.115.250401. URL: http://link.aps.org/doi/10.1103/PhysRevLett.115.250401.

[102] Lynden K. Shalm et al. “Strong Loophole-Free Test of Local Realism*”. In: *Phys. Rev. Lett.* 115 (25 2015), p. 250402. DOI: 10.1103/PhysRevLett.115.250402. URL: http://link.aps.org/doi/10.1103/PhysRevLett.115.250402.

[103] Johan Åberg. “Quantifying superposition”. 2006.

[104] Tillmann Baumgratz, Marcus Cramer, and Martin B Plenio. “Quantifying coherence”. In: *Physical review letters* 113.14 (2014), p. 140401.

[105] Frédéric Grosshans et al. “Quantum key distribution using gaussian-modulated coherent states.” In: *Nature* 421.6920 (Jan. 2003), pp. 238–41. ISSN: 0028-0836. DOI: 10.1038/nature01289. URL: http://www.ncbi.nlm.nih.gov/pubmed/12529636.

[106] Vittorio Giovannetti, Seth Lloyd, and Lorenzo Maccone. “Advances in Quantum Metrology”. In: *Nat. Photon.* 5 (2011), p. 222. DOI: 10.1038/nphoton.2011.35.

[107] *A little bit, better*. The Economist, 2015.

[108] Jonathan P. Dowling and Gerard J. Milburn. “Quantum technology: the second quantum revolution”. In: *Phil. Trans. Roy. Soc. A* 361.1809 (2003), p. 1655. DOI: 10.1098/rsta.2003.1227.

[109] Ryszard Horodecki et al. “Quantum entanglement”. In: *Rev. Mod. Phys.* 81 (2 2009), p. 865. DOI: 10.1103/RevModPhys.81.865.

[110] Kavan Modi et al. “The classical-quantum boundary for correlations: Discord and related measures”. In: *Rev. Mod. Phys.* 84 (4 2012), p. 1655. DOI: 10.1103/RevModPhys.84.1655.

[111] Nicolas Brunner et al. “Bell nonlocality”. In: *Rev. Mod. Phys.* 86 (2 2014), pp. 419–478. DOI: 10.1103/RevModPhys.86.419. URL: http://link.aps.org/doi/10.1103/RevModPhys.86.419.

[112] T. Baumgratz, M. Cramer, and M. B. Plenio. “Quantifying Coherence”. In: *Phys. Rev. Lett.* 113 (14 2014), p. 140401. DOI: 10.1103/PhysRevLett.113.140401.

[113] M. Lostaglio, D. Jennings, and T. Rudolph. “Description of quantum coherence in thermodynamic processes requires constraints beyond free energy”. In: *Nature Commun.* 6 (2015), p. 6383. DOI: 10.1038/ncomms7383.

[114] Varun Narasimhachar and Gilad Gour. “Low-temperature thermodynamics with quantum coherence”. In: *Nature Commun.* 6 (2015), p. 7689. DOI: 10.1038/ncomms8689.

[115] Alexander Streltsov, Gerardo Adesso, and Martin B Plenio. “Colloquium: Quantum coherence as a resource”. In: *Reviews of Modern Physics* 89.4 (2017), p. 041003.

[116] Yi Peng, Yong Jiang, and Heng Fan. “Maximally coherent states and coherence-preserving operations”. In: *Physical Review A* 93.3 (2016), p. 032326.

[117] Daniel Gottesman. In: *Chaos, Solitons & Fractals* 10 (1999), p. 1749. DOI: 10.1016/S0960-0779(98)00218-5.

[118] N. J. Cerf. In: *J. Mod. Opt.* 47 (2000), p. 197. DOI: 10.1080/09500340008244036.

[119] T. Hiroshima. In: *J. Phys. A: Math. Gen.* 34 (2001), p. 6907. DOI: 10.1088/0305-4470/34/35/316.

[120] R. F. Werner. “All teleportation and dense coding schemes”. In: *J. Phys. A: Math. Gen.* 34 (2001), p. 7094. DOI: 10.1088/0305-4470/34/35/332.

[121] Tillmann Baumgratz and Animesh Datta. “Quantum enhanced estimation of a multidimensional field”. In: *Physical Review Letters* 116.3 (2016), p. 030801.